VILNIUS GEDIMINAS TECHNICAL UNIVERSITY

Romualdas JUKNELEVIČIUS

RESEARCH ON BIODIESEL AND HYDROGEN CO-COMBUSTION PROCESS IN COMPRESSION IGNITION ENGINE

DOCTORAL DISSERTATION

TECHNOLOGICAL SCIENCES,
TRANSPORT ENGINEERING (T 003)

VGTU
LEIDYKLA
Vilnius TECHNIKA 2019

Doctoral dissertation was prepared at Vilnius Gediminas Technical University in 2014–2019.

Supervisor

Assoc. Prof. Dr Saugirdas PUKALSKAS (Vilnius Gediminas Technical University, Transport Engineering – T 003).

The Dissertation Defense Council of Scientific Field of Transport Engineering of Vilnius Gediminas Technical University:

Chairman

Prof. Dr Gintautas BUREIKA (Vilnius Gediminas Technical University, Transport Engineering – T 003).

Members:

Prof. Dr Stasys SLAVINSKAS (Vytautas Magnus University, Transport Engineering – T 003),

Dr Nerijus STRIŪGAS (Lithuanian Energy Institute, Energetics and Power Engineering – T 006),

Assoc. Prof. Dr Habil. Arkadiusz SZYMANEK (Czestochowa University of Technology, Poland, Chemical Engineering – T 005),

Assoc. Prof. Dr Gediminas VAIČIŪNAS (Vilnius Gediminas Technical University, Transport Engineering – T 003).

The dissertation will be defended at the public meeting of the Dissertation Defense Council of Transport Engineering in the Senate Hall of Vilnius Gediminas Technical University at **10 a. m. on 8 July 2019**.

Address: Saulėtekio al. 11, LT-10223 Vilnius, Lithuania.
Tel.: +370 5 274 4956; fax +370 5 270 0112; e-mail: doktor@vgtu.lt

A notification on the intend defending of the dissertation was send on 7 June 2019. A copy of the doctoral dissertation is available for review at VGTU repository http://dspace.vgtu.lt, at the Library of Vilnius Gediminas Technical University (Saulėtekio al. 14, LT-10223 Vilnius, Lithuania), at the Library of Klaipėda University (K. Donelaičio st. 3, LT-92144 Klaipėda, Lithuania), at the Library of Vytautas Magnus University (K. Donelaičio st. 52-215 rm.), LT-44244 Kaunas, Lithuania) and at the Library of Kaunas University of Technology (K. Donelaičio st. 20, LT-44239 Kaunas, Lithuania).

VGTU leidyklos TECHNIKA 023-M mokslo literatūros knyga

ISBN 978-609-476-182-9

romualdas.juknelevicius@vgtu.lt

VILNIAUS GEDIMINO TECHNIKOS UNIVERSITETAS

Romualdas JUKNELEVIČIUS

BIODYZELINO IR VANDENILIO BENDRO DEGIMO PROCESO SLĖGINIO UŽDEGIMO VARIKLYJE TYRIMAS

DAKTARO DISERTACIJA

TECHNOLOGIJOS MOKSLAI,
TRANSPORTO INŽINERIJA (T 003)

VGTU
LEIDYKLA
Vilnius TECHNIKA 2019

Disertacija rengta 2014–2019 metais Vilniaus Gedimino technikos universitete.

Vadovas

doc. dr. Saugirdas PUKALSKAS (Vilniaus Gedimino technikos universitetas, transporto inžinerija – T 003).

Vilniaus Gedimino technikos universiteto Transporto inžinerijos mokslo krypties disertacijos gynimo taryba:

Pirmininkas

prof. dr. Gintautas BUREIKA (Vilniaus Gedimino technikos universitetas, transporto inžinerija – T 003).

Nariai:

prof. dr. Stasys SLAVINSKAS (Vytauto Didžiojo universitetas, transporto inžinerija – T 003),

dr. Nerijus STRIŪGAS (Lietuvos energetikos institutas, energetika ir termoinžinerija – T 006),

doc. habil. dr. Arkadiusz SZYMANEK (Čenstachavos technologijos universitetas, Lenkija, chemijos inžinerija – T 005),

doc. dr. Gediminas VAIČIŪNAS (Vilniaus Gedimino technikos universitetas, transporto inžinerija – T 003).

Disertacija bus ginama viešame Transporto inžinerijos mokslo krypties disertacijos gynimo tarybos posėdyje **2019 m. liepos 8 d. 10 val.** Vilniaus Gedimino technikos universiteto senato posėdžių salėje.

Adresas: Saulėtekio al. 11, LT-10223 Vilnius, Lietuva.
Tel.: (8 5) 274 4956; faksas (8 5) 270 0112; el. paštas doktor@vgtu.lt

Pranešimai apie numatomą ginti disertaciją išsiusti 2019 m. birželio 7 d.

Disertaciją galima peržiūrėti VGTU talpykloje http://dspace.vgtu.lt ir Vilniaus Gedimino technikos universiteto bibliotekoje (Saulėtekio al. 14, LT-10223 Vilnius, Lietuva), Klaipėdos universiteto (K. Donelaičio g. 3, LT-92144 Klaipėda, Lietuva), Vytauto Didžiojo universiteto (K. Donelaičio g. 52-215 kab., LT-44244 Kaunas, Lietuva), Kauno technologijos universiteto (K. Donelaičio g. 20, LT-44239 Kaunas, Lietuva).

Abstract

Increasing environmental pollution, concerns about oil price, traffic related health effects and depletion of fossil fuel resources are forcing humanity to limit the consumption or to look for new forms of energy. The cleanest power suitable for the road transport would be the electric energy produced of the clean sources such as solar, hydro, wind power and stored in batteries or extracted from hydrogen using fuel cell technology. However, the limitted range of driven distance are the obstacle for today battery electric cars. The lack of hydrogen fuelling stations, high price of hydrogen and expensive materials, limits the outbreake of the fuel cell technology. According to experts, hybrid systems including both electric and internal combustion engines consuming the renewable fuels would be the main power plant of vehicles decreasing the exhaust emissions of the internal combustion engine remains the important research subject for the time beeing.

This dissertation work presents the study of performance, efficiency and ecological indicators of the co-combustion process of hydrogen with various renewable biomass based biofuels and their blends in the compression ignition engine. Experimental investigation and numerical simulation methods were applied in order to have a complex understanding of biodiesel fuels and influence of hydrogen on the engine work cycle.

Introductory chapter presents the formulation of the problem, object and importance of the thesis, aim and the tasks of the work. The scientific novelty, theoretical and practical value of results obtained during experiments, and the list of published scientific publications by the author are presented.

The scientific literature according to the theme of the thesis overviewed in the first chapter. The composition of biomass based biofuels with transestherification and hydrotreatening processes, heating values of the fuel and other features were reviewed according to other scientist's works. The influence of the main parameters on CI engine efficiency and emission parameters were discussed.

The second chapter represents the set-up of engines used at experiment, its methodology, calculations of heating values of the fuel mixtures used in experiment, calculations of hydrogen energy share according to the biodiesel flow rate, calculation of mass fraction burned, theoretical analysis of the rate of heat release, numerical simulation of performed experiments are discussed.

The results of experiments obtained during tests of biodiesel and hydrogen fuel mixtures, numerical analysis and simulation of mentioned fuel mixtures presented in the third chapter. Research of various hydrogen energy share revealed that, higher engine efficiency and lower exhaust gas emissions in CI engine can be achieved.

11 scientific papers focused on the subject of the doctoral thesis have been published: 2 – in publications of the *Clarivate Analytics Web of Science* database with citation index; 1 – in *Conference Proceedings* publications of the *Clarivate Analytics Web of Science* database; 5 – in publications of other international database; 3 – in publications of other reviewable scientific publications.

Reziumė

Transporto sukeliama aplinkos tarša, didėjantis jos poveikis sveikatai, naftos kainų nestabilumas, augantis iškastinio kuro išteklių eikvojimas verčia žmoniją riboti vartojimą ir ieškoti naujų energijos formų. Švariausia energija, tinkama kelių transportui, būtų elektros energija, išgauta iš švarių šaltinių, tokių kaip saulės, vandens ir vėjo jėgainės, ir saugoma baterijose arba išgaunamos iš vandenilio panaudojant kuro elementų technologijas. Tačiau ribota baterijų talpa yra didžiausia kliūtis šiandieniniams elektromobiliams. Vandenilio degalinių stoka, aukšta vandenilio kaina ir brangios medžiagos, naudojamos kuro elementų elektros generatoriuose, riboja vandenilio kuro elementų panaudojimą sausumos transporte. Pasak ekspertų, hibridinės sistemos, naudojančios elektrinius ir vidaus degimo variklius, veikiančius atsinaujinančiais degalais, artimiausiu metu būtų pagrindinė transporto priemonių jėgainė. Jose naudojami vidaus degimo varikliai turėtų būti mažiau taršūs ir todėl yra svarbus tyrimo objektas.

Šioje disertacijoje pateikiamas įvairių atsinaujinančių biodyzelino rūšių ir jų mišinių su vandeniliu panaudojimo slėginio uždegimo variklyje, efektyvumo ir ekologinių rodiklių tyrimas. Darbo eigoje buvo panaudoti eksperimentiniai tyrimai ir skaitiniai modeliavimo metodai, siekiant išsiaiškinti biodyzelino ir vandenilio mišinio įtaką variklio parametrams.

Įvadiniame skyriuje pristatomos problemos, darbo objekto ir reikšmės, tikslo ir uždaočių genezė. Taip pat pateikta eksperimentų metu gautų rezultatų mokslinis naujumas, teorinė ir praktinė vertė bei autoriaus paskelbti moksliniai straipsniai.

Pirmajame skyriuje apžvelgta mokslinė literatūra disertacijos tema. Pagal kitų mokslininkų darbus atlikta iš biomasės išgaunamų biodegalų, jų transesterifikavimo ir hidrinimo proceso, biodyzelino šilumingumo ir kitų savybių apžvalga. Aptarta pagrindinių savybių įtaka slėginio uždegimo variklio efektyvumui ir išmetamųjų teršalų parametrams.

Antrajame skyriuje pateikiama eksperimente panaudota įranga, eksperimente naudojamų degalų energetinių verčių santykio skaičiavimo metodika, sudegusios mišinio dalies skaičiavimo metodika, šilumos išsiskyrimo greičio įvertinimo analizė, aptariamas atliktų eksperimentų skaitinis modeliavimas.

Trečiame skyriuje pateikti atliktų eksperimentų rezultatai, gauti atliekant biodyzelino ir vandenilio mišinių bandymus, bandymų modeliavimas ir skaitinė analizė. Bandymai atlikti su įvairiomis vandenilio energijos dalimis parodė daug žadančius rezultatus, didesnį variklio efektyvumą ir mažesnį kenksmingų teršalų išmetimą slėginio uždegimo variklyje.

Disertacijos tema buvo publikuota 11 mokslinių straipsnių: 2 – *Clarivate Analytics Web of Science* duomenų bazės leidiniuose, turinčiuose citavimo rodiklį; 1 – *Clarivate Analytics Web of Science* duomenų bazės *Conference Proceedings* leidiniuose; 5 – kitų tarptautinių duomenų bazių leidiniuose; 3 – kituose recenzuojamuose mokslo leidiniuose.

Notations

Symbols

a – combustion efficiency parameter of the Wiebe function;
A_p – piston surface;
b_e – brake specific fuel consumption;
B_{volH} – volume flow rate of hydrogen;
B_{wtH} – mass flow rate of hydrogen;
B_{wtLF} – mass flow rate of liquid fuel;
CO – carbon monoxide;
CO_2 – carbon dioxide;
D – cylinder bore;
deg – degree;
dQ – heat release;
$dQ/d\varphi$ – rate of heat release;
$dp/d\varphi$ – pressure-rise in cylinder;
H_2 – hydrogen molecule;
HC – hydrocarbon;
H_{wtH} – lower heating value of hydrogen by mass;
H_{wtLF} – lower heating value of liquid fuel by mass;
i – number of cylinders of the engine;
K_L – dependence factor on temperature increase;

lpm – liters per minute;
m_{Hcycl} – mass flow rate of hydrogen per cycle;
m_{LFcycl} – mass flow rate of liquid fuel per cycle;
m_{frH} – mass fraction of the hydrogen in the mixture;
m_{frLF} – mass fraction of the liquid fuel in the mixture;
M_H – molar mass of hydrogen;
Mt/y – million tons per year;
m_v – combustion intensity shape parameter;
n – engine speed;
n_c – constant of proportionality;
N – number of moles of main reactants;
N_0 – number of moles of main reactants at the start of combustion;
N_e – number of effective centres;
N_A – Avogadro constant ($6.022140857 \cdot 10^{23}$ mol^{-1});
N_2 – nitrogen atom;
NO_x – nitrogen oxides;
NO – nitrogen monoxide;
O_2 – oxygen molecule;
OH – hydroxyl radical;
P_{ind} – indicated power;
p – pressure;
p_{cyl} – in-cylinder pressure;
p_{ind} – indicated pressure;
p_H – pressure of hydrogen;
$p_{H@STP}$ – pressure of hydrogen at STP;
p_{max} – maximum in-cylinder pressure;
p_{STP} – pressure of hydrogen at STP;
Q_{cycl} – amount of heat released during engine work cycle;
Q_{Hcycl} – amount of heat released during combustion of hydrogen per cycle;
Q_{LFcycl} – amount of heat released during combustion of liquid fuel per cycle;
R – result of function;
S_p – displacement of the piston;
t – time;
t_c – combustion duration (time related);
T_{cyl} – temperature in the cylinder;
T_{ex} – exhaust gas temperature;
T_{in} – intake gas temperature;
T_{inj} – injection duration of LF;
T_H – temperature of hydrogen;
$T_{H@STP}$ – temperature of hydrogen at STP;
T_{LF} – temperature of liquid fuel (diesel or biodiesel);
T_{max} – maximum in-cylinder temperature;

V – volume;
V_i – in-cylinder volume of combustion chamber;
V_{SOC} – in-cylinder volume at the time of start of combustion;
V_{EOC} – in-cylinder volume at the time of end of combustion;
V_c – clearance volume (compression volume);
V_s – swept volume (stroke volume);
V_b – volume of the burned fraction;
V_u – volume of the unburned fraction;
V_{air} – volume flow rate of air;
V_H – volume flow rate of hydrogen;
V_{airLF} – stoichiometric flow rate of air for liquid fuel;
V_{airH} – stoichiometric flow rate of air for hydrogen;
V_{Hcycl} – volume flow rate of hydrogen per cycle;
V_{LFcycl} – volume flow rate of LF per cycle;
vol – volume;
wt – weight;
x – mass fraction burned;
y_n – independent variables of the function;
Z – increment;
δp – uncertainity of in-cylinder pressure;
δV – uncertainity of instantaineous volume displacement;
$\delta BMEP$ – uncertainity of the brake mean effective pressure;
δm_{LF} – uncertainity of the mass flow rate of liquid fuel;
δm_H – uncertainity of the mass flow rate of hydrogen;
δR – uncertainity of the result;
δp – uncertainty of in-cylinder pressure;
δTd – uncertainty of pressure transducer;
δAm – uncertainty of amplifier;
δDa – uncertainty of data acquisition module;
$\delta \eta_e$ – uncertainty of the *BTE*;
δx_n – uncertainity of the independent variables;
Δp – in-cylinder pressure rise (difference);
Δp_c – in-cylinder pressure rise due to combustion;
Δp_v – in-cylinder pressure rise due to the volume change;
Δp^*_c – normalized in-cylinder pressure rise;
$\Delta \varphi_c$ – combustion duration;
η_e – brake thermal efficiency;
η_i – indicated thermal efficiency;
η_v – volumetric efficiency;
η_{ch} – charging efficiency;
ε – compression ratio;
λ – air-fuel ratio;

κ – polytropic exponent;
μ – mean value;
ρ_H – density of the hydrogen;
ρ_{LF} – density of the liquid fuel;
τ – number of engine strokes;
φ – crank angle degree from the start of combustion;
φ_c – combustion duration (crank angle);
φ_i – liquid fuel injection timing;
φ_0 – start of combustion;
φ_{pmax} – crank angle of maximum in-cylinder pressure.

Abbreviations

AFR – air-fuel ratio;
AFR_{volLF} – stoichiometric volume air – fuel ratio of liquid fuel;
AFR_{volH} – stoichiometric volume air – fuel ratio of hydrogen;
ATR – auto-thermal reforming;
AVL – Anstalt für Verbrennungskraftmaschinen (Germ.);
aBDC – after bottom dead center;
aTDC – after top dead center;
bBDC – before bottom dead center;
BEV – battery electric vehicle;
bTDC – before top dead center;
BMEP – brake mean effective pressure;
BSFC – brake specific fuel consumption;
BTE – brake thermal efficiency;
BTL – biomass to liquid fuel based on the Fischer-Tropsch process;
DF – diesel fuel;
CA – crank angle;
CAD – crank angle degree;
CA 0–10 – crank angle interval from the start of combustion to the 10% MFB;
CA 10–90 – crank angle interval from the 10% MFB to the 90% MFB;
CD – combustion duration;
C/H – carbon to hydrogen ratio;
CI – compressed ignition;
CNG – compressed natural gas;
CN – cetane number;
CP – cloud point;
DF – diesel fuel;
DI – direct injection;
CFPP – cold filter plugging point;
CPOX – catalytic partial oxidation;

CR – compression ratio;
ECU – electronic control unit;
EGR – exhaust gas recirculation;
EOC – end of combustion;
FA – fatty acid;
FAME – fatty acid methyl esther;
FC – fuel cell;
FCEV – fuel cell electric vehicle;
FFA – free fatty acid;
FTS – Fischer-Tropsch synthesis;
GHG – green-house gas;
GTL – gas to liquid fuel based on the Fischer-Tropsch process;
HCCI – homogeneous charge compression ignition;
HCNG – hydrogen enriched compressed natural gas;
HES – hydrogen energy share;
H0 – HES = 0%
H16 – HES = 16%
HRF – high reactivity fuel;
HVO – neat hydro-treated vegetable oil;
HVO+$H_2$16% – HVO and hydrogen mixture with HES = 16%;
HFRR – high frequency reciprocating rig;
IMEP – indicated mean effective preassure;
ISFC – indicated specific fuel consumption;
ITE – indicated thermal efficiency;
ICE – internal combustion engine;
IV – iodine value;
LF – liquid fuel;
LFL – lower flammability limit;
LHV – lower heating value;
LL – low load;
LRF – low reactivity fuel;
MFB – mass fraction burned;
ML – medium load;
NExBTL – trademark of Neste hydrotreated vegetable oil;
NL – nominal load;
NTP – normal conditions for temperature and pressure (20 °C and 101325 kPa);
PCCI – premixed charge compression ignition;
PFI – port fuel injection;
PRO Diesel – mixture of 15% (vol.) NExBTL with fossil diesel fuel;
PRO Diesel+$H_2$16% – PRO Diesel – hydrogen mixture with HES = 16%;
PEM – proton exchange membrane;
PM – particulate matter;

PWM – pulse width modulation;
POX – partial oxidation;
PP – pour point;
RCCI – reactivity controlled compression ignition;
RME – neat rapeseed methyl esther;
RME+$H_2$16% – RME and hydrogen mixture with HES = 16%;
RME7 – mixture of 7% (vol.) RME with fossil DF in accordance to the standard EN 590:2013;
RME7+$H_2$16% – RME7 and hydrogen mixture with HES = 16%;
ROHR – rate of heat released;
SMD – sauter mean diameter;
SMR – steam methane reforming;
SOEC – solid oxide electrolysis cells;
SOC – start of combustion;
SOI – start of injection;
STP – standard conditions for temperature and pressure (0 ºC and 10^5 Pa);
TDC – top dead center;
XTL – material X to liquid fuel based on the Fischer-Tropsch process;
ULSD – ultra-low sulphur diesel.

Notions

Abnormal combustion – phenomena of extremely rapid release of much of the chemical energy, causing high pressures and propogation of pressure waves of substantial amplitude across the combustion chamber (Heywood 1988).

Auto-ignition – the acceleration of oxidation reaction rates due to the heat release becoming in excess of prevailing losses to the surrounding without the aid of deliberate external ignition sources (Karim 2015).

Biodiesel – renewable liquid fuel produced by transesterification of any vegetable oils or other oils and fats consisting largely of triglyceride (EN 14214:2008).

Co-combustion – the thermochemical reaction of more than one fuel to produce the power.

Dual fuel engine – an engine where a mixture of gaseous fuel and air is ignited by the injection of pilot diesel fuel (Karim 2015).

Hydrotreated biodiesel – renewable liquid fuel produced by catalytic hydrogenation of the same triglyceride feedstocks used to produce biodiesel (EN 15940:2016).

Knock – the noise, which is transmitted through the engine structure when abnormal combustion occurs (Heywood 1988).

Contents

[1] The annexes are supplied in the attached compact disc.

Introduction

Formulation of the Problem

The development of global economy directed towards the increasing consumption of fossil fuels, which cause the increasing of the global warming. The result of this phenomenon is dramatic melting of mountain glaciers and arctic ice, increased floods over the last decades. In 2015, global CO_2 emissions reached 32.3 Gt CO_2, while the whole transport fleet accounted for 7.75 Gt CO_2. With increased emissions of cars and trucks by 68 % since 1990, it accounts 75% of the whole transport fleet CO_2 emissions – 5.8 Gt CO_2 (International Energy Agency Highlights, 2017). The International Panel of Climate Change (IPCC) suggests that a permanent concentration of CO_2 at the level of 550 ppm would lead to the increase of the Earth's temperature by ~3 °C above pre-industrial levels. At the Paris International Climate Conference, in December 2015, 195 countries signed the universal global climate agreement with an action plan to avoid serious climate changes leading to the catastrophic consequences. Governments took the commitment to keep the global average temperature 'well below' 2 °C above pre-industrial levels. The EC took the commitment up to year 2050 decrease the toxic emissions by 80–95% in compare to 1990. While the transport must reduce its emissions on 60% by 2050 in compare to 1990 (Conference of the Parties 2015). These regulations affect the oil production with consequences on the growth of

the World economy (Murray *et al.* 2012). The impact on the growth of economy and location of the oil reserves in the critical regions, implicates the research of alternative and sustainable energy resources. The research of alternative fuel features, the combustion process and engine controls are the tools to reduce emissions and maintain the efficiency parameters.

EU established the stringent emission regulations for transition from current situation to the year 2020–2021. To reduce the emissions according to EU regulations and to maintain the consumption of 26.5 l/100 km diesel by truck-trailer, means a fully computerized, expensive exhaust system and well-balanced onboard control of all energy consumers of the truck. The alternative for above mentioned could be use of alternative fuels, including hydrogen and biomass based biodiesel. US Department of Energy considers that as long as the FC technology will reach the higher efficiency of hydrogen utilization, the use of hydrogen in IC engines can serve as a technological platform that would help the development of a hydrogen infrastructure (U.S. Department of Energy 2006).

The thermodynamic and combustion physical properties makes the hydrogen quite promising alternative of the fuel for the road transport. Although use of the pure hydrogen for IC engines are hardly possible, the co-combustion with biomass based biofuels produced of sustainable sources supplied by reliable suppliers makes it the subject of research interest.

Relevance of the Thesis

The Directive of the European Parliament on the deployment of alternative fuels infrastructure of 2013 (Directive of the European Parliament 2013), announced that hydrogen and biofuels as alternative fuels can replace petroleum derived fuels and assist to reduce emissions of IC engine. European Commission Decision of 25 July 2016 announced the Work Programme 2016–2017 „Smart, green and integrated transport“ (European Comission 2016). The aim of the programme is to achieve a European transport system that is resource-efficient, climate and environmentally friendly, benefits the economy and society. Special attention will be given to the research of resource efficiency, through the use of innovative propulsion systems, to reduce the dependence of the transport on fossil fuels and undertake of alternative fuels. With such efforts the required level of mitigation of climate change and pollution should be achieved in the transport sector.

The present petroleum diesel engines running on lean burn are forced by EC regulations towards the lower emissions while customers needs the sufficient efficiency. One of the ways to improve lean burn CI engines, is the use of gaseous fuel hydrogen with high flame speed and high LHV leading to the improvement of engine efficiency and emission parameters. The low C/H ratio hydrogen in co-

combustion with biodiesel initiate to step forward towards the implementation of the decissions of European Commission.

The co-combustion of hydrogen with biodiesel intended to power CI engines and satisfy the required level of regulatoins. However, due to the challenges related to the extremely low density of hydrogen, affecting the engine volumetric efficiency and power, cycle-by-cylcle variations of hydrogen combustion, dependance of hydrogen energy fraction on air-fuel ratio, load and engine speed, the use of hydrogen needs for more deep investigation to provide the methodology for assessing the impact of hydrogen use on engine performance parameters.

Considering the different reactivity features of the hydrogen as low reactivity with low CN and biomass based fuel as the high reactivity with high CN the reactivity controlled compression ignition (RCCI) strategy is available. Further research of RCCI mode operation on co-combustion of hydrogen and biomass based fuel is the challeng because of very limited pole of available literature and research articles on above subject. Different fuel blends could be used to create the reactivity gradient at different operating conditions of CI engine: the high cetane fuel at low load and a low cetane fuel at nominal load. Therefore, it is available to operate CI engine with fuel mixtures covering the range from the high cetane to the low cetane, depending on the operating regime. The hydrogen energy share can be the tool to handle the engine operation with various AFR or loads. However the extremely fast laminar flame speed, high auto-ignition temperature and small quenching distance of hydrogen are the main challenges to employ it as low reactivity fuel of the RCCI mode operation. The injection timing, duration and multiple injection impulses of the biofuel are the tools to manage the co-combustion with hydrogen. The abnormal combustion also needs to be researched as there are gaps in the knowledge of that phenomenon at the RCCI mode operation.

The Object of Research

The co-combustion process parameters of the hydrogen with first- and second-generation biomass based biofuels (and their blends with petroleum diesel), in the compression ignition engine with supply of hydrogen to the intake manifold and injection of biofuel directly into the cylinder.

The Aim of the Thesis

After investigation of the hydrogen co-combustion with pure biodiesel as well as it blends with petroleum diesel in the compression ignition engine, make a suggestion on methodology for assessing the impact of hydrogen use on engine performance parameters.

The Tasks of the Thesis

The following tasks were concluded to achieve the aim of the thesis:

1. To analyze the properties of hydrogen, biofuels and their blends with petroleum diesel, to plan the experiment of a compression ignition engine and to develop a numerical algorithm.
2. To examine the effect of the hydrogen energy fraction in co-combustion with RME and HVO and it blends with petroleum diesel on the maximum in-cylinder pressure, combustion duration of initial (CA 0–10) and main (CA 10–90) phases, the auto-ignition delay period and ROHR.
3. To determine the influence of the hydrogen energy share on the emission parameters of the engine.
4. To determine the boundary of hydrogen energy share at various engine loads when the phenomena of abnormal combustion (pressure oscilation) occurs.

Research Methodology

Experimental, theoretical and numerical simulation investigation methods are applied in present dissertation.

Experiments were carried out with a single-cylinder, normaly aspirated compression ignition engine, without EGR. The data collecting and processing was performed by *SAWIR* software developed in the *Delphi 6.0* programming environment.

During bench tests, in-cylinder pressure sensor *Kistler 6061B*, intake air and exhaust gas temperature sensors, exhaust gas analyzer *Bosch BEA 350*, smoke analyer *Maha MDO 2 LON*, biofuel injection duration controller, biofuel consumption gauge, hydrogen gas flow meter *COMMON CGR-01* were used.

Numerical simulation model of the experimental engine was developed with *AVL BOOST* software and was applied in order to get combustion process data and simulate the engine combustion process. The simulation of the temperature

change in the constant volume combustion chamber performed with the *CHEMKIN* software.

Scientific Novelty of the Thesis

1. Determined the influence of the hydrogen energy share on hydrogen co-combustion with biodiesel and/ or its mixtures with petroleum diesel on the efficiency and emissions parameters of the compression ignition engine.
2. Developed a new methodology for the calculation of the energy share ratio in depend of the liquid fuel injection time and hydrogen volume flow rate according to the choosen hydrogen energy share and indicated mean effective pressure, including evaluation of indicated thermal efficiency.
3. Applied the hydrogen co-combustion with biodiesel and/ or its mixtures with petroleum diesel in RCCI engine mode.
4. Developed and applied the numerical modeling technique to analyze engine parameters under the lean mixture with a hydrogen energy share (50-80%) exceding the experimental limits.

Practical Value of the Research Findings

1. The hydrogen (with 20–23% of energy share) can be used to reduce the indicated fuel consumption and exhaust emissions of automotive diesel engines. This is especially important dealing with the problem of air pollution of big cities. The adjustment of the liquid fuel injection timing, duration and injection impulses can result in even higher diesel engine efficiency.
2. The energy regeneration system of diesel locomotives can be utilized to produce the hydrogen, which can be used to reduce the consumption and exhaust emissions of the petroleum fuel.
3. On the basis of the author's research results, the guidance methods and renewal startegies of companie‘s fleet vehicles can be developed with use of hydrogen for diesel engines.

The Defended Statements

The following statements based on the results of present thesis may serve as the official hypotheses to be defended:

1. The hydrogen volume fraction lower than 3.0–3.1 % in the mixture is not sufficient to reach the lower flamability limit (LFL) of the hydrogen, which determines the sluggish flame propagation speed during combustion, the low rate of heat release and the lower p_{max} in compare to the pure biodiesel.
2. Increasing of the hydrogen energy share in co-combustion of hydrogen with RME, HVO and their blends with petroleum diesel at all loads resulted the increase of indicated thermal efficiency and reduction of indicated specific fuel consumption.
3. In co-combustion of the hydrogen with RME, HVO and their blends with petroleum diesel, the increase in hydrogen energy share shortens both the initial (CA 0–10) and the main (CA 10–90) combustion phases.
4. The NO emission decreased due to the sluggish flame propagation rate when the hydrogen energy share was low but further increase of the hydrogen fraction NO increased. The CO and HC, on the contrary: increased with the low HES and decreased with further increase of the hydrogen energy share.
5. Smokiness was reduced by increased hydrogen energy share with all engine loads.

Approval of the Research Findings

11 scientific papers focused on the subject of the doctoral thesis have been published: 2 – in publications of the *Clarivate Analytics Web of Science* database with citation index; 1 – in *Conference Proceedings* publications of the *Clarivate Analytics Web of Science* database; 5 – in publications of other international database; 3 – in publications of other reviewable scientific publications.

The obtained experimental data was presented at the following scientific conferences:

- "44th International Scientific Congress on Powertrain and Transport Means European KONES 2018". Czestachwa – Wisla, Poland.
- "22nd International scientific conference Transport means 2018". Trakai, Lithuania.

- "3rd International Hydrogen Technologies Congress (IHTEC-2018)". Alanya/Antalya, Turkey.
- 9th International Conference of Hydrogen Production (ICH2P/ICRIC-2018)". Zagreb, Croatia.
- "SAE International. International Powertrains, Fuels & Lubricants Meeting 2018". Heidelberg, Germany.

Structure of the Dissertation

The dissertation consists of an introduction, three chapters, general conclusions, the list of references, the list of scientific publications by the author of the thesis and summary in Lithuanian.
The scope of thesis is 146 text pages, excluding annexes. In order to prepare the thesis, the author referenced 174 publications, other sources and included in the text 60 numbered formulas, 68 figures and 15 tables.

Acknowledgments

Author would like to acknowledge scientific supervisor Assoc. Prof. Dr Saugirdas Pukalskas for the guidance during PhD studies and for the support to complete this thesis. I am thankful to him for giving me the freedom to explore, for feedback when required, for his confidence in my work and for his openess.

Significant progress in understanding of hydrogen combustion was made during my Erasmus+ practice at Czestachowa University of Technology under supervision of Assoc. Prof. Dr Habil. Stanislaw Szwaja. I am indebted him for his guidance, inovative ideas, incontrovertible criticism and the invaluable time he bestowed me when I have performed the experiment and written this thesis. This thesis was partially realized within the project: "Dietary, Power and Economic Potential of Sida Hermaphrodita Cultivation on Fallow Land" (No. BIOSTRATEG1/270745/2/NCBR/2015) financed by the National Center for Research and Development of Poland.

I also take oportunity to express my gratitude to Assoc. Prof. Dr Fanhua Ma for providing the support during my one-year doctoral studies at Tsinghua University in Beijing. I am thankful for the discussions, sharing of ideas and wide brain storms in the "HCNG Reasearch Group" guided by Prof. F. Ma. In this group doctoral students from the whole World were involved in the inter-continental China–EU projects of the "Belt and Road Initiative", financed by China.

I would like to thank all my teachers, colleagues, dedicated staff members and assitants at Vilnius Gediminas Technical University, Tsinghua University, Czenstachwa University of Technology for providing the best possible support. Their suggestions, comments, helpful discussions and support in many aspects helped me to achieve the goal. My sincere thanks to Dr Alfredas Rimkus, Paulius Stravinskas, Dr Michał Gruca, Dr Michał Pyrc, Dr Hao Duan, Dr Roopesh Kumar Mehra. I express my acknowledgement and gratitude to Dr Vilius Bartulis, Assoc. Prof. Dr Edgar Sokolovskij, Prof. Dr Gvidonas Labeckas, Prof. Dr Vytautas Bučinskas for incentive during my PhD studies, and my former teachers Prof. Dr Habil. Alvydas Pikūnas (1949–2019), Prof. Dr Habil. Renius Žeromaskas (1937–2011), Dr Leonas Gastila (1918–2011) for encouragment before doctoral studies.

I am thankful to our Lord Jesus for giving me the belief in my capabilities, trustworthiness to others, for His care in my daily life.

Finally, I express my sincere thank to my wife Jolita and my son Dominykas for understang, patience and continued moral support during entire period of my doctoral studies. I also express gratitude to my cousins who passed away: Dr Habil. Kostantas Kazakevičius (1942–1997) and Prof. Dr Habil. Juozas Jakimavčius (1943–2000). Several times they invited me to the World of research and science, however it takes me a long time to make the decision.

1

Features, Application, Relevance of Biodiesel and Hydrogen in Diesel Engines

This Chapter reviews the features, relevance, and perspectives of hydroegen and various renewable fuels, such as biofuels. Properties and features of hydrogen, different biofuels and their mixtures with petroleum diesel are analysed and presented in compare to the sole petroleum diesel fuel. This Chapter concludes in formulating of main objective and tasks of present investigation. According to the chapter's theme, several publications were published in following scientific publications: Juknelevičius *et al.* (2019); Juknelevičius (2018); Rimkus *et al.* (2018a); Mehra *et al.* (2018); Mehra *et al.* (2017); Juknelevičius *et al.* (2018a); Juknelevičius *et al.* (2018b); Juknelevičius *et al.* (2018c); Juknelevičius *et al.* (2018d); Rimkus *et al.* (2015).

1.1. Biomass Based Biofuel

Today of biomass produced biofuels are first, second and third-generation. Their use may diminish the emissions levels, as the lower C/H ratio of biofuels causes the reduction of CO_2 emission. Most biofuels today produced from commonly available, edible feedstock and classified as first-generation. They can offer some CO_2 benefits and can help improve domestic energy security (Silvestrini *et al.* 2010, Raslavičius *et al.* 2014). Biofuels produced from second-generation biomass does not compete with food production; however high raw material costs are still an issue in making it processes economically attractive (Hilbers *et al.* 2015). Another problem related to the production of biofuels is the ratio between the price of energy produced and its production costs (Murphy *et al.* 2010). This ratio should be no more than 3:1 to cover the cost of infrastructure and transportation, and now this ratio is only 1.3:1 (Hilbers *et al.* 2015).

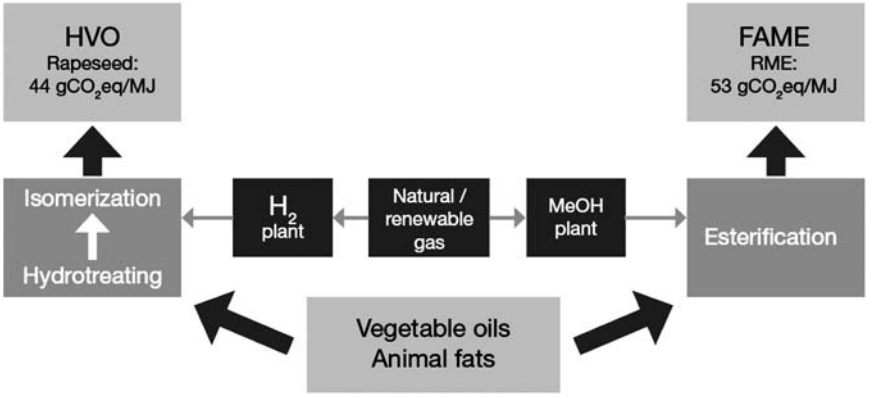

Fig. 1.1. The transesterification and hydrotreating processes with inputs and outputs for HVO and FAME production with default well-to-tank GHG values (Engman *et al.* 2016)

The main feedstocks of biofuels are vegetable oils and animal fats containing fatty acids. Vegetable oils comprise of a mixture of triglycerides. While esters of glycerol and unsaturated fatty acids are components of the triglycerides. During the esterification of triglycerides with catalyst (methanol) a mixture of fatty acid methyl esters (FAME) and glycerol are extracted. The glycerol is also considered as engine fuel (Grab-Rogalinski *et al.* 2016). Usually FAME is referred as the conventional biodiesel, while hydrotreated biodiesel is the fuel produced in a an alternative way to the esterification of triglycerides. During the

hydro treating process of triglycerides, the HVO produced of the same triglyceride feedstock, which can be used to produce FAME or Rapeseed Methyl Ester as well (Fig. 1.1). However, FAME and HVO are the different products, with different chemical structure and physical properties.

FAME can be produced of any vegetable oils or other oils and fats consisting largely of triglyceride. The most common first generation FAME sources in the past and up to the present are:

- rapeseed (*Brassica napus*) oil (RME);
- palm (*Elaeis guineensis*, *Elaeis oleifera*) oil;
- coconut (*Cocos nucifera*) oil;
- soybean (*Glycine max*) oil;
- sunflower (*Helianthus annuus*) oil;
- peanut oil and corn oil.

Experiments performed with RME and it blends with petroleum diesel revealed that the blend of RME up to 30 wt% with petroleum diesel is possible. However, the EN 590 standard limits blending of petroleum diesel with up to 7 vol% of RME, due to some biofuel properties to be discussed further. In this diserattion author used blend of petroleum diesel with 7 vol% of RME and marked it as RME7.

Finish scientists together with Neste Oil Corporation developed the HVO technology and named it NExBTL (an acronym for “next generation biomass-to-liquid”). The NExBTL is renewable diesel produced from second-generation feeedstock‘s: palm, soybean, rapeseed oils. The fat fractions of the waste of food, fish and slaughterhouse industries are suitable raw material for the renewable diesel as well (Engman *et al.* 2016).

1.1.1. Biodiesel

The physical and chemical properties of biodiesel are dependant substantially on feedstock and composition of FA. The main issue to ensure the quality of the biodiesel is the limitation of undesirable components that can negatively influence fuel properties and performance. These undesirable components are formed during the transesterification reaction such as glycerol. Others can be caused by residual catalyst or carried from the feedstocks such as trace elements (Na, K, S, P, Ca and Mg). These elements are limited by biodiesel standard EN 14214. Biodiesel should be as free of free fatty acid as possible, because FFA may cause corrosion and have elevated melting points (Knothe *et al.* 2005). The composition including major FA and fuel-related properties of the biodiesel along with standard of biofuels – EN 14214:2008 presented at the Table 1.1.

The biodiesel contains considerable oxygen content (10–11%) which results in about a 12% lower mass heating value. However, due to higher density by 6%,

and lower mass stoichiometric AFR its energy content of the stoichiometric mixture is about 1.8% higher than ULSD. The different FAME have different LHV. For example, the LHV of palm biodiesel is 36.5–36.9 MJ/kg; Jatropha is 39.2 MJ/kg, Pongamia oil is 43.4 MJ/kg. The majority of researchers reported that FAME from different sources has lower calorific value than the ULSD.

Table 1.1. Biodiesel's composition and main properties (Knothe *et al.* 2005; Hoekman *et al.* 2012; Piaszyk 2012; Mahmadul *et al.* 2017)

Properties / features	EN 14214:2008	Palm oil	Soybean oil	Rapeseed oil	Beef tallow	Jatropha oil	Pongamia or Karanja oil
		Biodiesel from edible oil sources			Biodiesel from non-edible oil sources		
Palmitic FA $C_{16}H_{32}O_2$, 16:0, %	–	39.3–45.7	9.6–13.6	4.2	24.5–27.1	12.8–17	3.7–9.8
Stearic FA $C_{18}H_{36}O_2$, 18:0, %	–	4.2	2.4–6.0	1.6	13.7–22.7	6.1	2.4–8.9
Oleic FA $C_{18}H_{34}O_2$, 18:1, %	–	38.4–44.2	21.3–26.1	51.7–67.3	38.1–46.3	33.7–47.1	44.5–72.2
Linoleic FA $C_{18}H_{32}O_2$, 18:2, %	–	7.7–11.3	49–57.1	18.7–24.3	4.4	30.1–42.3	10.8–18.3
Density, kg/m³ at 15°C and 1.01 bar	860–900	864.4	913.8	882	877	879.5	931
Kinematic viscosity, mm²/s at 40 °C	3.5–5.0	4.50	4.04	4.44	4.82	4.80	6.13
Cetane number	Min. 51	54.6	51.5	54.4	58.8	51.6	55
Lower heating value, MJ/kg	Min. 35	36.5–36.9	37.3	36.8–37.4	36.5–39.8	39.2	43.4
Flash point, °C	Min. 120	135	76	170	150	135	95
Pour point, °C	Max. 0	15	2	−12	9	2	3
Cloud point, °C	–	16	9	−3.3	12	2.7	7
Iodine number, g I_2/100 g	Max. 120	54	128–143	111	35–48	104	86.5–91

The molar mass of biodiesel (294.5–318.5 g/mol) is higher than petroleum ULSD (142.3–212.4 g/mol), which is reflected in slightly higher distillation temperatures. While density can vary from 807.3 kg/m^3 for coconut oil to 931 kg/m^3

for Pongamia FAME (Mahmadul *et al.* 2017). The density of the FAME measured using ASTM standard D1298 and EN ISO 1676 methods (Ashraful *et al.* 2014). The mass flow rate of the fuel depends on it density and thus influence the efficiency of fuel injection and combustion quality (Chauhan *et al.* 2010; Chauhan *et al.* 2012). The efficiency of the fuel injection is related to the atomization of the fuel. A fuel with lower density is characterized by better atomization, therefore the density affects the engine performance due to the different mass of injected fuel (Bahadur *et al.* 1995). The density of the fuel is related to the engine emissions and the high density of the fuel causes high emissions of the PM and NO_x (Ali *et al.* 1995; Szybist *et al.* 2007).

The density is related to the viscosity and cetane number of the fuel (Rahman *et al.* 2017; Atabani *et al.* 2014). High kinematic viscosity of fatty compounds is a major reason why neat vegetable oils are abandoned as alternative ULSD. The chain length of carbon atoms and number of double bonds affects the kinematic viscosity of each fatty acid alkyl esters. Viscosity increases with increase of the chain length and with rise of saturation (Knothe *et al.* 2016). The palm oil with 39.3–45.7% of saturated palmitic FA has higher viscosity (4.50 mm^2/s) in compare with soyabean oil (4.04 mm^2/s) conatining 49–57.1% of unsaturated linoleic FA.

The viscosity strongly influences the atomization and spray characteristics of a fuel injection and affects the possible formation of engine deposits (Mofijur *et al.* 2013). The incomplete combustion and difficulties related to the cold weather conditions, are caused by the increase of viscosity due to decrease of temperature. (Alptekin *et al.* 2009; Ghazali *et al.* 2015). Higher viscosity of the biodiesel results in a larger fuel droplet at injection, which further worsen the combustion quality and release the higher exhaust emission. The large molecular mass and large chemical structure are the main features influencing the fact that the kinematic viscosity of the biodiesel is higher than ULSD (Liaquat *at al.* 2012; Liaquat *at al.* 2013; McCarthy *el al.* 2011; Meng *et al.* 2008; Misra *et al.* 2011; Atabani *et al.* 2012; Bhuiya *et al.* 2016).

The two reference compounds on the cetane scale show that the CN decreases with decreasing the length of the chain and with increasing of the branching. Aromatic compounds, which are dominant in ULSD, have low CN. The higher value of CN provides the benefits, regarding engine performance and emissions while biodiesel used (Knothe *et al.* 2003). CN is an important indicator of ULSD quality as it relates to the ignition behavior: the higher the CN, the shorter the ignition delay time. The fuel having lower CN takes the time to start the combustion and causes higher HC and PM emissions. Thus, in general the shorter ignition delay time is desirable. FAME fuels with high amounts of saturates have a higher CN; while the FAME with high amounts of unsaturated have a low CN. Some FAME fuel has CN higher than that of petroleum diesel; beef tallow biodiesel CN = 58.8; some FAME fuels has lower than petroleum diesel; Jatropha

CN = 51 (Mofijur *et al.* 2014; Mofijur *et al.* 2015). However, HVO has much higher CN than FAME and petroleum diesel.

Flash point is the lowest temperature at which the fuel vaporation is sufficient to produce an inflammable mixture of the fuel vapor and air above the fuel surface when the fuel is heated under STP. The FAME fuels in general have a higher flash point than ULSD which means that biodiesel is safer for transportation and storage purpose (Atadashi *et al.* 2010; Jain *et al.* 2010; Dwivedi *et al.* 2014). Biodiesel flash point may be influenced by the chemical properties of the biodiesel such as the total number of carbon atoms and the number of double bonds (Mahmadul *et al.* 2017). According to EN 14214 standard limit flash point of biodiesel is 120 °C. Few of them (such as soyabean biodiesel, Pongamia biodiesel) has lower than the limit prescribed by standard.

Cloud and pour point are fuel features aiming to evaluate fuel performance at low ambient temperatures. This done by cooling the fuel up to the limit where the fuel can still flow, but immediately turns into a wax crystal (Kinast 2003).

The pour point and the cloud point are the crucial parameters of biodiesel, at the cold weather conditions. The high amount of fatty acid resulted in higher cloud and pour point of biodiesel than ULSD. Transesterification does not modify the FA composition, therefore biodiesel produced from feedstocks containing higher fractions of particularly saturated and long-chain fatty acid tends to have relatively low cold flow properties. Due to its content of saturated compounds, beef tallow methyl ester has CP = 12 °C (Tab. 1.2), palm oil methyl ester CP = 16 °C. In contrast, feedstocks with relatively low fractions of saturated long-chain fatty acid yield biodiesel with much lower CP and PP. Thus, feedstocks such RME CP = −3.3 °C, Jatropha biodiesel CP = 2.7 °C. Typical way to solve that problem at the low temperature to blend biodiesel with ULSD.

Iodine value (IV) is the measure to determine the unsaturation of FA in the way of measuring the amount of I_2 that reacts by addition to carbon–carbon double bonds (Hoekman *et al.* 2012). The IV is measured in a 100 g iodine sample that can be added to double bonds of any fatty acid or oil chain. EN 14214 has a max. specification of 120 mg I_2/100 g FAME. Coconut-derived biodiesel was found by several authors with the lowest iodine value of 18.5 due to its high saturation, while beef tallow biodiesel has 35–48. Hoekman *et al.* (2012) reported that *Camelina sativa* has the highest iodine number of 152.8, followed by safflower biodiesel – 141, while soyabean biodiesel has 128–143 according to review of Mahmadul *et al.* (2017). Moreover, the authors found that RME iodine value of 111, is just under the max. value of EN 14214.

The major benefits of FAME fuel is easier production, more cost efficient and less time consuming than ULSD. FAME can reduce the need for maintenance. It stimulates sustainable rural development, because it produced locally, does not need to be drilled, transported, or refined. It is safe to handle, more biodegradable, and reduces some tailpipe emissions.

FAME has some disadvantages as it emits higher NO_x emission than petroleum diesel. Because of higher cloud point, FAME freezing in cold weather, causing a cold weather starting. Large molecular mass and chemical structure of FAME leads to a problem in pumping, combustion, and atomization of the injection system of a CI engine. FAME fuel decrease the power by 5% compared to that of petroleum diesel. During the long-term operation, the formation of injector deposits, plugging of filters, lines and injectors occurs because of the high viscosity (Atadashhi *et al.* 2010; Demirbas 2008).

1.1.2. Hydrotreated Biodiesel

HVO is the hydrotreated biodiesel with lower density than that of ULSD and biodiesel (FAME). The HVO fuel is a low aromatic, fully paraffinic, light fraction hydrocarbon, and contains no sulphur and oxygen. The properties of HVO are similar to that of GTL and BTL diesel fuels produced by Fischer-Tropsch synthesis (Aatola *et al.* 2008) from natural gas and biomass (Table 1.2).

Table 1.2. The main properties of GTL diesel, BTL diesel, HVO and ULSD (Aatola *et al.* 2008; Gill *et al.* 2011; Sajjad *et al.* 2014; Labeckas *et al.* 2014; Engman *et al.* 2016)

Properties	EN 590 EN 12916	GTL diesel (FTS)	BTL diesel (FTS)	HVO	ULSD
Composition, % (wt)	–	84.9–85.4, 13.99–15.1	85.79, 12.54	84.5–85 C, 15–15.5 H	84–87 C, 13–16 H
Density, kg/m³ at 15 °C and 1.01 bar	820–845	768–785	761.2	779.7	830.5
Lower heating value, MJ/kg	–	34.5–49.3	44.58	44.04	42.95
Auto-ignition temp. at STP, °C	–	220	–	~ 210	250
Kinematic viscosity, mm²/s at 40 °C	2.0–4.5	4.441	1.550	2.867	2.070
Lubricity HFRR, corrected wear scar diameter 1.4, μm at 60 °C	Max. 460	355–570	–	351	360–590
Flash point, °C	Min. 55	63–99	55 <	61	56
Pour point, °C	–	–27–(–2.5)	–20.5	–	–35–(–32)
Cloud point, °C	Max. –34	–17–3	–15.5	–34–(–5)	–22
Iodine number, g I_2/100 g	–	1.22	–	–	6
Total aromatics, % (wt)	7–42	2.3–3.0	3.2	0.3	24
C/H ratio (wt)	–	5.67	6.84	5.60	6.90
Cetane number (CN)	Min. 51	75	80	75–99	51.5

The feedstock composition has influence on properties of the HVO produced. For instance, the presence of unsaturated fatty acids are the cause of oxidation stability concerns, while the presence of saturated ones is the cause of cold flow problems (Zaccheria *et al.* 2009). Feedstocks of the HVO and FAME contain the same major unsaturated acids: oleic acid (18:1), linoleic acid (18:2) and linolenic acid (18:3). The degree of unsaturation of fatty acids expressed by the iodine value, i.e. the amount of iodine that have reacted with 100 g of product. The lower the index, the greater the degree of saturation. Hydrogenation leads to increase of the saturation, CN and oxidative stability. That cause the lower iodine value of HVO in compare to FAME (Table 1.1).

Fuel distributors more readily accept the hydrotreated biodiesel than transesterified biodiesels, because paraffinic fuels have better stability during the storage (Kuronen *et al.* 2007). This feature enables the logistic and transportation of HVO, GTL and BTL diesels using the same current distribution network. With respect to the lifecycle environmental impact the HVO outperforms transesterified FAME biodiesels and FTS BTL when fuels are produced from the same feedstock. (Sunde *et al.* 2011).

HVO meets EN 15940:2016 requirements for paraffinic ULSD. This standard covers also synthetic FTS products GTL, BTL and CTL. The common FAME specification prescribed by the EN 14214:2008 is not valid for HVO since it consists of hydrocarbons only. The low density of the HVO – 779.7 kg/m^3 is the reason why HVO does not meet the EN 590:2013 specification of the lower density limit – 820 kg/m^3 (Standard EN 590). For that reason, up to 30% (wt) HVO can be blended with ULSD to meet the EN 590 specification. However, due to blending the cold flow properties became worse and flow improvers such as Keroflux 3566 and Infineum R288 are used (Simacek *et al.* 2010).

The other ways for upgrading of cold flow properties of HVO reported in the reserch papers are based on the hydrogenation technology. Isomerization and reaction temperature control are addition ways on top of flow improvers (No 2014). The low-temperature properties of HVO can be upgraded by subsequent catalytic isomerization of *n*-paraffins (Simacek *et al.* 2011). The Pt/ZSM-22, Pt/ZSM-23, Pt/SAPO-11, Pt/SAPO-41 catalysts were found to be very effective for the isomerization of HVO according to Hanscok *et al.* (2007). While the original CFPP of sunflower HVO was +23 °C, they obtained the CFPP ranges from –18 to –14 °C. That was the result of isomerization of the sunflower HVO with Pt anchored to zeolite HZSM 22 at temperatures of 280–370 °C, under the pressure of 3.5–8 MPa.

Simacek *et al.* (2011) carried ot the study, of the physico-chemical properties of sunflower HVO at 360–420 °C and 18 MPa to investigate the effect of hydrogenetion temperature on the cold flow properties of neat HVO and blends with ULSD. They found that properties were very close to those of a ULSD when

reaction temperature was 420 °C. The low-temperature properties were improved without any separate isomerization process than temperature.

The volumetric heating value of HVO is lower than that of ULSD, because of the lower density by 6%. Therefore, a larger volume of HVO is required in order to achieve a given *BMEP*. Thus, the volumetric fuel consumption increases compared to ULSD. However, as the density of HVO is lower than that of ULSD, the weight based fuel consumption actually decreases with HVO. However, the wheight heating value of HVO is 44.04 MJ/kg that is higher in compare to the ULSD, because of the fact that C/H ratio of HVO is lower (5.60) in compare to 6.90 of standard ULSD.

The other most dramatic difference between ULSD and HVO is the cetane number. The CN of HVO and FTS diesels (GTL and BTL) are much higher (more than 75) in compare to ULSD (min. 51 required by the standatd EN 590:2013), because of its nature as a mixture of *n*-paraffins (alkanes) and *i*-paraffins (Engman *et al.* 2016). Most of *n*-paraffins contain 70–90% of *n*-heptadecane and *n*-octadecane and assists to reach high CN. However, they mostly influence the poor low-temperature properties and thus prevent their use as a DF blending component in concentrations higher than 5–10% (No 2014).

High CN is the advantage for NO_x emissions and the lower carbon content of this fuel (5.60), make the combustion less susceptible for soot formation. More specifically, as the CN is a measure of the ignition delay of the fuel (Heywood 1988), due to the high CN of HVO the shorter is the ignition delay than other reference fuels. Moreover, the auto-ignition temperature of HVO is lower than ULSD and that leads to further shortening of of the ignition delay.

Sole HVO, in general, has low lubricity due to the absence of sulphur and oxygen compounds (Lapuerta *et al.* 2011). However, similar doses of additives that used to improve the lubricity of ULSD can be used to improve the lubricity of HVO fuel also (Kuronen *et al.* 2007).

1.2. Features of Hydrogen as Fuel of Internal Combustion Engine

Early in the 20th century, hydrogen has been recognized as a fuel having some highly desirable properties, for application it as a fuel in ICE. With development of automobile industry, it was recognized that due to special properties and safety concerns, the use of hydrogen as engine fuel needs more research on ICE. Hydrogen when combusted with only with oxygen produces only water but when combusted in air it produces water and oxides of nitrogen. These features make the hydrogen an attractive fuel to reduce the green house gas emissions and to meet the stringent environmental requirements. However, oxides of nitrogen are

the issue to be fixed. Properties of hydrogen generaly discussed in compare with methane by most authors (Saravanan *et al.* 2008; Verhelst *et al.* 2009; Fayaz *et al.* 2012; Karim 2007; Salvi *et al.* 2015). Comparative properties of hydrogen with methane are shown at the Table 1.3.

Hydrogen has some unique combustion properties, such as a wide flammability limit, low ignition energy, and very fast flame propagation rate, which ensures prompt ignition (Saravanan *et al.* 2007). On the contrary, low density and wide flammability limit of hydrogen imposes the safety and storage problems. The lower ratio of fuel weight to that of weight of the fuel storage system is one of the major challenges in the on-board hydrogen storage for vehicles (Salvi *et al.* 2015). At atmospheric conditions hydrogen must be stored as pressurized gas at 300–700 bar or as a liquid.

Table 1.3. Hydrogen and methane properties (Karim 2007; Verhelst *et al.* 2009; Szwaja 2010; Salvi *et al.* 2015)

Properties		Hydrogen	Methane
Physical properties	Chemical formula	H_2	CH_4
	Density, kg/m³ at NTP	0.0837	0.6512
	Molar mass, g/mol	2.016	16.043
	Boiling point, °C	–253	–161.5
Thermodynamic properties	Lower heating value, MJ/kg	120	50
	Lower heating value, MJ/Nm³	10.7	35.8
	Stoichiometric air-fuel ratio, kg/kg	34.2	17.1
	Stoichiometric air-fuel ratio, Nm³/Nm³	2.6	9.3
	Heating value of stoichiometric mixture, MJ/kg	3.40	2.75
	Heating value of stoichiometric mixture, MJ/Nm³	3.17	3.47
	Diffusion coefficient into air, cm²/s at NTP	0.61	0.189
	Thermal conductivity, mW/mK at STP	182	34
	Kinematic viscosity, mm²/s at 40°C	118	17.2
Combustion properties	Flammability limits, vol% at NTP	4–75	5.3–15.0
	Minimum ignition energy, mJ	0.02	0.28
	Laminar flame speed, m/s at NTP	2.65–3.25	0.38
	Auto-ignition temperature,°C	585	540
	Adiabatic flame temperature,°C	2045	1917
	Minimum quenching distance, mm at NTP	0.64	2.03
	Air–fuel equivalence ratio (λ)	0.14–10	0.6–2
	Fuel–air equivalence ratio (φ)	7.1–0.1	1.67–0.5

Gaseous hydrogen, with a density of 0.0837 kg/m³ consists 6.8% the density of air and 12.8% the density of methane. Hydrogen can be converted to the liquid below its boiling point of 20 K (–253 ºC), which is the second lowest boiling point of all substances, second only to the helium. Liquid hydrogen has density of 70.8 kg/m^3, which is 7% the density of water and occupies 848 times less volume than it does in its gaseous state. Even as a liquid, hydrogen is not very dense. One cubic meter of water (H_2O) contains 111 kg of H_2, while one cubic meter of liquid hydrogen contains only 71 kg of H_2. Water contains more mass of hydrogen than hydrogen itself, because of its tight molecular structure and intermolecular hydrogen bonds. The molecules of hydrogen gas are smaller than other gases, and it can diffuse through many materials. This property makes hydrogen more difficult to contain than other gases. Hydrogen leaks are dangerous in that they pose a risk of fire where they mix with air (Perry *et al.* 1997).

The LHV of hydrogen is 120 MJ/kg, more than twice higher than methane and 2.8 times higher than DF. The difference between the internal (DI mode) and external (PFI mode) mixture formation of hydrogen is significant, due to the low volumetric parameters of hydrogen, such as volumetric LHV (10.7 MJ/m^3), stoichiometric AFR on volume basis (2.6 Nm^3/ Nm^3), volumetric heating value of stoichiometric mixture (3.17 MJ/m^3). The LHV of hydrogen-air mixture with PFI compared with methane and other fossil fuels is lower. However, with DI mode, mixture LHV is much higher. Theoretical power density increase by 33% for hydrogen when switching from PFI to DI (Verhelst *et al.* 2009). CI engines with DI of hydrogen into combustion chamber has higher performance indicators, however such construction is technically more complex and needs special hydrogen injectors (Pischinger 2014).

The auto-ignition temperature of hydrogen is 585 °C is by 40 deg higher than methane and much higher in compare to the DF, therefore the compression ratio can be increased for the CI engine, but on other hand, the use of pure hydrogen in CI is hardly possible (Saravanan *et al.* 2008).

Szwaja (2010) emphasized that high auto-ignition temperature and octane number of hydrogen is an important factor of resistance to the knock occurrence. Moreover, the resistance to the knock occurance increase with decrease of hydrogen volume share of the mixture, enabled by the extremely lean air-fuel equivalence ratio of 10. Nevertheless, the fast combustion of hydrogen-air mixture results in unstable flame propagation accompanied with the pressure oscillations of high amplitude of 100 kPa. These high frequency oscilations are the reason of knock occurance.

The wide flammability limits of hydrogen-air mixture within a range of 4–75 vol%, allows a wide range of engine power output through changes in the mixture equivalence ratio. This feature allows run the engine with very lean operation (λ = 10) and the reduce NO_x emissions. The flammability limits widen

with increase of temperature (Fig. 1.2). According to the Schroeder *et al.* (2004), dependence of the LFL on temperature can be expressed by the formula:

$$LFL = LFL_0 \cdot (1 - K_L \cdot (T - T_0)). \tag{1.1}$$

Here: LFL_0 – LFL at 0ºC, K_L – dependence factor on temperature increase, $K_L = 0.000157\ K^{-1}$, T – designated temperature, $T_0 = 273.15$ ºC.

The lower flammability limit dropps to 2 vol% at 300 °C, however, with increase of pressure up to 5 MPa the LFL increase from 4% to 5.6% (Fig. 1.3). Further, with increase of pressure up to 15 MPa no changes has been noticed.

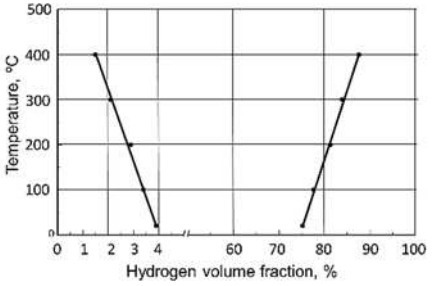

Fig. 1.2. Influence of temperature on LFL and UFL of air-hydrogen mixtures (Schroeder, Holtapels 2004)

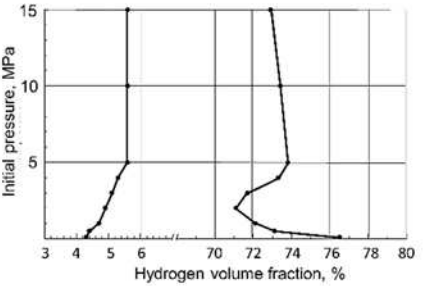

Fig. 1.3. Influence of pressure on LFL and UFL of air-hydrogen mixtures (Schroeder, Holtapels 2004)

For mixture as lean as 4 vol% hydrogen in air is still flammable, but burns incompletely. In the real situations, the lower flammabilty limit may be below or above 4 vol% depending on conditions. The exact value of the flammability limit is not well known today, however it is important for safety reasons. The broad ignition limits creates the higher risk of backfiring into intake manifold for PFI mode (Wierzba *et al.* 2001). Therefore it is recomended to equip the hydrogen fuelled CI engine with gas flash back arrestor for safety reasons. The total elimination of backfiring is possible with DI of hydrogen to the combustion chamber of CI engine. However due to the high diffusion coefficient of hydrogen into air, the homogenity of hydrogen-air mixture will be lost and increased the cyclic variations. Such case could lead to the combustion deterioration of hydrogen-air mixture and combustion when exhaust valve open (Szwaja 2010).

Verhelst *et al.* (2009) lists the properties of hydrogen–air mixtures, at stoichiometric ($\lambda = 1$) and at the lean operation ($\lambda = 4$), compared to the stoichiometric methane–air and iso-octane–air mixtures. Listed survey was done on the comprehensive analysis of the works of Glassman (1987), Molnarne *et al.* (2003)

and Perry *et al.* (1997). The laminar burning velocity of stoichiometric hydrogen–air mixture is in the range of 2.65–3.25 m/s at NTP. At the stoichiometric operation ($\lambda = 1$), high burning speed increases the efficiency of burning process, but at the same time it causes significantly higher wall-heat losses and also considerably higher material stresses as well as higher noise emission. However, at the lean-burn strategies with $\lambda = 2$, the burning velecity is 0.7–1.2, while with $\lambda = 4$, the burning velocity can be twenty times lower (Verhelst *et al.* 2009). For mixtures close to stoichiometry, due to the high burning velocity and high adiabatic flame temperature, significantly increase the NO_x emissions.

The minimum ignition energy of a hydrogen-air mixture is 0.02 mJ and contains 1/14 of the ignition energy required for a methane-air mixture according to the most articles. Detailed research on the ignition energy, provids that it depends on equivalence ratio and hydrogen volume concentration of the mixture. Ono *et al.* (2007) measured the minimum ignition energy using a capacitive spark discharge. It was only 0.017 mJ for hydrogen concentrations of 22–26% for a spark gap of 0.5 mm. Using a 2 mm gap, the minimum ignition energy was about 0.05 mJ and more or less constant for hydrogen volume concentrations between 10% and 50% ($\lambda = 0.42–3.77$). However it increased suddenlly when concentration of dropped below 10%.

The benefit of the low minimum ignition energy is ignition of the lean hydrogen-air mixture and prompt ignition. But low minimum ignition energy will increase possibility for hydrogen-air mixture in the combustion chamber to be ignited by any other source (Momirlan *et al.* 2005).

Hydrogen has remarkably high values of capability to disperse in air, such as kinematic viscosity, thermal conductivity and diffusion coefficient, in comparison to methane and DF. Such differences together with its extremely low density help to give hydrogen its unique diffusive and heat transfer characteristics (Karim 2007). The high diffusivity of hydrogen, when injected to a combustion chamber of CI engine decrease the heterogeneity of a diesel spray which makes the mixture better premixed with air and more homogeneous. The increased homogeneity of the mixture provides better conditions for the completeness of combustion. In addition, the homogeneity of the mixture leads to faster combustion and it becomes closer to constant volume causing an increase of the indicated thermal efficiency (Szwaja *et al.* 2009). However at the lean-burn strategies with $\lambda = 4$, diffusivity decrease by 36.2% and at the same worsen the homogetinty of the air-fuel mixture.

The quenching distance measures how close hydrogen flames can travel closer to the cylinder wall before they extinguish. The quenching distance for hydrogen is about 0.64 mm compare to methane which is 2.03 mm. The smaller the distance, more difficult to quench the flame and this will increase the tendency

for backfire. Experimentally quenching distance can be derived from the relation between minimum ignitions energy and the spark gap size (Fayaz *et al.* 2012).

1.3. Review of Research on Hydrogen and Diesel Fuel Use in Compression Ignition Engine

1.3.1. Hydrogen only operation

The idea to implement the hydrogen, as a clean, renewable and efficient fuel, for the operation of the R. Diesel designed engine was and still is under investigation. Homan *et al.* (1979) back in 1978, conducted CI engine with hydrogen gas only. Researchers soon realised that the operation range was very limited due to the high resistance of hydrogen to auto-ignition. The resistance of hydrogen to auto-ignition could not be resolved even at CR of 29:1. Later it was investigated the feasibility of the hydrogen fuelled CI engine with the assistance of a glow plug. The results revealed that glow plug ignition is the way to provide reliable ignition and smooth engine operation. The hydrogen ignition delay was very short and the *IMEP* were higher than the corresponding results obtained with DF. However, significant cycle-to-cycle variations in the ignition delay, associated with the large amplitude pressure oscillations (further investigated by Szwaja *et al.* 2009) observed. The NO_x concentrations measured in the exhaust gas were significantly higher (Dimitriou *et al.* 2017).

Ikegami *et al.* (1982) investigated the possibility of establishing a hydrogen fuelled CI engine using a swirl chamber. Researchers performed two different engine aspiration systems. One was dealing with the compression ignition on an air-aspirated engine system, and another with an engine operating with an argon-oxygen charge. It was suggested that both pilot injection and fuel leakage from the injector could aid ignition of the hydrogen fuel, bringing almost smooth operation. The result indicated that ignition and engine operation are satisfactory without any hot surface to assist ignition.

Fukuma *et al.* (1986) studied hydrogen DI where cylinder charge ignition was achieved by using a glow plug as a hot surface and one injector nozzle with only one hole. They identified a slow flame propagation through the heterogeneous mixture, and achieved better performance with an eight-hole nozzle injector.

Welch *et al.* (1990) conducted investigations of the DI hydrogen engine at a compression ratio of 17 with a hot surface assisting ignition. Results indicated that the hydrogen fueled CI engine can produce higher power than an ordinary diesel fueled CI engine with lower emissions than the same engine operated with DF. *ITE* for lower brake loads were above 50%. They also identified an exponential dependence between the rate of pressure rise and the engine load. This

increase can be explained by a higher temperature at the end of compression due to a larger mass of hot residual gases. Another positive feature is reduced NO_x emissions compared to the ordinary diesel engine (Antunes 2010).

The auto-ignition behaviour of sole hydrogen was also investigated by Naber *et al.* (1998) and Tsujimura *et al.* (2003). Naber and co-authors performed experiments in a constant volume combustion vessel under TDC diesel engine conditions. They changed the following parameters: the injection pressure, temperature of the injected fuel, the orifice diameter, the ambient gas pressure, temperature and composition. They revealed the same as did Tsujimura (2003) with relation to the Arrhenius correlation between temperature and ignition delay. However the influence of other parameters was not so important. During experiments with gas densities at the TDC diesel engine conditions, ignition delays of less than 1.0 ms were obtained for gas temperatures greater than 1120 K. They confirmed that in a diesel engine at reasonable TDC conditions the compression ignition of hydrogen is possible (Szwaja *et al.* 2009).

Tsujimura *et al.* (2003) assess the the auto-ignition of hydrogen jets in a constant volume vessel. Tsujimura focussed on the thermodynamic state of the ambient gas, which influenced the auto-ignition delay of hydrogen jets. He concluded that the temperature of ambient gas has an effect on the auto-ignition delay of the hydrogen jet. The auto-ignition delay was linearly dependant on the temperature in the Arrhenius coordinates when ambient gas temperatures were below 1100 K. For temperatures higher than 1100 K, the temperature dependence of the auto-ignition delay is weak, and the auto-ignition delay reaches a limited value.

Investigation results of Antunes *et al.* (2009) showed that the hydrogen DI in a CI engine gave a higher power to weight ratio when compared to conventional diesel fuelled CI operation, with the peak power being approximately 14% higher. The use of inlet air heating was required for the hydrogen fuelled engine to ensure satisfactory combustion, and a large increase in the peak in-cylinder pressure was observed. A significant efficiency advantage was found with the hydrogen fuelled CI engine achieving a *BTE* of approximately 42.8%, compared with 27.9% in the conventional DF mode. While the highest *BTE* of 48% was achieved with the hydrogen fulled HCCI mode.

The DI hydrogen fuelled CI engine can provide good speed and load control, however control of the in-cylinder gas pressure and pressure rise rates, and the consequent mechanical stress on the piston rings and piston crank mechanism are related to the reliability of the CI engine. Therefore number of HCCI engine research groups around the world have recognised the potential advantages of this mode of operation in terms of thermal efficiency and emissions. The main difficulty with HCCI operation is the engine controllability, and until now no commercial HCCI engine has been offered on the market (Antunes 2010).

A hydrogen HCCI engine operation based on the induction or injection of hydrogen during the intake stroke, after the exhaust valve closed and formation of the homogenious air-hydrogen charge thanks to the high diffusivity of the hydrogen. Hydrogen HCCI engines distinguishing with a feasibility of homogeneous and very lean combustion, giving reduced NO_x emissions and high *BTE* due to the fast combustion. However they have very complicated and limited controllability when load variations are present during operation.

A pure hydrogen fueled engine under the HCCI mode during investigation of Szwaja *et al.* (2009) performed unstable because of uncontrolled SOC and it occurs within the range of 15–6 CAD bTDC. It was assumed that hydrogen is probably ignited by several hot places of combustion chamber and the piston surface. Moreover, the SOC occurs too early to generate the maximum break torque, because due to the fast combustion, 50% MFB and in-cylinder peak pressure are located bTDC. Thus, both EGR and/or leaning of the air-hydrogen mixture could be applied to improve the engine work cycle. These measures are vital to reduce the knock effect as well, because the stoichiometric air-hydrogen mixture during combustion under the HCCI mode, generates high knock.

1.3.2. Co-Combustion of Hydrogen with Diesel Fuel

The use of sole hydrogen for combustion engines are hardly possible, but it co-combustion with DF makes it the subject of research interest. Moreover, it is widely known, that there is no single fuel solution for the future transport because the availability and cost of alternative fuels differ between the modes. Researchers found that during combustion of hydrogen with DF in the CI engine, it produces less CO, HC and sulfur oxides. However, addition of hydrogen leads to increase of combustion noise, which occurred due to the high speed of hydrogen combustion (Miyamoto *et al.* 2011). The sharp increase of temperature, resulting the rapid NO_x formation. Though Saravanan *et al.* (2008) noticed that with the supply of more than 30% HES, the NO_x concentration decreased. However, the *BTE* increased from 22.8% to 27.9% when CI engine was supplied with less than 30% HES.

During tests (Szwaja *et al.* 2009) carried out with a CI engine operated with hydrogen – DF mixture was noticed the shorter ignition lag and, in this way, decreased the rate of pressure rise. The entire combustion duration does not change significantly, with a HES of 5–15%. But with further increase of HES p_{max} increased and the HES of 17% provided favorable conditions for generating combustion knock.

Investigations of CI engine with addition of 0–20% (Sharma *et al.* 2018) and 0–40% HES (Zhou *et al.* 2014), revealed the decrease of peak in-cylinder pressure and peak heat release rate, associated with deterioration on *BTE* and

BSFC due to the low combustion efficiency of hydrogen. However, other experimental investigations (Zhou *et al.* 2016) revealed that the p_{max} and heat release rate increased at medium and high engine loads, as the pre-ignition occured at high engine load and engine speed.

The *BSFC* was reduced too with an increasing of HES (Deb *et al.* 2015) however noticed the improvement of the *BTE*. Conversely, it was also observed sharp increase in peak in-cylinder pressure p_{max} and the peak heat release rate values with the increasing hydrogen rate. Indicated specific CO, CO_2 and smoke emissions decrease (Syu-Ruei *et al.* 2015; Talibi *et al.* 2018; Koten 2018) with an increasing of HES.

Investigation of the low hydrogen fraction (Syu-Ruei *et al.* 2015; Koten 2018) effect on CI engine showed that *BSFC* decreased and *BTE* increased with an increased amount of hydrogen due to the higher flame speed of hydrogen and thus improved mixture formation. Nevertheless, the addition of hydrogen lowered NO_x emissions at the low load conditions, but increased at the high load, since the thermal NO_x dominated at the higher temperature (Sharma *et al.* 2018; Syu-Ruei *et al.* 2015; Koten 2018).

Decrease of NO_x emissions were noticed at all partial loads, but increase of 51.3% obtained at full load when Karagoz *et al.* (2015) examined the CI engine with addition of hydrogen together with intake air. While Dimitriou *et al.* (2018) noticed the increase of NO_x emission at medium load due to the high energy content of hydrogen fuel.

The combustion efficiency increased with hydrogen addition due to the excess air factor. If there is no proper excess air factor, NO_x emissions may decrease (White *et al.* 2006). As the hydrogen's flame speed is more than 10 times higher than DF, and lower heating value is 3 times higher than DF, therefore the presence of hydrogen causes the peak pressure rise, followed by the temperature rise and increase of NO_x emissions. Hydrogen diluting effect causes decrease of NO_x at partial loads but at full load condition, the peak temperature is outweighed and increase of NO_x emissions noticed.

Antunes *et al.* (2009) carried out tests with a CI engine operated with 20% of HES, shown that the NO_x emissions can decrease. The level of NO_x was approximately 20% lower than obtained under sole diesel operation. The concentration of NOx was low (200 ppm) at low loads, lean mixture and low in-cylinder temperatures, but with increase of the load NO_x increased. Although the peak pressure in-cylinder was higher in the hydrogen-fuelled mode due to the higher fuel burn rate and it do not have an adverse effect on NO_x formation. This suggests that the peak gas temperature was lower in the hydrogen-fuelled mode due to enhanced air-fuel mixture and it homogenity.

The addition of hydrogen in combination with various aftertreatment-emission control technologies are used for restriction of NO_x emissions as well.

Investigation (Resitoglu *et al.* 2017) of CI engine with SCR revealed that hydrogen is a promising reductant of NO_x when used in combination with SCR.

Results from experiments (Tsujimura *et al.* 2017) show that increase of hydrogen into the engine makes ignition delay shortened that also affects main combustion phase. The trend of exhaust opacity decreased steadily with increase of hydrogen. Amounts of hydrogen addition by energy share were limited to nearly 35% due to combustion knock occurring at nominal load. However, other experiment (Dimitriou *et al.* 2018) was performed with HES up to 98% at low load conditions, without any engine operation implications. This condition provided a simultaneous reduction of carbon and NO_x emission of over 90% while soot emissions were dropped by 85% compared to the conventional diesel-only operation.

These and other articles have shown that hydrogen addition has a positive effect on the CO, CO_2, smoke emissions but most of them pointed out the increase of NO_x emissions. However it's not easy to define the common opinion on influence of hydrogen fraction on performance parameters such as in-cylinder pressure, *BTE*, *BSFC*. The different experimental setup, hydrogen fractions, engine speeds and load range used during experiments makes it difficult to compare the results and conclusions.

1.4. Review of Research on Biodiesel and Hydrogen Use in Compression Ignition Engine

Many researchers to establish suitability and feasibility of biodiesel as an alternate fuel have evaluated performance and emission behaviour of the CI engines with various biodiesels. Currently, there are more than 350 oil-bearing crops identified as suitable for the production of biodiesel (Tamilselvan *et al.* 2017). Due to the various compositions of esters, physical and chemical properties of biodiesels, their suitability to qualify as alternate fuels for CI engines, need in critical analysis. Hence, it is indispensible to study the performance, combustion and emission characteristics of biodiesels for adopting them as alternate fuels for CI engines.

1.4.1. Biodiesel only operation

The results of the dynamometer and on road vehicle tests performed by Sugiyama *et al.* (2012) revealed that the high CN and low aromatics fraction of the HVO reduced HC and PM emissions, and is capable to improve *BSFC*. Lebedevas *et al.* (2013) revealed that the performance and emission indicators of the diesel engine running on blends of *Camelina sativa* biodiesel of 30 vol% with petrol

DF was negligible. However, the properties of fuel containing *Camelina sativa* biodiesel makes considerably worse than RME in the course of the storage.

Labeckas *et al.* (2014) conducted experimental study with CI engine with 5–15 vol% amount of ethanol blend with DF, and ethanol (15 vol%), DF (80 vol%), RME (5 vol%) blend (E15B). They revealed that the oxygen mass content of the mixture reflects changes of the auto-ignition delay time caused by the use of E15B blend more predictably than the CN does. The auto-ignition delay for mostly oxygenated blend E15B was 15.4% longer than DF (0.78 ms) and the *BSFC* was higher. The lower emissions of NO_x, CO, HC along with positive changes in exhaust opacities revealed an importance of the fuel oxygen bound.

Experimental research of Rimkus *et al.* (2015) at the average speed and various brake torque of CI engine, with ULSD and BTL (15%) blend indicated decrease of the *BSFC* on 2.6% and increase of efficiency on 2.0%. The CO_2 and HC were reduced, due to the lower carbon-hydrogen ratio and molecular chains of BTL. The lower aromatic hydrocarbons resulted a 16–18% reduction in smokiness. Furthermore this reduction was achieved because of the intense combustion in the range of main combustion phase (this phenomena reduced the HC concentrations as well). Moreover, the shorter auto-ignition delay due to the higher CN of the BTL and lower oxygen fraction caused the reduction of the ROHR by 12–20% in the initial combustion phase and a lower combustion temperature, which supports the reduction of NO_x by 9–12%.

Use of HRD by Singh *et al.* (2015) showed the reduction of PM, CO and HC emissions as well as *BSFC*, when compared to petrol DF. However, NO_x increased by 26%. The results performed by Ewphun *et al.* (2017) showed that increasing HVO fraction at the fuel content decreased the ignition delay, flame temperature, soot concentration and NO_x concentration. However, with decrease of the oxygen concentration by EGR, effected contrariwise. A combination of EGR with supercharger resulted in decreased flame temperature, ignition delay and soot concentration, compared to sole EGR conditions.

During the tests performed by Pirjola *et al.* (2017), the substitution of DF with HVO, the emissions of NO_x reduced by 20% and PM by 44%. Bhardwaj *et al.* (2015) noted that the HVO fuelling resulted in about 50% reduction in smoke emissions and 43% reduction in gravimetric PM flow. These and other studies (Aatola *et al.* 2008; Murtonen *et al.* 2009; Lehto *et al.* 2011; Imperato *et al.* 2011; Pflaum *et al.* 2010; Erkkila *et al.* 2011) conducted with the CI engines fueled with HVO showed that HVO reduce NO_x, soot emissions and deposit formation in the cylinder, therefore HVO has beneficial fuel for the CI engine.

1.4.2. Co-Combustion of Biodiesel with Hydrogen

Subsequent studies of the CI engine operated with hydrogen – biodiesel mixtures (Serin *et al.* 2018; Chaichan *et al.* 2018; Chelladorai *et al.* 2018; Tüccar *et al.* 2018; Jegadheesan *et al.* 2017; Rocha *et al.* 2017; Barrios *et al.* 2017; Aldhaidhawi *et al.* 2017; Baltacioglu *et al.* 2016; Zhou *et al.* 2014) show that emissions and performance parameters are dependent on injection timing of biodiesel, its duration, *BMEP*, MFB and engine speed. The hydrogen being no carbon fuel can reduce the CO and PM emissions, and provide high flame propagation, because of extremely low ignition energy so that provides higher brake thermal efficiencies.

Experiments carried out on the CI engine (Aldhaidhawi *et al.* 2017) with petrol DF blended with 20 vol% of RME and different HES of 0–5%, revealed the lower engine performance, efficiency, and emissions except the NO_x, which slightly increased. Addition of hydrogen to the fuel blend, the CO emissions, smoke, and total unburned hydrocarbon emissions (THC) decreased, while the NO_x kept the same increasing trend. The addition of hydrogen has not a significant effect on ignition delay.

During the investigation (Rocha *et al.* 2017) performed on a diesel – generator, hydrogen was supplied with HES of 5–24% to the diesel – biodiesel (7%) blend (B7). With increase of the HES, CO_2, CO and HC emissions decreased. But the emissions of nitrogen oxides increased due to the increase of the in-cylinder temperature. There was also noticed an increase of the peak pressure and heat release rate, since B7 ignition delay was reduced due to increase of the HES.

The petroleum DF tested with addition of 7% FAME on a CI engine with EGR (Barrios *et al.* 2017). No significant increase of NO_x was observed at each test conditions; however, HES of 25% caused a reduction of p_{max} and decrease by 22% of CO_2 emission at the lowest load and middle speed.

Lower torque and higher *BSFC* were measured when the CI engine was fuelled with petroleum diesel – tea seed oil (*Camellia oleifera*) biodiesel blends (10 vol% and 20 vol%) instead of neat petroleum diesel fuel (Serin *et al.* 2018). Hydrogen enrichment (5 l/min and 10 l/min) improved the torque and decreased the *BSFC* by 8,13% for both test fuels. Furthermore, hydrogen enrichment reduced CO and CO_2 emissions by 36,13% and 14,65% respectively. Increasing flow rate of hydrogen fuel from 5 l/min to 10 l/min further improved performance parameters and emissions except of increment of NO_x emissions up to 75.51%.

The CI engine performance tests of hydrogen addition to the blend of 20% pomegranate seed (*Punica granatum*) oil biodiesel with 80 vol% of petrol DF (B20) has positive effect on power output and BSCF (Tüccar *et al.* 2018). It has been found that the disadvantage caused by low CN of pomegranate seed oil biodiesel, can be eliminated by the addition of petrol DF. According to experimental

data, use of pomegranate seed oil biodiesel reduces CO emissions. However, use of pomegranate seed oil reduces engine power and increases the NO_x emissions.

The neat *Pongamia pinnata* biodiesel fueled CI engine with 10 l/min of hydrogen provided only 0.33% increase of *BTE* compared with petroleum diesel, and increase of 3.24% to neat *Pongamia pinnata* biodiesel at NL (80%) conditions (Jegadheesan *et al.* 2017). However, severe knocking observed if supply of hydrogen increased above 10 l/min. The emission of HC decreased by 13 ppm, CO decreased by 0.02 vol% and CO_2 decreased 3.8 vol% for *Pongamia pinnata* biodiesel with induction of hydrogen at 10 l/min to that of neat biodiesel at NL (80%) conditions. The performance parameters of *Pongamia pinnata* biodiesel supplied with 4 l/min of hydrogen induction is close to the neat biodiesel without much optimistic change. The increase of hydrogen addition to biodiesel, the overall performance increases, while emission were reduced with except of NO_x.

Chelladorai *et al.* (2018) investigated the effect of hydrogen addition to the CI engine fuelled with grapeseed oil. At full load, the max. *BTE* with petroleum diesel, petroleum diesel – grapeseed biodiesel blend and neat grapeseed biodiesel has increased from 32.34%, 30.28% and 25.94% to 36.04%, 33.97% and 30.95% for a HES of 14.46%, 14.1% and 12.8% respectively. Ignition delay period increased with hydrogen induction as a result of reduced oxygen concentration. This increase of ignition delay was from 9º CA to 13º CA for diesel, 6º CA to 10º CA for petroleum diesel – grapeseed biodiesel blend and 11º CA to 15º CA for neat grapeseed biodiesel for a HES of 14.46%, 14.1% and 12.8% respectively.

Chaichan (2018) examined the EGR of CI engine on emissions levels and performance supplied with neat sunflower oil (*Helianthus annuus*) biodiesel with hydrogen. 20 vol% of gaseous hydrogen was supplied to the air at the intake manifold. The hydrogen co-combustion with the sunflower biodiesel without EGR enhanced the *BTE* of CI engine by 12.9%, the PM level declined by 42%, while NO_x was 1211 ppm at the NL, in compare to the petroleum diesel operation. The utilization of free carbon fuel (hydrogen) decreases the particulate matter. The PM increased when EGR was employed though at lower levels than with pteroleum diesel operation. However, hydrogen combustion with sunflower biodiesel resulted in the formation of NO_x because of the high flame temperature. High amounts of EGR was helpful in diminishing NO_x levels, but decreases the performance level.

The high reactivity fuel – biodiesel or hydrotreated biodiesel (high cetane number) coupled with the low reactivity fuel – hydrogen (low cetane number), is well suited for the RCCI strategy. RCCI is a dual fuel combustion technology that uses in-cylinder fuel blending with at least two fuels of different reactivity. The process involved in RCCI includes the introduction of a low reactivity fuel (H_2) into the cylinder to create a homogeneous air-fuel mixture. The high reactivity biodiesel then injected directly into the combustion chamber (Reitz *et al.*

2015). The large difference of reactivity between the two fuels (biodiesel and H_2) can optimize the combustion phasing, duration and extend the operable load range while sustaining low exhaust opacity and high thermal efficiencies (Cardera *et al.* 2017).

1.5. Relevance and Perspective of Biodiesel and Hydrogen Use in Compression Ignition Engine

The EU road transport fleet consumed 195 314.81 million tons of ULSD and 88 325.16 million tons of petrol in 2010, with projections of 214 344.5 million tons of ULSD and 72 895.9 million tons of petrol in 2018 (Flach *et al.* 2017). This tendency generated by more than double increase of diesel penetration among new cars registrations. It was noticed in EU during the period of 1995–2010 increase of new diesel cars registrations from 23% to 51%, while the diesel cars in EU shared 35.5% in 2010 (Automobile industry pocket guide 2014). The increase trend of ULSD noticed in Lithuania as well. The whole fleet of Lithuanian road transport consumed 1.51 million tons of liquid fuel in 2010, including 1.01 million tons (67%) of ULSD. While in 2017, whole fleet of Lithuanioan transport consumed 1.828 million tons of liquid fuel, including 1.495 million tons (82%) of ULSD, including 0.058 million tons of biodiesel (Lithuanian Department of Statistics 2018). Diesel engines are widely used for all kinds of transport in Lithuania because of their high fuel efficiency, low fuel consumption and reasonable price. There has been a steady growth of ULSD consumption between 1995 and 2008, which has experienced a 210% increase, while the consumption of petrol decreased by 70% (Raslavičius *et al*. 2014).

Recently, scientists from the National Aeronautics and Space Administration (NASA) reported that CO_2 from human actions continues to increase above levels have not been seen in hundreds of thousands of years (Othman *et al.* 2017). Agreeing to this statement the International Energy Agency (IEA) informed that since the beginning of the Industrial Revolution in the middle of 19th century, human activities increased by 44% the atmospheric concentration of CO_2, from 280 ppm to 403 ppm in 2016. Increase have been also noticed as follows: in the levels of the CH_4: from 1570 ppb in 1980 to 1850 ppb in 2016 and the N_2O: from 300 ppb in 1980 to 330 ppb in 2016 (Bhardwaj *et al.* 2015). In terms of CO_2 equivalents, the atmosphere in 2016 contained 489 ppm, of which 403 is CO_2 alone and the rest comes from other gases.

To keep control of above-mentioned emissions and to satisfy the emission obligations require the research progress and development of engine technologies. The use of renewable fuels has the potential to reduce the emissions and,

thus mitigate the effects of the environmental crisis of climate change. Among the current renewable fuels are alternative biomass based biofuels.

The current alternative, first generation, biomass based biofuels are produced from commonly available, edible feedstock's using well-established conversion technologies (Hoekman *et al.* 2012; Raslavičius *et al.* 2014; Hilbers *et al.* 2015). The second-generation biomass based biofuels are not competitors of the food industry. The high price of feedstock materials are an issue in making biofuel economically attractive. The other issue associated with production of biofuels is the energy return on energy invested. This ratio should be at least 3:1 to cover for infrastructure and transportation, while now it is approximately 1.3:1 for biofuels (Hilbers *et al.* 2015).

The physical properties and the availability in the globe makes the hydrogen the other quite attractive alternative fuel for road transport. Verhelst *et al.* (2009) described the long-term scenario of hydrogen usage as an energy source including it qualitative and quantitative descriptions in order to implement the transition towards clean and sustainable energy. The authors demonstrated the importance of variety of hydrogen-based energy technologies, which enable the efficient and economical way to ensure energy needs. The most efficient way to use hydrogen is a fuel cell technology, which is twice as efficient as an IC engine. The hydrogen could be the clean fuel – energy carrier to supply the FC electric energy to the road transport. Fuel cells could replace CI engines in trains, ships, but the main problem is high cost of hydrogen and lack of refueling network (European Commission 2015).

Although the use of sole hydrogen for combustion engines are hardly possible, the co-combustion with various fuels including renewable fuels makes it the subject of research interest. Moreover, it is widely known, that there is no single fuel solution for the future transport because the availability and cost of alternative fuels differ between the modes.

The co-combustion of hydrogen and biodiesel as dual fuel in CI engines provides the higher thermal efficiency and reduces hydrocarbon emissions based on two factors. Hydrogen is carbon free fuel, and biodiesel provides the extra oxygen in the composition. The hydrogen – biodiesel mode CI engines has a potential for penetration of the hydrogen in the industry. The large scale engines such as co-generation power units and ships has considerable amount of wasted energy to recover and accumulate as hydrogen, which can be used to drive engines and comply with the environment requirements. The hydrogen – biodiesel mode operation can support projects where hydrogen is produced from renewable or waste heat recovery sources, with biodiesel used as pilot fuel with the remaining amount of the energy supplied by the hydrogen.

The design of biodiesel and hydrogen dual fuel homogeneous charge compression ignition (HCCI) engine and CI engine with direct injection of hydrogen

can be derived from existing engine models. However development in the control of the rate of pressure rise for both modes of operation and on the control of the ignition timing for the HCCI mode is required. High performance HCCI and DI biodiesel – hydrogen engines can be suitable for use in a wide range of applications: road, marine and rail applications, as well as stationary power generation systems (Antunes 2009).

Liquid hydrogen still it is the challenging potential for use in IC engines, however there are very little prospects for its wide application in the near future. Few main factors that are obstacles for use of liquid hydrogen are: the need in cryogenic technology for storage and very low density which represents approximately four times the volume of DF for the same energy (Karim 2007).

The conclusion of this relevance and perspective overview would be that the extraordinary physical properties of hydrogen make it use as much as promissing and questionable. The carefull and precise researches with possibly new approaches need to be developed and validated. The improvement of understanding of the hydrogen engine operation can contribute the achievment of the higher thermal efficiencies.

1.6. Conclusions of the 1st Chapter and Formulation of the Thesis Tasks

The overview of alternative fuels, its features, results of tests and papers of researchers guide to the following conclusions:

1. Governments of the Globe, EU authorities promote to use the alternative fuels in a transport sector. Biomass based fuels, such as FAME, HVO and gaseous fuel – hydrogen are suitable alternative and the research and development of these fuels are motivated in the whole world.
2. Hydrogen has potential in co-combustion with biomass based fuels in CI engines because of its physical and chemical properties. Hydrogen can improve the combustion process of CI engine. However, various amounts of hydrogen fraction can influence and change efficiency and ecological parameters in different ways.
3. The only hydrogen fuelled CI engine can provide good speed and load control, however control of the in-cylinder gas pressure and pressure rise rates, and the consequent mechanical stress on engine parts are related to the reliability of the CI engine.
4. The hydrogen HCCI engine operation with the port injection of hydrogen distinguishing with a feasibility of homogeneous and very lean combus-

tion, giving reduced NO_x emissions and high *BTE* due to the fast combustion. However, the main difficulty with HCCI operation is the engine controllability when load variations are present during the operation.

5. High reactivity fuel – biodiesel (high cetane number) coupled with the low reactivity fuel – hydrogen (low cetane number), is well suited for the reactivity controlled compression ignition (RCCI) strategy.
6. Co-combustion of hydrogen with ULSD in CI engine produce less emissions except increase of NO_x as the result of sharp temperature-rise. The increase of in-cylinder pressure p_{max} and the peak of heat release rate was observed with the increase of hydrogen fraction leading to the improved *BTE* decrease of the *BSFC*.
7. The studies conducted with the CI engines fueled with hydrotreated biodiesel, revealed that biodiesel reduces the NO_x, soot emissions and deposit formation in the cylinder, therefore it has to be beneficial fuel for the CI engine.
8. The co-combustion of hydrogen and biodiesel as dual fuel in CI engines provides the higher thermal efficiency and reduces hydrocarbon emission as hydrogen is carbon free fuel. Unfortunately, the release of high temperature causes higher concentrations of NO.

According to the conclusions of the first chapter, the tasks of the thesis are as follows:

1. To evaluate features of the various biofuels and fuel mixtures to develop the experimental and numerical investigation methodology of the compression ignition engine.
2. To examine the effect of the hydrogen fraction in co-combustion with RME and HVO and it mixtures with petroleum diesel on the maximum in-cylinder pressure, combustion duration of CA 0–10, CA 10–90, start of combustion, the auto-ignition delay period and ROHR.
3. To determine the influence of the hydrogen energy share on the CO, CO_2, NO, HC emissions and exhaust opacity parameters.
4. To determine the HES at various engine loads when phenomena of abnormal combustion appears.

2

Methodology of Research on Hydrogen Co-Combustion with Biodiesel

The experimental tests and numerical simulation research methodology was chosen and adopted, according to the tasks of the thesis. The methodology used during tests were presented in several international scientific conferences and published in scientific journals: Juknelevičius (2018); Rimkus *et al.* (2018a); Juknelevičius *et al.* (2018a); Juknelevičius *et al.* (2018b); Juknelevičius *et al.* (2018c).

The object of the research is the co-combustion of hydrogen with biomass-based biofuels in the compression ignition engine to determine the influence of the hydrogen energy share on the performance and emission parameters. The compression ignition engine with dual fuel mode (gaseous – hydrogen, liquid – biofiel), makes the fuel supply system more complicated in compare to the sole fuel application. It gets more complicated when operating with four cylinder engine, as the modifications required for specific needs of experiment must be done for four injectors, sensors etc. The single cylinder engine was choosen as simple, easy to maintain and less expensive for experiment.

The supply system of liquid fuel was adopted in order to adjust the amount of injected liquid fuel, as the hydrogen energy share was set by volumetric amount. The adjustment of the amount of injected fuel has been managed by the

electronicaly controlled unit. The unit enables the adjustment of the duration of the injection time in μs in order to obtain required amount of injected fuel. The supply chain of the hydrogen installed to the existing compression ignition engine contains the connection tube with the valve installed to the intake manifold.

The experimental setup, hydrogen and liquid fuel measuring, hydrogen energy share calculation methods, measuring equipment are presented more detailed in the following chapters.

Experiments were carried out during 2017–2018 at the Institute of Thermal Machinery of Czestochowa University of Technology. The research group of the University was funded by the National Center for Research and Development of Poland within the project "Dietary, Power and Economic Potential of Sida Hermaphrodita Cultivation on Fallow Land", project code BIOSTRATEG1/270745/2/NCBR/2015.

2.1. Set-up of Experimental Engine

The single-cylinder stationary compression ignition engine Andoria S320 (Fig. 2.1) was equipped with common rail three-piston radial-high pressure pump Bosch CR/CP1S3 driven by 2.2 kW electric motor GL-90L2-4. The other CELMA Type 2Sf200 L6/4A electric motor used as the starter-generator for CI engine. After CI engine starts to run, it delivers energy by two driving V-belts to electric motor, now performing as generator. The CI engine was set to operate at the constant speed of 965 rpm ± 0.85%. The generated electric power was supplied to the power grid chain and can be measured. The technical specifications of the CI test engine given at the Table 2.1.

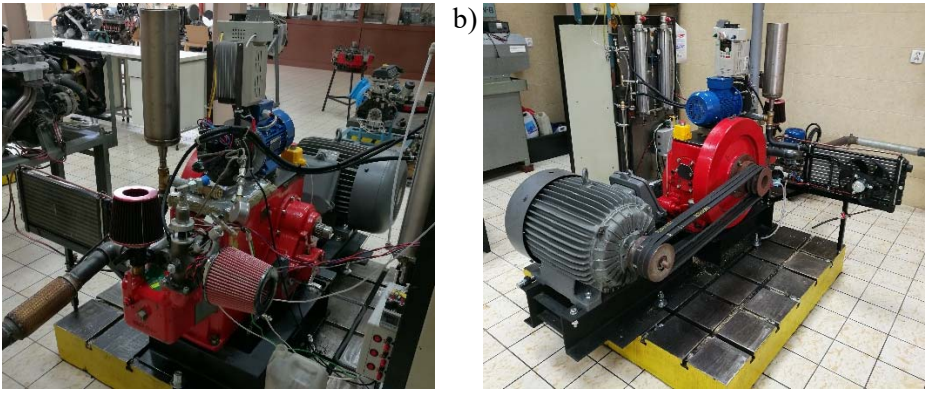

Fig. 2.1. Andoria S320 experimental engine with CELMA Type 2Sf200 L6/4A electric starter-generator: a) CI engine; b) electric starter-generator

Table 2.1. Technical specifications of the test engine Andoria S320

Parameter	Value
Number of cylinders	1
Bore diameter, mm	120
Piston stroke, mm	160
Displacement, cm^3	1810
Compression ratio	17
Rated power, kW/HP	13.2/18
Rated speed, rpm	1500
Peak torque, Nm	84.4
Peak torque speed, rpm	1200
Length of connecting road, mm	275
Intake valve opening	23° bTDC
Intake valve closing	40° aBDC
Exhaust valve opening	46° bBDC
Exhaust valve closing	17° aTDC

Each experiment conducted at the various *IMEP*. The *IMEP* managed by changing the liquid (biodiesel) and gaseous fuel (H_2) supply to the combustion chamber. The low reactivity fuel – hydrogen supplied by the plastic connection tube through the valve installed to the intake manifold. In the intake manifold, the hydrogen mixed with air supplied after pass through the air filter. Thus the homogeneous air – hydrogen mixture get into the combustion chamber of the engine. In the combustion chamber the homogeneous air – hydrogen mixture under the elevated heat and pressure ignited by injected liquid fuel.

The consumption of liquid fuel measured by stopwatch. The liquid biodiesel consumption was measured by stopwatch of the consumption of 9.62 cm^3 or 41 cm^3 of the liquid fuel measured by flow meter (pos. no. 4). The accuracy of the fuel consumption measurement was 0.5%.

Hydrogen was supplied into the engine intake manifold out of the ballon of 165 bar with a two-stage pressure regulator (pos. no. 9) to reduce its pressure to 1 bar, which was the pressure of the hydrogen gas supply line. Hydrogen consumption was measured using the gas meter COMMON CGR-01 (pos. no. 10) which measures volumetric values. The measuring range of gas meter 0.16–650 m^3/h, with accurancy of <± 2% in the auxiliary range, while < ±2% in the basic range in accordance with the requirements of the EN12480 standard.

A firebreak valve (pos. no. 11) was installed just upstream of the air intake manifold to prevent flashback phenomenon.The completely experimental installation presented at the Fig. 2.2.

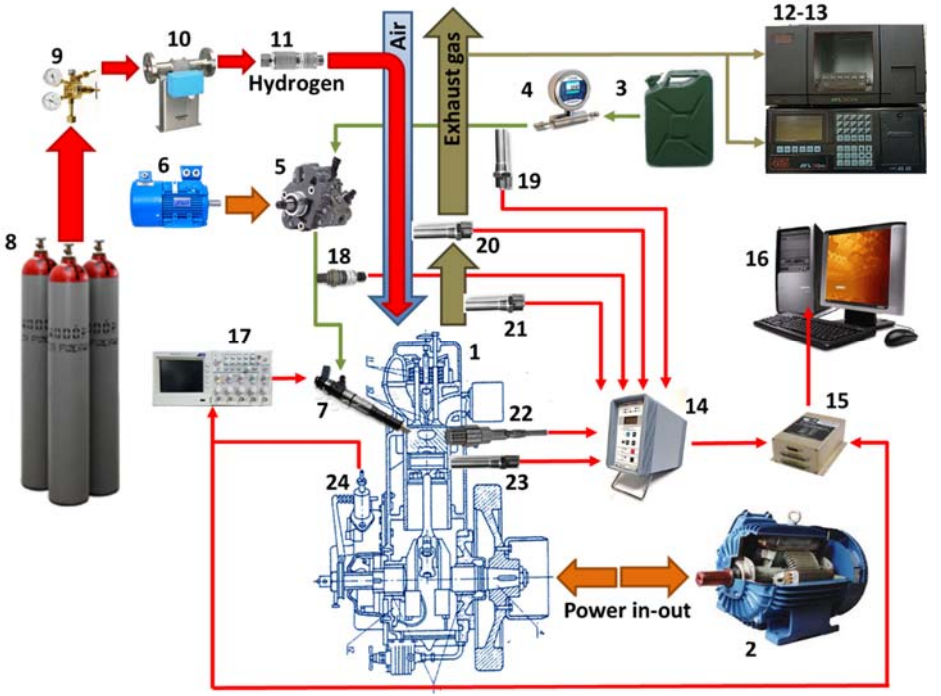

Fig. 2.2. Experimental installation. 1 – CI engine; 2 – electricity generator; 3 – diesel fuel tank; 4 – diesel fuel flow meter; 5 – DF high pressure pump; 6 – DF pump drive el. engine; 7 – DF common rail injector; 8 – hydrogen high-pressure balloon; 9 – hydrogen one-stage pressure reducer; 10 – hydrogen flow meter; 11 – hydrogen firebreak arrestor; 12 – smoke analyser; 13 – emissions analyser; 14 – amplifier & A/D converter; 15 – data acquisition system; 16 – PC – SAWIR; 17 – DF injection controller with osciloscope; 18 – DF pressure sensor; 19 – DF temperature sensor; 20 – inlet air temperature sensor; 21 – exhaust gas temperature sensor; 22 – in-cylinder pressure sensor; 23 – engine temp. sensor; 24 – CA encoder

The high-pressure fuel pump supplies the fuel to the single common rail Bosch diesel injector 0445110076. The amount of the injected fuel was managed electronically by injection controller, conected to the Tektronix TDS2012C osciloscope. The Tektronix TDS2012C osciloscope provides the on-line in-cylinder pressure data with diesel injector needle lift trace. Before experiment, the Bosch diesel injector 0445110076 was tested and calibrated at the authorized diesel service P.H.U. “Gora Bosch & Delphi Diesel”. The Bosch diesel injector 0445110076 test and calibration results are given at the Table 2.2.

Table 2.2. Calibration data of the Bosch common rail fuel injector 0445110076 obtained at the "Gora Bosch & Delphi Diesel"

Measure	Incection duration, μs	Pressure, MPa	Measure time, s	Injection rate	
				Manufacturer given value, mm^3/h	Measured value, mm^3/h
Leak test	0	140	200	35±35	8.55
Full load test	1000	135	90	53.7±4	54.53
Partial load test	500	80	40	19.3±3.4	18.95
Idle gear test	600	25	40	4.4±2.1	3.6
Pilot injection test	160	80	40	2±1.3	2.04

The exhaust gas emissions were measured with Bosch BEA 350 (CO, CO_2, HC, NO_x) and Maha MDO 2 LON (smoke) analysers. The measurement range and accuracy of the analysers given at the Table 2.3.

Table 2.3. Measurement range and accuracy of the Bosch BEA 350 and Maha MDO 2 LON gas analysers

Parameter	Exhaust gas emission analyzer	Measurement range	Accuracy
CO, %vol	Bosch BEA 350	0–10	±0.001
CO_2, %vol		0–18	±0.1
HC, ppm vol		0–9999	±1
O_2, %vol		0–22	±0.01
λ		0.5–9.999	±0.001
NO, ppm vol		0–5000	< ±1
Degree of opacity, %	Maha MDO 2 LON	0–100	±0.1%

In-cylinder pressure *p* data acquisition and record system on real time basis consists of:

1. In-cylinder pressure *p* traced by piezo sensor Kistler 6061B installed instead of the preheating plug. Data provided at the Tab. 2.4.
2. Charge amplifier of the pressure data – Kistler type 5011.
3. CA encoder Kistler type 2612C.
4. Data acquisition converter Measurement Computing Corporation PCI-DAS 6036.
5. PC software SAWIR (*System Analizy Wykresu Indykatorowego w Rzeczywistym czasie* (Polish) – System of the Indicator Chart Analysis at the Real Time).

The measurement range of the charge amplifier Kistler type 5011 is 10–990 000 pC, output voltage 10 V, output currency 5 mA, output resistance 10 Ω, frequency 0–200 kHz, range of operation temperature 0–50 ºC.

Table 2.4. Technical data of the pressure piezo sensor Kistler 6061B

Parameter	Data
Measuring range, bar	0–250
Sensitivity, pC/bar	25
Sensitivity change 50±35 °C, %	≤ ±0.5
Natural frequency, kHz	90
Acceleration sensitivity (radial), bar/g	≤0.001
Operating temperature, ºC	< +50–+350
Thermo shock at 9 bar *IMEP* and 1500 rpm, bar	Δp ≤ ±0.2
Insulation resistance at 20 ºC, TΩ	>10
Shock resistance, g	2000

The speed range of Kistler type 2612C encoder up to 15 000 rpm, temperature range (–28) – (+80) ºC, distribution capacity up to 1 deg.

Data acquisition converter PCI-DAS 6036 registers the data into PC memory within the sufficient period of time to perform the calculation. PCI-DAS 6036 has 8 analog inputs in the symmetric system. Resolution of coverter – 16 bits, maximum sampling frequency – 200 kS/s, two 16 bit analog output (update speed 10 kS/s), memory buffer with capacity of 8196 tests. Software InstalCal is installed to the PCI-DAS 6036 converter for calibration and test as well as self-calibration of the analog input and analog output lines are available. Data acquisition application is controlled by the software SAWIR was developed using programming environment Delphi 6.0 of Windows operating system.

The indicated pressure data measured by piezo sensor Kistler 6061B used to calculate the indicated engine work or indicated specific amount of energy performed as the result of gas pressure on the piston. The indicated pressure p_i is the ratio of indicated specific amount of energy L_{ind} to the stroke volume V_s (Heywood 1988):

$$p_i = \frac{L_{ind}}{V_s} = \frac{\int pdV}{V_s}. \tag{2.1}$$

The numerator $\int pdV$ in relation of p–V express the engine work performed. The work performed by engine is the area enclosed by the pressure curve at the p–V graph as a function of the cylinder volume and it can be determined after deduction the the p–V graph areas:

$$p_i = \frac{(\int_{361}^{540} pdV - \int_{181}^{360} pdV) - (\int_{541}^{720} pdV - \int_{1}^{180} pdV)}{V_s}. \quad (2.2)$$

The SAWIR generated print-screen of the on-line data depicted at the Fig. 2.3.

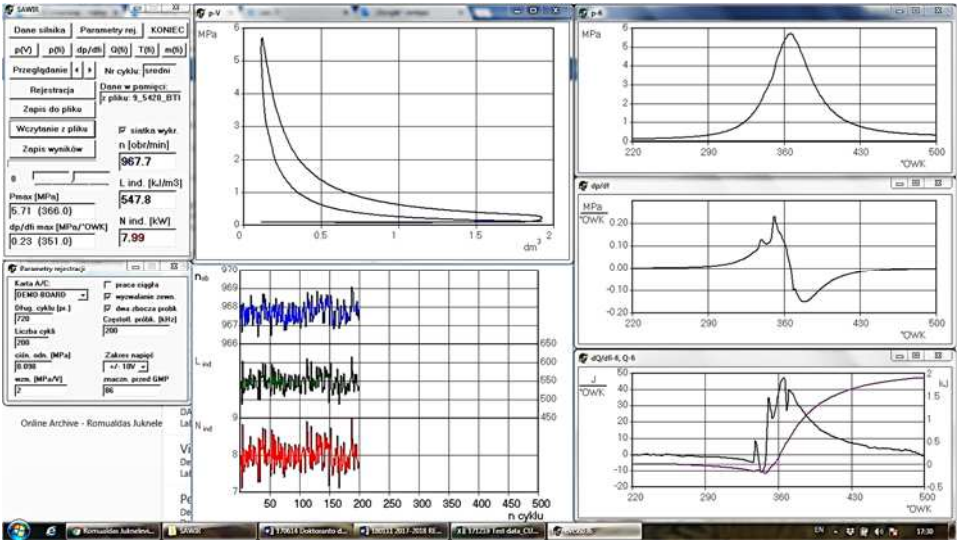

Fig. 2.3. SAWIR generated data screen: *p–V* diagram, engine speed – *n*; indicated specific amount of energy – L_{ind}; indicated power – P_{ind}; in-cylinder pressure – p_{cyl}; pressure-rise – $dp/d\varphi$; rate of heat release – $dQ/d\varphi$; in-cylinder temperature T_{cyl} and MFB

During the each test SAWIR collects several data available in txt format for the transition it into the other (Excel, MatLab) files for the following analysis. The test series consisted of 200 consequtive combustion cycles with the individual data of:

- engine speed – *n*;
- indicated specific amount of energy L_{ind};
- indicated power P_{ind};
- CA of the in-cylinder max. pressure p_{max};
- CA of the max. pressure-rise $dp/d\varphi$;
- rate of heat release $dQ/d\varphi$;
- in-cylinder max. temperature T_{max};
- CA location of 50% of MFB;

– temperature of air (and hydrogen gas) at the inlet manifold T_{in};
– temperature of exhaust gas T_{ex};
– temperature of liquid fuel (diesel or biodiesel) T_{LF}.

The mean values of 200 consequtive combustion cycles within the range of 0–720 CAD are collected:

– in-cylinder pressure p_{cyl};
– volume of combustion chamber V;
– pressure-rise $dp/d\varphi$;
– rate of heat release $dQ/d\varphi$;
– in-cylinder temperature T_{cyl}.

2.2. Biodiesel Used in Experiments

During the tests performed at the Czestachowa University of Technology in Poland the locally supplied biodiesel (Pol. *olej napędowy* – ON) from the oil refinery Orlen Południe S.A. was used and in this thesis denoted as RME7. Orlen RME7 satisfied the requirements of standard EN 590:2009 in accordance to the Directive 2009/30/EC, which defines properties of the ULSD sold at retail and limits the content of the RME to max. 7 vol% (Table 2.5).

Other fuels such as pure hydrotreated biodiesel NExBTL and PRO Diesel (the blend of 15 vol% of NExBTL with ULSD) were supplied by Neste Oyj. Pure biodiesel NExBTL meets the standard EN 15940:2016. The EN 14214 specification is not valid for NExBTL because it consists of hydrocarbons only. The NExBTL meets the standard EN 590:2009 with exeption of density. The NExBTL meets US standard ASTM D975 and Canadian CGSB-3.517 as well. If NExBTL is used in a blend with EN 590 ULSD in case of PRO Diesel, NExBTL does not need to meet EN15940 requirements because NExBTL is fully mixable with ULSD. The EN 590 is applied only for the final fuel blend set by the EN 590.

Table 2.5. Fuel properties (Hoekman *et al.* 2012; Labeckas *et al.* 2014; Rapsoila 2017; Neste Certificate of Analysis 2017; Neste PRO Diesel Product Data Sheet 2017; Aatola *et al.* 2008)

Properties	RME	RME7	NExBTL	PRO Diesel
Composition (wt), %	77.5–77.9 C, 11.3–11.7 H, 10.8 O	81.9 C, 11.9 H, 6.2 O	84.8 C, 15.2 H	85.8 C, 14 H
Density, kg/m³ at 15°C and 1.01 bar	883.7	838.7	779.4	789.3
Molar mass, g/mol	294.5–318.5	205.3	212.4–254.5	142.3–254.5

End of Table 2.5

Properties	RME	RME7	NExBTL	PRO Diesel
Lower heating value, MJ/kg	37.4	42.14	43.7	43.2
Lower heating value, MJ/Nm³	32700	36095	34092	35750
Stoichiometric air-fuel ratio (wt), kg/kg	12.4	14.35	14.9	14.56
Stoichiometric air-fuel ratio (vol), Nm³/Nm³	9139	10032	9678	9577
Heating value of stoichiometric mixture, MJ/kg	2.79	2.74	2.75	2.78
Heating value of stoichiometric mixture, MJ/Nm³	3.58	3.60	3.52	3.73
Auto-ignition temperature at STP, °C	342	~ 260	~ 210	–
Flammability limits at NTP (vol), %	0.8–10	0.6–7.5	–	–
Kinematic viscosity, mm²/s at 40 °C	4.528	3.5–5.0	2.867	1.979
Aromatics (wt), %	–	23.2	0.3	13
Cetane number	51.7	51.7	74.3	65
Carbon to hydrogen ratio (C/H)	6.5	6.9	5.6	5.6

The neat RME supplied by UAB Rapsoila (Lithuania) was used for tests. There are small amounts of contaminants such as glycerols and diaglycerols are formed during the production of RME. These contaminants can cause the engine operational problems, therefore, EN 14214 standard and the US standard ASTM D6751 limit the amount of contaminants in biodiesel.

2.3. Calculations of Hydrogen Energy Share for Various Hydrogen–Biodiesel Blends

In order to obtain CI engine performance efficiency and emission parameters at certain *IMEP* the flow rates of hydrogen and biodiesel must be determined. Moreover author intent to perform tests with addition of various HES to the biodiesel. The test bed instalation of single-cylinder CI engine enable to measure the rate of dual fuel supply: volume rate of hydrogen (dm³/s) and injection duration of biodiesel (μs). Soft-ware SAWIR collects the data of 200 consequtive combustion cycles and provides the *IMEP* generated during the individual test.

The calculation matrix to determine the volume flow rate of hydrogen and injection duration of LF presened at the Fig. 2.4.

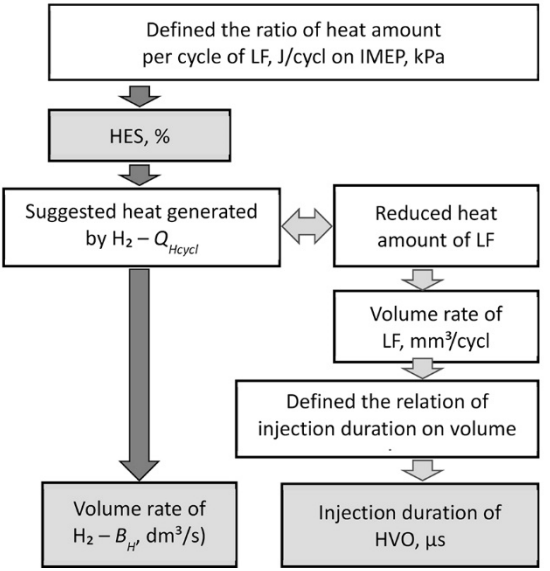

Fig. 2.4. Calculation matrix to determine the volume rate of hydrogen and injection duration of LF

On the basis of the initial tests performed with neat biodiesel spieces, linear regression was defined as relationship between an *IMEP* as the scalar dependent variable y and heat generated by the measuerd cyclic amount of the fuel Q_{cycl} (J/cycl) as explanatory variables x (or independent variables). The linear regression was defined for each tested fuel. Obtained equations of linear regression with its R-squared values presented at the Table 2.6.

Table 2.6. Relationship of cyclic heat amount Q_{cycl}, J/cycl on *IMEP* for tesed fuels

Liquid fuel	Q_{cycl}, J/cycl	R^2
RME7 (Orlen)	6.0297· *IMEP* – 131.5	0.9313
RME7 (Neste)	6.4641· *IMEP* – 219.36	0.9578
RME (Rapsoila)	6.4378· *IMEP* – 218.09	0.9315
ProDiesel (Neste)	6.6877· *IMEP* – 194.92	0.9516
NExBTL (Neste)	5.8838· *IMEP* – 119.38	0.9774

The heat amount per cycle for the tested fuel was determined for the relative *IMEP*. The author suggested the *IMEP* within the range of 280–410 kPa as the low load (LL), 440–585 kPa as the medium load (ML) and 610–670 kPa as the nominal load (NL) for calculation of the heat amount per cycle. The *IMEP* was one of parameters changed with each of tested fuels. The other parameter was HES. According to the selected HES was determined the heat amount released during combustion of hydrogen per cycle Q_{Hcycl} by this expression:

$$Q_{Hcycl} = HES \times Q_{cycl}. \tag{2.3}$$

Here HES – hydrogen energy share, %; Q_{cycl} – heat amount released during engine work cycle, J/cycl.

Mass flow rate of hydrogen per cycle:

$$m_{Hcycl} = \frac{Q_{Hcycl}}{H_{wtH}}. \tag{2.4}$$

Here H_{wtH} – lower heating value of hydrogen by mass, MJ/kg.

Mass of hydrogen is density dependable. Density was determined with expression:

$$\rho_H = \frac{M_H}{R} \times \frac{p_{H@STP} + p_H}{T_{H@STP} + T_H}. \tag{2.5}$$

Here M_H – molar mass of hydrogen, g/mol; R – universal gass constant = 8.314 J/mol·K; $p_{H@STP}$ – pressure of hydrogen at STP, kPa; p_H – pressure of hydrogen gass during the test, kPa; $T_{H@STP}$ – temperature of hydrogen gass at STP, K; T_H – temperature of hydrogen gass during the test, K.

The volume rate of hydrogen per cycle V_{Hcycl}, mm^3/cycl:

$$V_{Hcycl} = \frac{m_{Hcycl}}{\rho_H}. \tag{2.6}$$

Here m_{Hcycl} – mass flow rate of hydrogen per cycle, g/cycl; ρ_H – density of hydrogen, g/mm^3.

Volume flow rate of hydrogen in dm^3/s supplied from hydrogen ballon to the intake manifold:

$$B_{volH} = V_{Hcycl} \cdot \frac{n}{60} \cdot \frac{1}{2} \cdot 10^{-6}. \tag{2.7}$$

Here V_{Hcycl} – volume rate of hydrogen per cycle, mm^3/cycl; n – engine speed, rpm.

The reduced cyclic heat amount released during combustion of liquid fuel (biodiesel) defined by formula:

$$Q_{LFcycl} = Q_{cycl} - Q_{Hcycl}\,. \tag{2.8}$$

The reduced cyclic volume flow rate of liquid fuel:

$$V_{LFcycl} = Q_{LFcycl} / (H_{wtLF} \times \rho_{LF}). \tag{2.9}$$

Here: H_{wtLF} – lower heating value of liquid fuel by mass, MJ/kg: ρ_{LF} – density of liquid fuel, g/mm^3.

Injection duration T_{inj}, μs was defined as linear regression on the data basis of previous tests. The linear regression was defined as relationship between a injection duration T_{inj} as the scalar dependent variable and cyclic volume flow rate of liquid fuel V_{LFcycl} as explanatory variables (or independent variables). The linear regression was defined for each tested fuel. The data presented at the Table 2.7.

Table 2.7. Relationship of injection duration T_{inj}, μs of LF on amount of liquid fuel per cycle V_{LFcycl} for various LF

Liquid fuel	T_{inj}, μs	R^2
RME7 (Orlen)	52.587· V_{LFcycl} – 27.672	0.9225
RME7 (Neste)	47.474· V_{LFcycl} + 263.8	0.9992
RME (Rapsoila)	43.518· V_{LFcycl} + 207.41	0.9974
ProDiesel (Neste)	48.353· V_{LFcycl} + 273.24	0.9936
NExBTL (Neste)	49.959· V_{LFcycl} + 148.8	0.9962

Diesel fuel – RME7 (Neste), PRO-Diesel (Neste), pure biofuel HVO (Neste) and pure RME (Rapsoila) were used for tests with 0–44% hydrogen energy share. The amount of liquid fuel and hydrogen were calculated and supplied to the cylinder on the basis of required hydrogen energy share. As the presence of hydrogen effects the combustion duration and other parameters, the start of the liquid fuel injection timing φ was set at the fixed position, enabling to compare and analyze several MFB profiles at various HES. During the test with HES = 0% the position of 50% MFB, which corresponds to the peak of indicative pressure in cylinder, was targeted to be within the 8–12 CAD aTDC and injection timing φ_{i1} was determined. Then at the lowest HES (depending on the used biofuel the HES was within 12–19%) the position of 50 % MFB was targeted to be within the 8–12 deg CA and injection timing φ_{i2} was determined. Then the subsequent tests were performed with increase of HES, but with fixed injection timing φ_{i2}.

2.4. Calculation of Mass Fraction Burned

Gerald M. Rassweiler (1903–1978) and Lloyd Withrow (1889–1992) developed the method for calculation of the MFB. It is based on calculation of the ratio of the difference between the measured pressure and the polytrophic pressure to the total fuel energy. It is commonly used because of its relative simplicity and computational efficiency. This method, known also as a single-zone heat release method (Rassweiler *et al.* 1938). It is based on the assumption that, during combustion process, the in-cylinder pressure-rise Δp over a given CA interval $\Delta\varphi$, is the sum of pressure rise due to the piston motion Δp_v and the pressure-rise due to the combustion Δp_c:

$$\Delta p = \Delta p_v + \Delta p_c. \tag{2.10}$$

They approximated the whole combustion process with a series of small CA increments. The air-fuel mixture is compressed polytropically by the piston and then a small amount of air-fuel charge burn (Avarzaman 2002). This will continue throughout the combustion period. Since the combustion at each CA position occurs with the various cylinder volume, some reference volume must normalize the pressure rise due to the combustion.

Rassweiler *et al.* (1938) presented the following expression to determine the MFB:

$$MFB = \frac{Vp^{-\kappa} - V_{SOC}p^{-\kappa}}{V_{EOC}p^{-\kappa} - V_{SOC}p^{-\kappa}}. \tag{2.11}$$

Here V_{SOC} – the cylinder volume at the time of SOC; V_{EOC} – the cylinder volume at the time of EOC. This expression based upon assumption that the polytropic exponent κ is the same for the compression and expansion process. This formula is complicated in practical use as it is impossible to determine the EOC of each cycle.

Stone *et al.* (1987) gave a more practical derivation of this method. They assumed the Rasweiller and Withrow statement about two parts of pressure rise: pressure rise due to the piston motion Δp_v and the pressure rise due to combustion Δp_c, according formula 2.16. As the crank angle φ_i increments to the next value of φ_{i+1}, the volume changes from V_i to V_{i+1} and the pressure from p_i to p_{i+1}. Assuming that the polytropic process with exponent κ can model the pressure rise due to the change in volume, the following expression define the p–V relation:

$$p_i V_i^{\kappa} = p_{i+1} V_{i+1}^{\kappa} = const. \tag{2.12}$$

The pressure change due to the cylinder volume change caused of piston reciprocating motion can be defined as:

$$\Delta p_V = p_{V_{i+1}} - p_{V_i} = p_i \left[\left(V_i \middle/ V_{i+1} \right)^{\kappa} - 1 \right]. \tag{2.13}$$

While pressure change due to the combustion process:

$$\Delta p_c = p_{i+1} - p_i \left(V_i \middle/ V_{i+1} \right)^{\kappa}. \tag{2.14}$$

The volume V_i at each CA could be determined by formula:

$$V_i = V_c + A_p S_p. \tag{2.15}$$

Here: V_c – clearance volume; A_p – piston surface; S_p – displacement of the piston starting from TDC.

The compression and expansion processes were represented by polytropic *p–V* relation 2.12. The compression polytropic exponent κ_c was defined with *log(p)–log(V)* diagram, using two set points 50 ºCA and 100 ºCA bTDC. The linear regression slope between these points is the compression polytropic exponent κ. The expansion polytropic exponent κ_e was defined within the range of 60 ºCA and 110 ºCA aTDC.

Heywood (1988) presented the data of specific heats for unburned gas mixtures and specific heats for burned products of combustion, to determine the compression polytropic exponent κ_c and the expansion polytropic exponent κ_e. However the difference of these two exponents practically are marginal, author of this thesis remains only with compression polytropic exponent κ_c.

Due to change of the cylinder displacement, the pressure change referenced to the clearance volume, i.e. the volume at the TDC. This normalized pressure change is denoted Δp^*_c:

$$\Delta p_c^* = \Delta p_c \frac{V_i}{V_c}. \tag{2.16}$$

The large amplitude oscillations of normalized pressure within vicinity bTDC marks the SOC, while more significant oscillations of normalized pressure within the range of 60–130 ºCA aTDC marks the EOC. The EOC has been indicated when the process of pressure rise due to combustion stops.

Assuming that normalized pressure rise is proportional to the MFB – *x*, for *Z* increments of crank angle:

$$x_i = \frac{\sum_0^i \Delta p_c^*}{\sum_0^Z \Delta p_c^*}. \tag{2.17}$$

In this expression numerator – Δp^*_c at each CA position i of combustion duration, denominator – sum of Δp^*_c values starting from SOC to the EOC:

$$\sum_0^Z \Delta p_c^* = \sum_0^Z \left[p_{i+1} - p_i \left(V_i \middle/ V_{i+1} \right)^{\kappa} \right] \cdot \frac{V_i}{V_c}. \tag{2.18}$$

The calculation of $\sum_0^i \Delta p_c^*$ starting from SOC, in some cases results the negative values and thus makes the MFB negative. However, MFB can not be negative and author assumed that SOC is at the moment when values of $\sum_0^i \Delta p_c^*$ change to positive.

The MFB profile was determined on the basis of the absolute pressure trace for the each combustion event. For the accuracy of the evaluation, the pressure diagrams averaged and then the rate of MFB was calculated. Assuming, that the cumulative heat release is directly proportional to the mass of the fuel burnt, then, the ROHR directly correspond to the dimensionless rate of MFB. From the MFB profile, the 10%, 50% and 90% MFB were determined. The CA 0–10 was defined as the CA interval from the SOC to the CA of 10% MFB, while CA 10–90 was defined as the CA interval from the 10% MFB to the CA of 90% MFB. There are three phases of MFB analyzed in the thesis.

I phase (0–10% MFB) is the initial combustion phase related to the SOC influenced by combustion delay and laminar flame speed. The combustion at this phase is quasi-laminar, propogated from source of combustion, and further at the EOC tranfering to the turbulent combustion. The flame propagation at this phase is very important for further process of combustion (Szwaja 2010).

II phase (10–90% MFB) is the main combustion phase with clearly expressed turbulent character. There are two types of combustion. Premixed combustion occurs when homogeneous mixture formed at I phase and further lasts at II phase. The diffusion combustion occurs when heterogeneous mixture is formed at the distinctly separated air and fuel areas. The flame propagation become slower than that of premixed combustion, as it is located at the areas of combustible mixture of air-fuel only. Premixed combustion actually not befall in case of hydrogen combustion, with external mixture formation.

III phase (90–100% MFB) – the final phase of combustion with combustion of the residue of air-fuel mixture. Only high temperature contrinutes and supports the combustion process.

The middle phase of combustion (50% MFB) is analyzed as well, because it well correlates with the peak of indicated in-cylinder pressure. The maximum of indicated in-cylinder pressure is located in vicinity of 8–12 CAD aTDC. The positioning of the 50% MFB in this region was considered as the indicator of the most favourable combustion with the highest performance indicators (Szwaja 2010).

2.5. Application of Wiebe Function

The combustion reactions in an ICE may proceed sequentially and parallelly with the formation of intermediate hydrocarbons and oxygen compounds, and free atoms and radicals. German origin, Soviet Union scientist Ivan Ivanovich Wiebe (1902–1969) called these intermediate compounds active centres (Wiebe 1962). Active centers are highly reactive, performs an important role in chemical kinetic reactions and are very relevant for their chains. For the beginning of reactions, a certain concentration of active centres are required and these centres can be generated by emitted heat or by compressed air–fuel mixture. During the combustion reaction of hydrogen emerge the water, and the leading role is played by reactions:

$$\text{Reaction I: } OH^{\bullet} + H_2 \rightleftarrows H_2O + H^{\bullet}; \tag{2.19}$$

$$\text{Reaction II: } H^{\bullet} + O_2 \rightleftarrows OH^{\bullet} + O^{\bullet}; \tag{2.20}$$

$$\text{Reaction III: } O^{\bullet} + H_2 \rightleftarrows OH^{\bullet} + H^{\bullet}. \tag{2.21}$$

The oxidation of CO can be represented by the following reaction cycle:

$$\text{Reaction IV: } OH^{\bullet} + CO \rightleftarrows CO_2 + H^{\bullet}; \tag{2.22}$$

$$\text{Reaction II: } H^{\bullet} + O_2 \rightleftarrows OH^{\bullet} + O^{\bullet}; \tag{2.23}$$

$$\text{Reaction V: } O^{\bullet} + CO \rightleftarrows CO_2. \tag{2.24}$$

These reactions may proceed sequentially and parallelly as shown in Fig. 2.5. Reactions in dotted-line cells are the *elementary reaction cycles*, whereas the reactions within the solid-line celles are the *effective reaction events*. The elementary reactions chain results in the formation of complete combustion products such as water and carbon dioxide and *active centres* such as hydroxyl radicals capable of initiating subsequent effective reaction events.

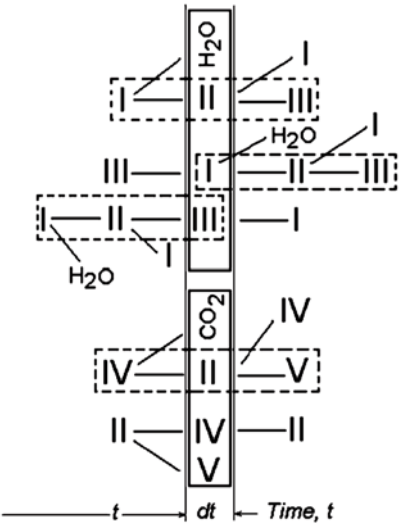

Fig. 2.5. Diagram of chemical processes, with elementary cycles (dotted-line), and effective events of chain reactions (solid line) as a function of time (Ghojel 2010)

The *active centres* initiate the *effective reaction events* and reaction chains. Wiebe stated that these events are *effective centres*. On the basis of this concept, Wiebe postulated that the increasing number of moles of the main reactants dN get involved in the effective reaction events within the time interval t to $t + dt$ is directly proportional to the substitution in the number of effective centres $dN_e - dN = n_c dN_e$ where n_c is the constant of proportionality. In differential form (Wiebe 1962):

$$-\left(\frac{dN}{dt}\right) = n_c\left(\frac{dN_e}{dt}\right). \tag{2.25}$$

Considering that N – the instantaneous number of molecules of the initial reactants, the relative density ρ of the effective centres will be defined as:

$$\rho = \left(dN_e/dt\right)\Big/_{N}. \tag{2.26}$$

Then equation (2.25) can now be written as:

$$-\frac{dN}{N} = n_c \rho dt. \tag{2.27}$$

Taking the logarithm of this equation and considering that N_0 – the number of mols of the main reactant of the combustion at the SOC, while N – the number of mols of the main reactant at any time of combustion:

$$\ln\frac{N}{N_0} = -\int_0^t n_c \rho dt; \tag{2.28}$$

$$\frac{N}{N_0} = e^{-\int_0^t n_c \rho dt}. \tag{2.29}$$

The MFB (expressed as x) of the initial reactants, at any time of combustion t can be defined as:

$$x = \frac{N_0 - N}{N_0} = 1 - \frac{N}{N_0}; \tag{2.30}$$

$$x = 1 - e^{-\int_0^t n_c \rho dt}. \tag{2.31}$$

The rate of burn fraction:

$$\frac{dx}{dt} = n_c \rho e^{-\int_0^t n_c \rho dt}. \tag{2.32}$$

The relative density of the effective centres can be expressed as $\rho = kt^{m_v}$, where k and m_v are constants. Constant m_v was named by I.I. Wiebe as the combustion characteristic exponent or the combustion intensity shape parameter of the function. If $n_c k = K$, equations of the burn fraction and rate of burn fraction at any time t can be transformed as follows:

$$x = 1 - e^{-\left[K/(m_v+1)\right]t^{m_v+1}}; \tag{2.33}$$

$$\frac{dx}{dt} = Kt^{m_v} e^{-\left[K/(m_v+1)\right]t^{m_v+1}}. \tag{2.34}$$

The combustion process in an IC engine is finite process and if the combustion duration is denoted t_c, the burn fraction:

$$x_c = 1 - e^{-\left[K/(m_v+1)\right]t_c^{m_v+1}}. \tag{2.35}$$

Taking the logarithm of equations (2.33) and (2.35) and dividing one by the other (Wiebe 1962):

$$x = 1 - e^{a(t/t_c)^{m_v+1}} = 1 - \exp\left[a\left(t/t_c\right)^{m_v+1} \right]. \tag{2.36}$$

Here $a = ln(1 - t_c)$ is the efficiency parameter of the function. The non-dimensional rate of burn fraction as function of time t can now be written as:

$$\frac{dx}{dt} = a\frac{m_v+1}{t_c}\left(\frac{t}{t_c}\right)^{m_v} e^{a\cdot\left(\frac{t}{t_c}\right)^{m_v+1}}. \tag{2.37}$$

This equation named single Wiebe function. The rate of burn fraction or the rate of heat release during combustion can be expressed as function of CA degree from the SOC – φ and combustion duration – φ_c instead of function of time t:

$$w_\varphi = \frac{dx}{d\varphi} = a\frac{m_v+1}{\varphi_C}\left(\frac{\varphi}{\varphi_C}\right)^{m_v} e^{a\cdot\left(\frac{\varphi}{\varphi_c}\right)^{m_v+1}}. \tag{2.38}$$

Here: $dx = \frac{dQ}{Q}$; Q – cyclic heat release rate.

I.I. Wiebe assumed that at the end of combustion when $x_d = 0.999$ the efficiency parameter $a = -6.90776$, while at $x_d = 0.990$ it increase $a = -4.60517$ (Ghojel 2010).

Integration of Wiebe function gives the MFB combusted from SOC:

$$x = \int \frac{dx}{d\varphi}\cdot d\varphi = 1 - e^{a\cdot\left(\frac{\varphi}{\varphi_c}\right)^{m_v+1}} = 1 - \exp\left[a\left(\frac{\varphi}{\varphi_c}\right)^{m_v+1} \right]. \tag{2.39}$$

Fig. 2.6 presents the dependence of ROHR and MFB on different combustion intensity shape parameter m_v at various CAD.

At lower m_v values, the combustion intensity is more concentrated at the beginning of the combustion process and with increasing m_v values, the combustion process intensity is at the middle or end of the combustion.

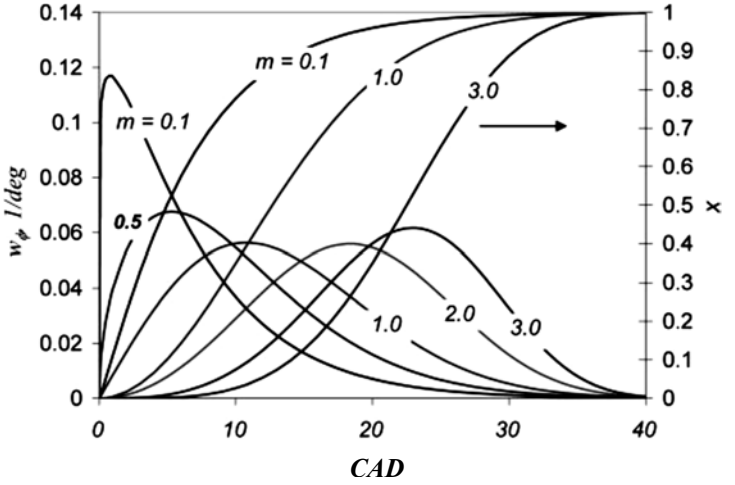

Fig. 2.6. The dependence of rate of heat release $w_\phi = dx/d\varphi$ and x = MFB on different combustion intensity shape parameter m_v (Ghojel 2010)

Fig. 2.7 presents the approximation of an actual heat release diagram of a CI engine measured during the experiment and by a Wiebe function.

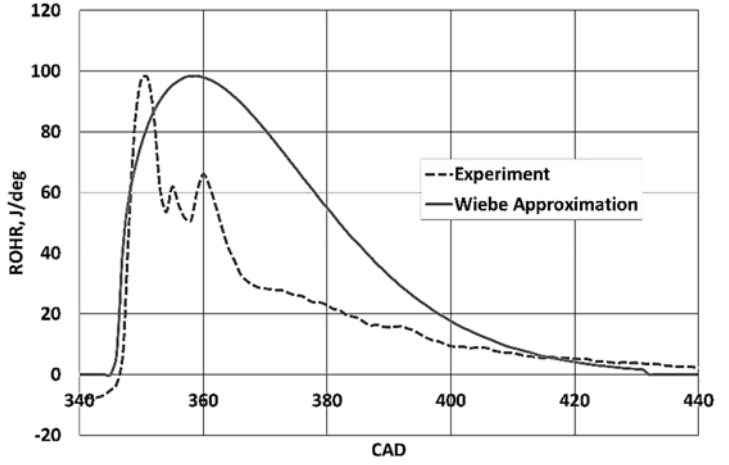

Fig. 2.7. The ROHR vs. CAD of experimental data and Wiebe Approximation

(2.38) and (2.39) equations were used as a combustion predictive model of the IC engines by relating its parameters to the fuel injection rate, ignition delay,

combustion duration and shape parameter. This form of the single Wiebe function become the standard used by most of known IC engine researchers: Miyamoto, Woschni, Anisits, Heywood. The single Wiebe function is the most useful when there is a need for a simple combustion model with high computational and algorythmic efficiency, for example: prediction of the engine thermodynamic cycle and emissions, analysis of HCCI or RCCI mode strategies, gaseous and dual fuel engines (Ghojel 2010).

2.6. Application of Wiebe Two Zone Function

The combustible mixture in the ccombustion chamber is considered homogenous. When combustion occurs there are formed unburned components of one zone with low temperature and combustion reaction products of other zone with high temperature. These zones are separated by the flame front where fuel oxidation takes place. The AVL BOOST numerical simulation model is based on these assumptions. Numerical simulation and analysis process of the software with Wiebe two zone function was employed for this thesis (AVL BOOST Theory 2011). The cylinder volume divided into two zones where burned charge V_b and unburned charge V_u contains total volume:

$$V_b + V_u = V. \tag{2.40}$$

The cylinder volume should be equal to sum of the volume changes and the sum of the different zone volumes must be equal to the cylinder volume:

$$\frac{dV_b}{d\varphi} + \frac{dV_u}{d\varphi} = \frac{dV}{d\varphi}. \tag{2.41}$$

The more detailed description of the thermodynamic engine model presented at the Appendix A.3.

The analysis of hydrogen co-combustion with biodiesel was performed with AVL BOOST subprogram BURN. The in-cylinder pressure traces obtained during performed experiments were placed into the BURN utility and the inverse calculations were done. The BURN calculated rate of heat release of each hydrogen – biodiesel fuel mixture, hydrogen energy share and engine load. The same calculation algorithms as for simulation were used for ROHR calculation. The calculations are based on the first law of thermodynamics.

The calculations were performed when intake and exhaust valves are closed and the high pressure-rise was indicated. The simulation of combustion processes were performed with developed simulation model with AVL BOOST software. Fig. 2.8 presents the AVL BOOST model for single-cylinder CI engine.

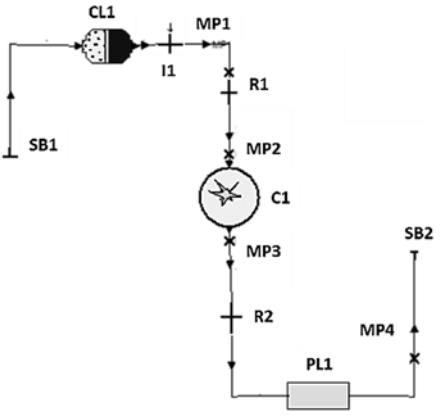

Fig. 2.8. The AVL BOOST simulation module of engine Andoria S320: I1 – H_2 injector; R1-2 – restrictors; SB1-2 – system boundaries; PL1 –exhaust manifold; CL1 – air cleaner; MP1-4 – measuring points; C1 – engine cylinder

AVL BOOST is the simulation software of engine cycles and gas exchanges that enables to build an engine model by selecting elements from a toolbox. These elements include cylinders, injectors, air filters, catalysts, intercoolers, turbochargers etc. connected by pipe elements (AVL BOOST 2011) . This AVL BOOST platform provides possibility to do advanced engine simulation in terms of cycle simulations, beneficial possibility of performing co-simulation with other simulation software and possibility of relatively easy implementation of user-defined models (Alqahtani *et al.* 2015).

2.7. Uncertainty and Error Calculations

Uncertainties and errors during performed tests occured as the result of calibration, measuring equipment accuracy and observation. The uncertainty of the test result was estimated according to the literature (Holman 2011). The result R of the test performed is the function expressed with an additive form:

$$R = \delta_1 y_1 + \delta_2 y_2 + \ldots + \delta_n y_n. \tag{2.42}$$

Here: R – result of function, $y_1, y_2, y_3,\ldots,y_n$ – independent variables of the function. The partial derivatives of independent variables for use in equation 2.48 are:

$$\frac{\partial R}{\partial y_i} = \delta_i. \tag{2.43}$$

The uncertainties of the result R or independent variables may be expressed as:

$$\delta R = \sqrt{\left(\frac{\partial R}{\partial y_1}\Delta y_1\right)^2 + \left(\frac{\partial R}{\partial y_2}\Delta y_2\right)^2 + ... + \left(\frac{\partial R}{\partial y_n}\Delta y_n\right)^2} = \sqrt{\sum_{i=1}^{Z}\left(\frac{\partial R}{\partial y_i}\right)^2 \Delta y_i^2}. \quad (2.44)$$

Here δR – the uncertainty of the result. Using the equation 2.50 the uncertainty of the test results such as in-cylinder pressure, *IMEP, ISFC, ITE* were determined to prove accuracy of the experiment. It was assumed that engine speed n and LHV are accurate values and they have no influence on the measured values.

The uncertainty of the *IMEP* was can be determined from equation:

$$\delta IMEP = \sqrt{\delta p^2 + \delta V^2}. \quad (2.45)$$

Here $\delta IMEP$ – uncertainty of the *IMEP*; δp – uncertainty of in-cylinder pressure; δV – uncertainty of instantaneous cylinder displacement.

The uncertainty of the *ISFC* was determined considering accuracy of hydrogen flow meter and mass flow rate of liquid fuel:

$$\delta ISFC = \sqrt{\delta B_{volH}^2 + \delta m_{LF}^2 + \delta p^2 + \delta n^2}. \quad (2.46)$$

Here δB^2_{volH} – uncertainty of the volume flow rate of hydrogen; δm^2_{LF} – uncertainty of mass flow rate of liquid fuel; δn^2 – uncertainty of engine speed.

The uncertainty of the *ITE* was determined from equation:

$$\delta ITE = \sqrt{\left(\delta IMEP\right)^2 + \left(\delta ISFC\right)^2}. \quad (2.47)$$

Here δITE – uncertainty of the indicated thermal efficiency. Uncertainties of the following parameters such as in-cylinder pressure, engine torque, *IMEP, ISFC, ITE* are given at the Table 2.8.

Table 2.8. The uncertainty of parameters, measured during the test

Parameters	Uncertainty, %
In-cylinder pressure, p	±0.5
Engine speed, n	±0.85
IMEP	±2.1
ISFC	±2.5
ITE	±3.2

2.8. Conclusions of Chapter 2

The presentation and review of research methodology lead to the following chapter conclusions:

1. The hydrogen supply system to the Andoria S320 CI engine was designed and mounted. The hydrogen supply system enabled to control the hydrogen flow rate therefore it was possible to determine the required HES. The injection system enabled to control injection timing and duration of liquid fuel. The applied experimental basis is valuable for further investigation of hydrogen co-combustion with liquid fuels tests.
2. Composed and applied the algorithm related to the experimental assessment methods to determine the flow rate of hydrogen, injection timing and duration of liquid fuel to get required HES.
3. Explained and presented the method for calculation of the mass fraction burned, to determine the duration of premixed combustion, the main combustion phase and position of 50% MFB, corresponding to the peak of indicative pressure in cylinder.
4. According to the design and data of the CI engine, used for the experiments, the AVL BOOST numerical simulation and analysis model was applied and developed. It is usefull tool for the analysis of the combustion process of CI engine performance efficiency and emission parameters, when various biodiesel fuels are co-combusted with hydrogen.

3

Experimental and Numerical Investigation of Hydrogen Co-Combustion with Biodiesel in Compression Ignition Engine

This chapter presents an experimental investigation and numerical simulation results. Investigated influence of various hydrogen fractions on biodiesel with focus on the engine combustion process. Research results were published in following scientific publications: Juknelevičius (2018); Rimkus *et al.* (2018a); Juknelevičius *et al.* (2018a); Juknelevičius *et al.* (2018b); Juknelevičius *et al.* (2018c).

3.1. Research of Hydrogen Co-Combustion with Hydrotreated Biodiesel and with Biodiesel

3.1.1. Experimental Investigation

The single cylinder CI engine with combined fuel mixture formation was used for the tests. The external mixture formation was designed for supply of the homogeneus air – hydrogen mixture to the combustion chamber. The pure hydrotreated biodiesel or biodiesel with internal mixture formation was directly injected into

the combustion chamber, already filled up with the air – hydrogen mixture and initiate the combustion.

The presence of hydrogen in the combustion chamber has cons and pros in relation to the combustion process. Hydrogen leads to the improvement of the mixture homogeneity as the CI engines are suffering due to the heterogeneity of the injected liquid fuel. However, the low concentration of hydrogen until the LFL of hydrogen are not reached leads to the insufficiency of the speed of chain reactions to assist the intensive combustion. With increase of HES the extremely low minimum ignition energy of hydrogen can provoke the abnormal combustion.

After the SOC, the high speed combustion of hydrogen leads to the propagation of fast co-combustion with biodiesel. However, due to the high speed of hydrogen combustion, it burns first and fast, unless the injected biodiesel initiates the combustion. After the all charge of hydrogen has been burned, the combustion of biodiesel continues further to the end of combustion.

Two types of pure liquid biofuels were analysed: biodiesel – RME and hydrotreated biodiesel HVO. Tests performed under the LL, ML, NL and corresponding *IMEP* presented at the Table 3.1.

Table 3.1. Injection timing and *IMEP* at various composition of RME, HVO and HES

Test no.	Composition of combustible mixture	SOI φ_i, bTDC	Loads	*IMEP,* kPa
1	RME+H_2 0%	φ_{i1} = 16°	LL	265.5
2	RME+H_2 (19–44%)	φ_{i2} = 14°	LL	273.2–295.6
3	RME+H_2 0 %	22º	ML	379.7
4	RME+H_2 (16–42 %)	20º	ML	416.3–508.5
5	RME+H_2 0 %	28º	NL	519.2
6	RME+H_2 (16–36 %)	26º	NL	551.1–625.3
7	HVO+H_2 0%	18º	LL	344.9
8	HVO+H_2 (13–40%)	18º	LL	371.7–379.5
9	HVO+H_2 0%	24º	ML	519.8
10	HVO+H_2 (13–30%)	24º	ML	494.8–538.5
11	HVO+H_2 0%	28º	NL	651.8
12	HVO+H_2 (12–29%)	28º	NL	645.8–691.5

The set-up of the test engine presented at the Chapter 2.1 with technical specifications given at the Table 2.1 and experimental installation at the Fig. 2.2. The analysis of experiments based on in-cylinder pressure data acquisition. The impact of HES on combustion properties and combustion duration of the CI engine under fixed injection timing at three *IMEP* studied. The *IMEP* managed by changing the

supply of the liquid fuel and hydrogen (section 2.2, chapter 2). The low reactivity fuel – hydrogen supplied together with air into the intake manifold. In cylinder, homogeneous air – hydrogen mixture under the elevated heat and pressure self-ignited by injected high reactivity HVO.

The calculated relative equivalence ratio λ depicted at the Fig. 3.1.

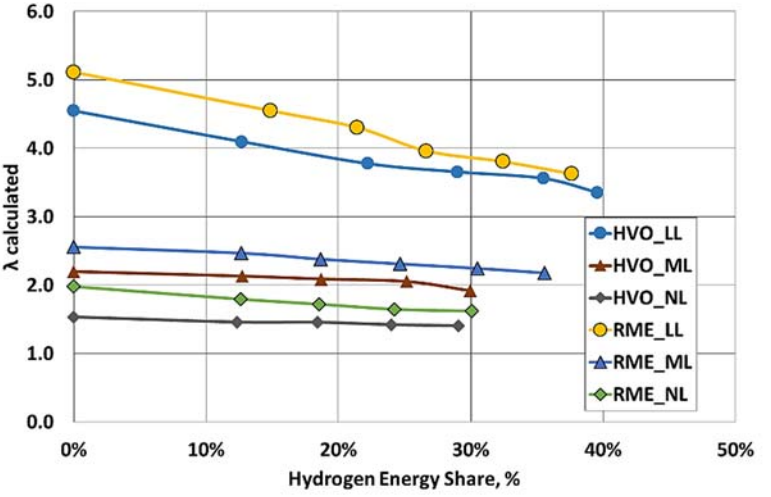

Fig. 3.1. Relative equivalence ratio λ vs. HES at various engine loads

As the relative equivalence ratio λ is the ratio of the air amount actually fed into the combustion chamber with stoichiometric (theoretical) amount of air, λ calculated using this formula:

$$\lambda = \frac{V_{air} - V_H}{V_{airLF} + V_{airH}}. \tag{3.1}$$

Here V_{air} – actual volume flow rate of air, dm^3/s; V_H – volume flow rate of hydrogen, dm^3/s; V_{airLF} – stoichiometric flow rate of air required for combustion of liquid fuel, dm^3/s; V_{airH} – stoichiometric flow rate of air for hydrogen, dm^3/s.

The volume flow rate of hydrogen was measured with H_2 flow meter (Fig. 2.2, pos. no. 10). The actual volume flow rate of air (Heywood 1988):

$$V_{air} = \frac{V_S \cdot n \cdot \eta_{ch}}{120}. \tag{3.2}$$

Here V_S – swept volume, dm^3; n – engine speed, rpm; η_{ch} – charging efficiency, considering the single cylinder engine assumed to be – 0.85.

The stoichiometric flow rate of air required for combustion of liquid fuel V_{airLF} and hydrogen V_{airH} considered as the product of the actual volume flow rate of fuel and the stoichiometric air – fuel ratio for the measured amount of fuel AFR_{volLF} and AFR_{volH}, respectively:

$$V_{airLF} = V_{LF} \cdot AFR_{volLF}; \tag{3.3}$$

$$V_{airH} = V_{H} \cdot AFR_{volH}. \tag{3.4}$$

The AFR_{volLF} and AFR_{volH} are presented at the Table 2.7, while V_{LF} and V_H were measured during the tests.

Typically for rich mixtures, λ is less than 1.0, while for lean mixtures, λ is greater than 1.0. However during the performed tests the λ always was greater than 1.0, and therefore author assumed that lean mixture considered at λ>3.0, while rich mixture considered within the range of 1.0<λ<2.0.

3.1.2. In-Cylinder Maximum Pressure and Analysis of Hydrogen Flamability Limits

In-cylinder maximum pressure curves for various hydrogen fractions are depicted at the Fig. 3.2.

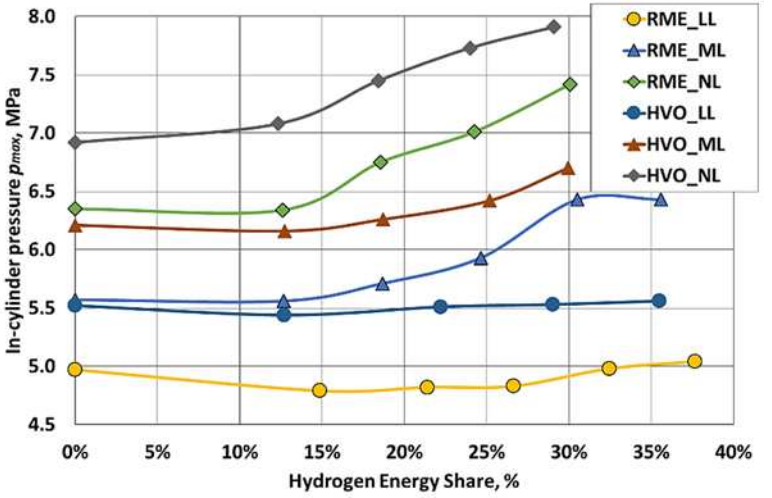

Fig. 3.2. In-cylinder maximum pressure vs. HES at various engine loads

The increase trend of in-cylinder maximum pressure was noticed with increase of HES more than 12% for HVO within the range of the LL and NL. The

increase of in-cylinder maximum pressure at LL was negligible (1%), at ML, it was 9% and at NL, increase of 14% was measured.

The negligible influence of hydrogen fraction at the LL and partially at the ML can be explained by the low volume fraction of the hydrogen in the combustion chamber. The volume fraction of H_2 at LL tests are within the range of 1.38–2.87%, which is below the lower flammability limit of hydrogen – 4% (Table 1.3) and the combustion was not intensified by presence of the hydrogen. The low volume fraction of H_2 at the LL has not significant influence in comparison to the ML and NL conditions. The lean hydrogen – air mixture does not support the flame propagation and results in rather low hydrogen combustion efficiency. When this boundary was exceeded, with HES more than 12–13% at the ML and NL, the combustion became more intensive, especially at the premixed phase and in-cylinder p_{max} increased. The influence of hydrogen volume fraction on the in-cylinder p_{max} depiced at the Fig. 3.3.

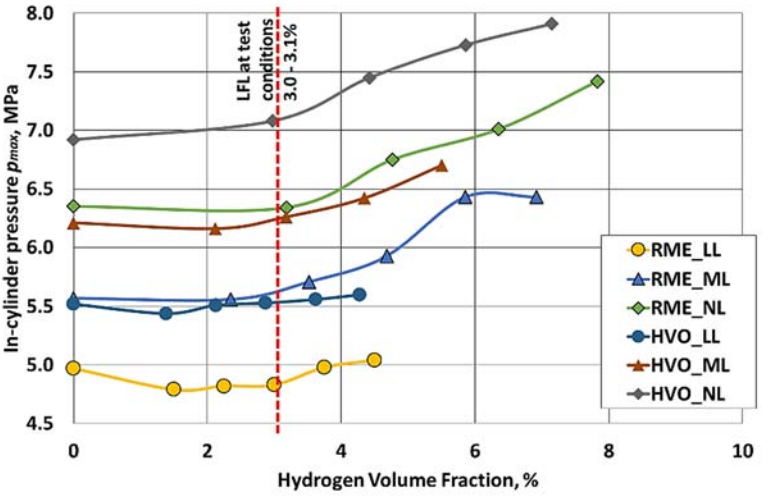

Fig. 3.3. In-cylinder maximum pressure vs. hydrogen volume fraction at various engine loads

The increase of in-cylinder maximum pressure commenced when HES overstep the 16% at the ML and NL with RME. The trace of in-cylinder maximum pressure at the LL decreased with HES of 15%. Further with HES = 15–27% does not changed significantly, and when HES overstepped 27%, the pressure began to rise. The in-cylinder pressure decreased during the lean burn of the λ = 3.49–3.92, unless addition of 15–27% HES. However, the main reason of this decrease is the low hydrogen volume fraction, which was far below of the LFL of hydrogen. The

hydrogen volume fraction at the HES of 15% was 1.5%, at the 21% HES – 2.25%, at the 27% HES – 3% and all these values were below the LFL of 4% (Table 1.3).

In-cylinder maximum pressure for RME increased at higher HES than with HVO; when hydrogen fraction was more than 15% at the ML and NL. However, at LL the influence of hydrogen fraction was negligible for RME. The max pressure with HVO was higher than that with RME at the whole test range of hydrogen fraction starting from 0%, because the start of combustion with HVO takes place earlier than with RME and pressure rise faster. The other reason of that phenomenon is that heating value of RME stoichiometric mixture is higher than that of HVO (Table 2.8).

There should be mentioned that with increase of temperature and pressure the flammability limits of the hydrogen-air mixture are changing. The actual SOC was in the temperature range of 415–435ºC during the experiments performed by author. According to the Schroeder *et al.* (2004), the LFL at 415–435ºC decreased to the boundary 1.5% of hydrogen volume fraction (Fig. 1.2). This decrease of LFL do not contribute the auto-ignition of hydrogen as the temperature is still too low (415–435ºC) and not sufficient for auto-ignition of hydrogen and to assist the intensity of combustion.

However, with increase of the pressure up to 5 MPa the LFL increased from 4% to 5.6% (Fig. 1.3). Therefore, at the moment of the SOC the pressure was 3.98 MPa and the LFL was 3.0–3.1% of hydrogen volume fraction (Fig. 3.3). We can conclude that only with HES of 32%, LFL was achieved and hydrogen effectively co-combusted with injected RME. Before that, the lean mixture of air – hydrogen with RME is still flammable but non-coherent, it burns incompletely and does not make positive effect on the combustion intensity and engine performance. The more detailed discussion on the reasons of this phenomenon provided further in the subchapter 3.1.4. The same explanation related to the poor performance of p_{max} with low HES = 16%, rich fuel mixtures at ML ($\lambda = 2.12$) and NL ($\lambda = 1.54$).

In-cylinder pressure data analysis performed using AVL BOOST software with increase of HES verified the increase of combustion intensity. That topic discussed further in the subchapter 3.1.6.

3.1.3. Engine Performance

Experiments revealed that with the hydrogen – RME mixture operation achieved the higher in-cylinder pressure than a sole RME operation. However, the *ISFC* decreases with increase of HES and at the medium ($\lambda = 1.95–2.15$) and nominal loads ($\lambda = 1.44–1.66$) has the highest decrease of *ISFC* by 28% in compare to sole RME because of increase of the mass flow rate of hydrogen (Fig. 3.6). Hydrogen due to high flame speed and short quenching distance extends the flammability

range of RME – hydrogen mixture, ensures the complete combustion of RME especially under higher load conditions, which provides reduced *ISFC* (Baltacioglu *et al.* 2016). The substitution of RME by hydrogen makes positive affect on *ISFC*.

ISFC presented at the Fig. 3.7, considering $ISFC_{ULSD}$ and $ISFC_{H_2}$.

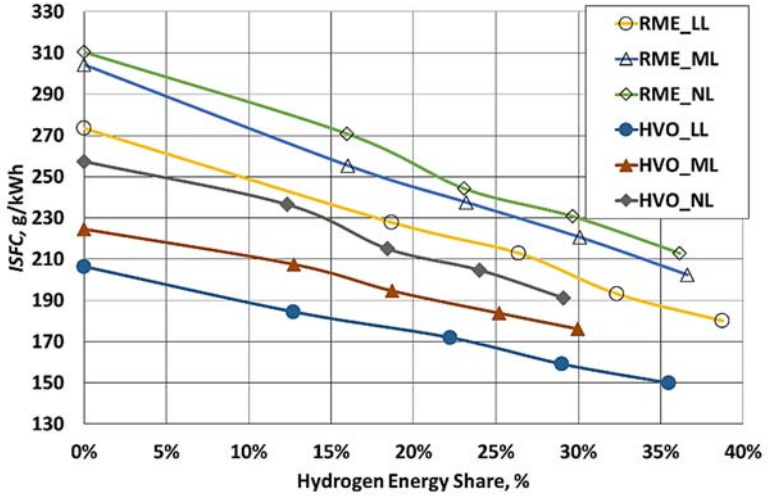

Fig. 3.6. *ISFC* vs. HES of RME and HVO at various engine loads

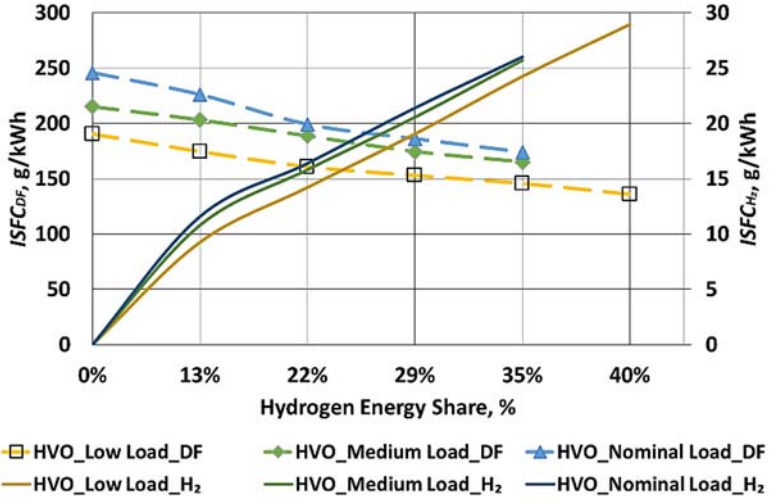

Fig. 3.7. $ISFC_{DF}$ and $ISFC_{H_2}$ vs. HES at various engine loads

With increase of HES the $ISFC_{H_2}$ increased linearly, while the $ISFC_{ULSD}$ decreased with increase of HES. The higher $ISFC_{ULSD}$ at the ML and NL can be attributed mainly to the higher mass flow rate of liquid fuel – HVO. The total *ISFC* decreased by 17.5% at NL, by 14% at ML and by 9% at LL with increase of HES, because of increase of the mass flow rate of hydrogen. The decrease of the total fuel mass flow rate by 10–13% was noticed at the ML and NL and by 22% at the LL with increase of HES. The substitution of HVO by hydrogen makes positive affect on total *ISFC*.

The increase trend of *ITE* during the test of RME was noticed with increase of the HES. The efficiency of the engine was higher with HVO, because of the *IMEP* during tests was higher than that of during tests with RME (Fig. 3.8). Considering that heating value of the stoichiometric mixture of RME is higher (2.79 MJ/kg) than HVO (2.75 MJ/kg), therefore the thermal efficiency of RME should be higher than that of HVO at the same *IMEP*.

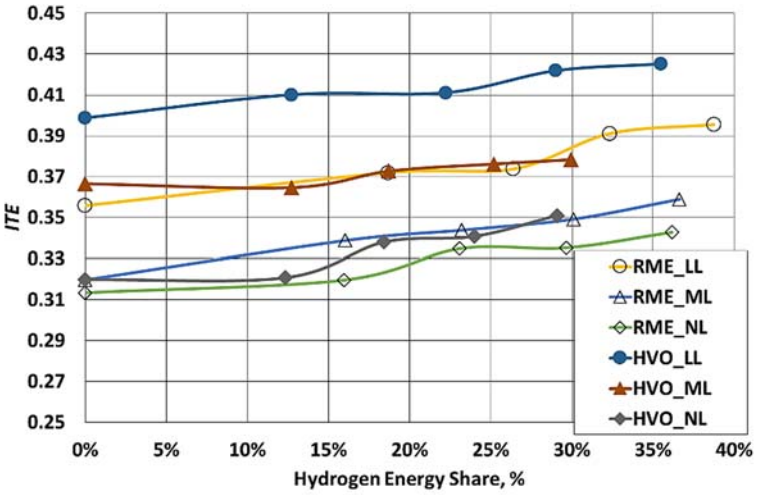

Fig. 3.8. *ITE* vs. HES of RME and HVO at various engine loads

The lower heating value of the fuel mixture did not change, with the same engine load, and therefore did not make any effect on *ITE*. The biggest influence on the thermal efficiency was made by increased mass flow rate of the hydrogen as the response to the decreased total fuel mass flow rate and *ISFC* (Fig. 3.7).

Due to the fast burn rate of hydrogen, the oxidation of hydrogen occurs with less heat losses to the walls of combustion chamber, improving the thermal efficiency. Thus, the increase of the HES should enhance the *ITE* at the rich fuel

mixture with nominal loads. However, there should be noted that hydrogen has extremely low quenching distance, which is smaller than biodiesel. Thus, the hydrogen flame can expand closer to cylinder walls, resulting in complete fuel combustion. Nevertheless, with the increase of HES the quenching assists the higher amount of heat transfer through the walls of the combustion chamber and thus worsening of the thermal efficiency. Moreover, the tests were performed with stationary single cylinder engine with displacement volume of nearly two liters corresponding to the combustion chamber surface area of 828 cm^2. This significantly big surface determintes the favaourable quenching conditions and high amount of heat losses through the wals of combustion chamber. Therefore, it was noticed that *ITE* was higher at the LL in compare to the NL during tests.

The engine‘s limited performance was achieved with with the HES of 42% at the ML and with HES of 36% at the NL when tested RME, while with HES = 30% at the ML and with HES = 36% at the NL when tested HVO. The hydrogen volume fraction was within the range of 6.91–7.83 with RME and 5.50–7.15% with HVO when abnormal combustion started.

In case of LL and lean mixture no abnormal combustion has been detected with increase of HES. However, with the increase of hydrogen fraction close to 50%, the amount of biodiesel becomes too small for stable ignition of the mixture. On the other hand with the decraese of hydrogen fraction to the limits less than 12–15%, it is supposed that such hydrogen fraction is too low for complete combustion confirmed with a high amount of unburnt hydrocarbon detected in the exhaust gas.

The phenomena of abnormal combustion was noticed with the relatively high hydrogen volume fraction i.e. HES. The hydrogen volume fraction is the factor that influence the minimum ignition energy of hydrogen. The minimum ignition energy of hydrogen increase to 0.05 mJ and more at the low volumetric concentration of hydrogen, which is lower than LFL. Meanwhile with increase of hydrogen volume fraction aproaching the stoichiometry, the ignition energy decrease to 0.017 mJ and high ambient temperature and pressure makes the reasonable conditions to the abnormal combustion. Furthermore the low quenching distance cause the increase of temperature of crevice parts, which become the active centers (initial centers) of the abnormal combustion.

The increase of HES shortens the auto-ignition delay and causes not only sudden increase of pressure-rise and ROHR, but can lead to the pin-shape pressure pulse appeared just after the sole hydrogen self-ignition, which reason could be the abnormal combustion. This self-ignition could be explained as the result of extremely low minimum ignition energy of hydrogen, that provides high probability of coincidental ignitions. The abnormal combustion can be avoided with the adjustment of the SOI, which makes positive effect on it. This arrangement discussed further at the subchapter 3.2.6.

The engine performance parameters obtained by the author and discussed above can be compared to the results and comments of other authors presented bellow.

Tsujimura *et al.* (2017) concluded that abnormal combustion is observed as HES is over 50% under nominal load operations. He thought that hydrogen flame could reach the walls of the combustion chamber faster than diesel therefore the temperature rise occurs with an increase of hydrogen energy share. It is not clarified the phenomena of hydrogen auto-ignition or surface ignition occurs near the combustion chamber walls as the abnormal combustion.

Dual fuelling of neat grapeseed oil with HES of 12.8% increases the thermal efficiency as a result of the considerably higher heating value of hydrogen, higher flame velocity and exponentially increasing reaction rates (Chelladorai *et al.* 2018). Maximum efficiency over the entire load range avoiding abnormal combustion corresponds to the HES of 33.97% for the neat grapeseed oil. With increase in HES, the specific energy consumption decreases owing to the significantly higher heating value compared to single grapeseed oil mode. The addition of hydrogen to *Pongamia pinata* increases the *BTE* and decreases the *BSFC* at all load conditions to a significant level (Jagedheesan *et al.* 2017). However, severe knocking observed with hydrogen induction above 10 lpm.

Rimkus *et al.* (2018) observed the influence of the extremely low hydrogen fraction, i.e hydrooxile gas (HHO) which contains only 0.14–0.18% volumetric fraction of hydrogen. They concluded that combustion of the chemically active hydrogen starts at the end of the compression in prior to the injection of liquid fuel. Such phenomena worsen the efficiency of the engine and increase concentrations of CO_2 and NO_x, however reduced the emissions of incomplete combustion CO and HC as well as smokiness. However tests carried out by author with hydrogen (not hydrooxile gas) did not revealed such phenomenon. Furthermore at the low volumetric hydrogen fraction which is lower than LFL (4%) the hydrogen co-combustion with diesel is inefficient. The evidence of that statement are poor performance of in-cylinder pressure until LFL was oversteped (Fig. 3.2 and 3.3), leading to the increased emissions of incomplete combustion CO and HC. The low hydrogen volume fraction leads to the insufficient amount of hydrogen radicals, which are main feedstock to compose the active hydroxyl radicals. That topic will be discussed in details further in the following subchapter.

The summary of the publications of other authors on the co-combustion of hydrogen and biodiesel with short remarks on performance and emissions parameters is presented at the Annex B.

3.1.4. Mass Fraction Burned and Combustion Temperature

The MFB was calculated as the cumulative heat release. The combustion duration of CA 0–10 and CA 10–90 was calculated at each *IMEP* and with each hydrogen fraction for RME and HVO according to the MFB profiles.

With the increase of HES the initial combustion duration of CA 0–10 (Fig. 3.9 and 3.10) was shortened due to the high premixed combustion rate and impact of higher laminar speed of hydrogen flame. Increase of hydrogen fraction also reduces the main combustion duration CA 10–90 (Fig. 3.11 and 3.12) which was accelerated by the initial combustion phase CA 0–10.

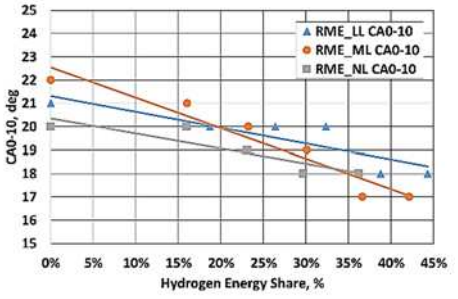

Fig. 3.9. The combustion phase CA 0– 10 at tested HES of RME

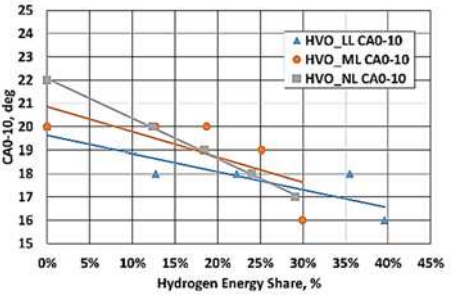

Fig. 3.10. The combustion phase CA 0–10 at tested HES of HVO

Hydrogen addition influences combustion phases: the main combustion phase and ignition delay time.

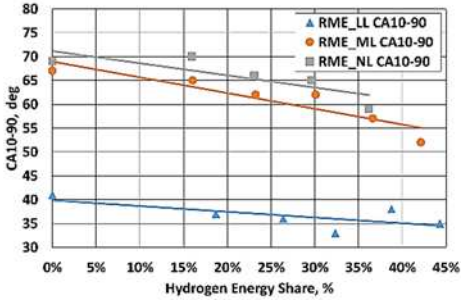

Fig. 3.11. The combustion phase CA 10–90 at tested HES of RME

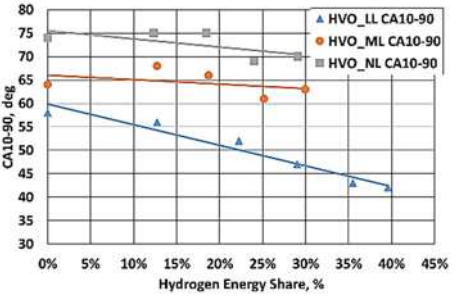

Fig. 3.12. The combustion phase CA 10–90 at tested HES of HVO

As it was observed, the initial combustion duration of CA 0–10 shortened from 22 to 17 CAD at NL. This is significant difference, which requires injection timing to be modified to optimal value. CA 10–90 also makes shorter by 5–16 CAD with HES increase that makes combustion closer to constant volume conditions, what leads to increase in engine thermal efficiency.

As it was mentioned before at the subchapetr 3.1.2, the combustion of the air – hydrogen mixture with liquid fuel at the low hydrogen volume fractions, burns incompletely and does not make positive effect on the combustion intensity and engine performance. The start of the ignition is the transition process from the preignition, when non-reacting air – hydrogen mixture with liquid fuel transforms into a combustion process with chain of reactions. The combustion process of hydrogen – oxygen has a relatively simple oxidation mechanism, however despite the simple composition of the hydrogen as fuel, it combustion requires more than 25 reactions between at least eight different species. Initial reaction of any kind of pure biodiesel could be expressed as:

$$RH + O_2 \rightleftarrows R^{\bullet} + HO_2^{\bullet}. \tag{3.5}$$

When air – hydrogen is supplied to the combustion chamber, parallel with above-mentioned reaction other reaction takes place:

$$H_2 + O_2 \rightleftarrows H^{\bullet} + HO_2^{\bullet}. \tag{3.6}$$

Now both liquid fuel and hydrogen take active part in preignition chemical process, while active radicals generated in the result of mentioned reactions, compete in between affecting the preignition process adversely. Moreover, due to the relatively low temperature (600–800 K) and pressure, partly active $H^{\bullet}$ radicals reacts in between and recombine the hydrogen molecule again:

$$H^{\bullet} + H^{\bullet} \rightleftarrows H_2. \tag{3.7}$$

The low hydrogen volume fraction generates insufficient amount of partly active $H^{\bullet}$ radicals, and further chain reactions not start as the $HO_2^{\bullet}$ radical is less reactive. Only after the concentration of $H^{\bullet}$ radicals increased to the certain level, the active radicals $OH^{\bullet}$ are formed with reaction:

$$H^{\bullet} + O_2 \rightleftarrows O^{\bullet} + OH^{\bullet}. \tag{3.8}$$

The formation of the active radicals $O^{\bullet}$ and especially $OH^{\bullet}$ rapidly activate the further ignition process, prescribed with the following chain propogation reactions, followed by chain branching reactions:

$$OH^{\bullet} + RH \rightleftarrows H_2O + R^{\bullet}; \tag{3.9}$$

$$OH^{\bullet} + H_2 \rightleftarrows H_2O + H^{\bullet}. \tag{3.10}$$

The duration of this chain of reactions is responsible for the auto-ignition delay. The hydrogen volume fraction exceeding LFL supports the shortening of the auto-ignition dealy.

The evidence of shortening of the auto-ignition delay confirmed the simulation of the temperature change (increase) in the constant volume combustion chamber (CVCC) with the CHEMKIN software, – the tool based on chemical kinetics mechanism, originally developed by Sandia National Laboratories in USA (Chemkin 2011). Author performed the simulation during the Erasmus+ practice at the Czestachowa University of Technology.

In order to compare various mixtures three simulations were performed with various ratios of the biodiesel and hydrogen. The temperature but not the pressure was analysed, because the temperature usually has a major effect on the rate of a chemical reaction.

The simulations performed with neat 1 mole of the biodiesel $C_{15}H_{32}$ – HVO. As additives were used various mole amounts of hydrogen: 1 mole of hydrogen in the first simulation (Fig. 3.13), while 2 moles of hydrogen in the second simulation (Fig. 3.14).

The mass fraction of the biodiesel for this simulation was calculated according to the formula 2.11:

$$m_{frLF} = \frac{m_{LF} \cdot 100}{m_{LF} + m_H} = \frac{212.47 \cdot 100}{212.47 + 1.01} = 99.5\% \cdot \tag{3.11}$$

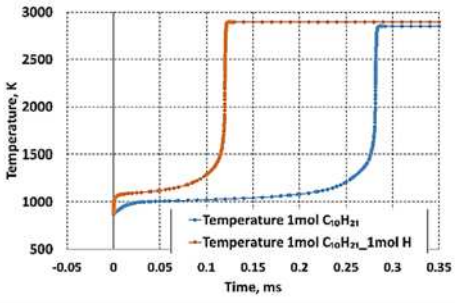

Fig. 3.13. The temperature vs. time with 1 mole fraction of hydrogen

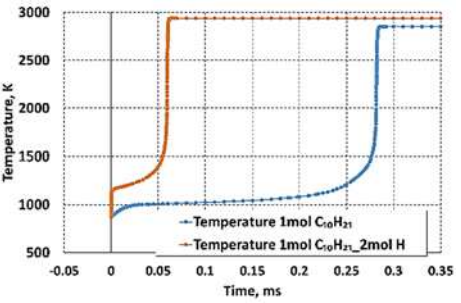

Fig. 3.14. The temperature vs. time with 2 mole fraction of hydrogen

Here m_{LF} = 212.47 g/mol, molar mass of biodiesel, m_H = 1.01 g/mol, molar mass of hydrogen. Then 1 mole mass fraction of the hydrogen m_{frH} = 0.5%, while 2 mole mass fraction will be 1%. The heating value of the combustion mixture

containing 1 mole of hydrogen and 1 mole of biodiesel was calculated by the formula 2.10:

$$H_{wtH-LF} = \frac{H_{wtLF} \cdot m_{frLF}}{100} + \frac{H_{wtH} \cdot m_{frH}}{100} =$$
$$43.7 \cdot 99.5\% + 120 \cdot 0.5\% = 44.08 \text{ MJ/kg.} \quad (3.12)$$

The 1 mole hydrogen energy fraction (HES) in the combustion bomb was 1.4%, while 2 mole hydrogen fraction – 2.7%.

The detailed analysis of the Fig. 3.13 and 3.14 revealed that combustion in both cases started at the same moment with first more rapid increase of temperature up to 1090 K due to the presence of 1 mole hydrogen and up to 1160 K influenced of 2 moles of hydrogen. The second sharp increase of temperature takes place within the certain period named by author, temperature increase lag or ROHR lag. This lag with biodiesel combustion was 0.28 ms and presence of the 1 mole hydrogen resulted in the shortening of the temperature increase lag by 0.16 ms. The presence of 2 hydrogen moles in the constant volume combustion chamber resulted in shortening of the ROHR lag by 0.22 ms. It can be concluded that increase of hydrogen mole fraction shortens the ROHR lag and at the same time auto-ignition delay.

3.1.5. Exhaust Emissions

The significant hydrogen fraction (more than 30%) decreased the CO and CO_2, as depicted in Fig. 3.15 and 3.16 respectively. However, with HVO within the range of the ML – NL, the CO increased by 13–15% when hydrogen fraction was 10–12% and further increase of HES decreased the CO. The similar trend was noticed with RME at the NL.

The RME has considerably higher C/H ratio than HVO, therfore it should lead to the higher carbon monoxide and carbon dioxide emissions. However, it shoul be considered that during performed tests the *IMEP* with HVO was higher on 30–35% than with RME. Considering that the difference of CO emissions are less than 20% if compare the RME and HVO, it can be concluded that the CO emissions are higher with RME than with HVO. The same conclusion is related to the CO_2 emissions. In fact both RME and HVO supports the considerable decrease of CO emissions when compare to the sole ULSD fuel. This phenomenon is explained by the presence of oxygen in the ester bonds of RME. The presence of oxygen supports higher amount of CO to be oxidized to CO_2.

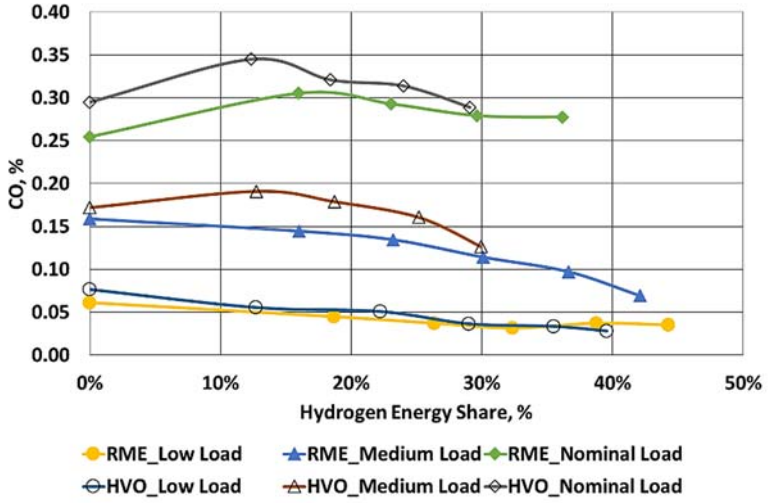

Fig. 3.15. The dependence of CO on fuel used, loads and HES

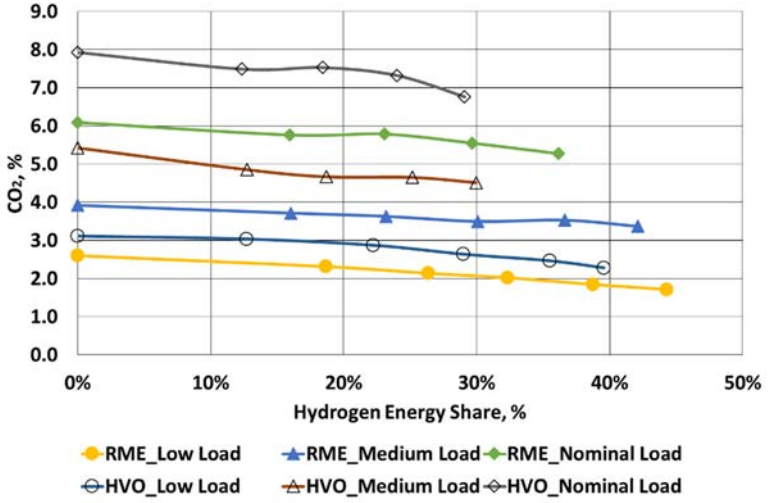

Fig. 3.16. The dependence of CO_2 on fuel used, loads and HES

The increased hydrogen increment rate caused the decrease of C/H ratio and that causes the reduction of CO and CO_2 emission in the exhaust gas as well as reduction of its exhaust opacity as shown at the Fig. 3.17.

Exhaust opacity decreases for both fuels RME, HVO with hydrogen increase, due to better premixing, shortening combustion duration and more effective flame penetration.

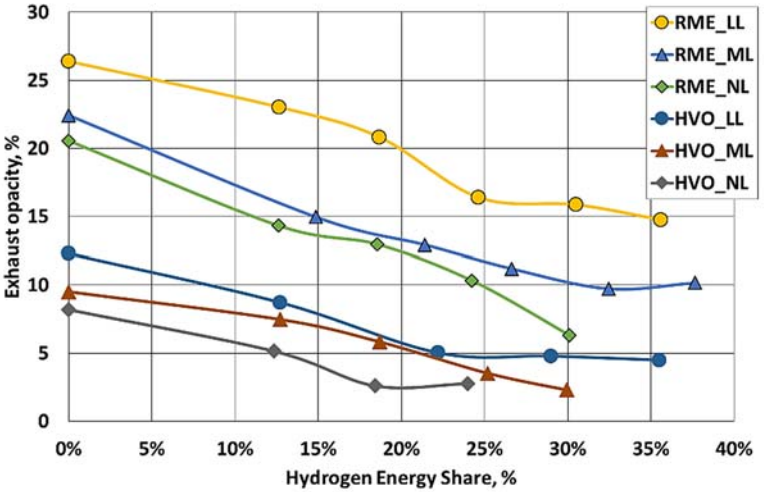

Fig. 3.17. The dependence of exhaust opacity on fuel used, loads and HES

The decrease of exhaust opacity as it shown at the Fig. 3.17, confirms the statement that with increase of HES the air and fuel mixture makes more homogenized. While the increase of hydrogen fraction in the mixture enhance the temperature and thus contribute the conditions for the formation of the NO (Fig. 3.18). The HES at the low load do not enhance the NO formation within the test range up to 40% HES. The highest increase of exhaust gas temperature with increase of HES, was measured within the range of 72–75 ºC at low load and medium load, while at nominal load it was 119 ºC. This increase of temperature determines the increase of NO from 770 ppm with HES = 0% to 1040 ppm with HES of 29%.

The addition of hydrogen up to 15% HES decreased the NO levels at ML and NL, however with the further HES increase of more than 15% NO increased significantly (Fig. 3.18). At the LL the increase of NO is negligible at the whole test range of HES because the lean hydrogen – air mixture does not support the flame propagation and results in low combustion temperature.

In general, NO increases and CO decreases with hydrogen increase above 10% during tests of both fuels and all engine loads. The increase of HES enhances the temperature, ROHR and contributes the increase of the NO. NO emission was lower for RME in comparison to HVO combustion.

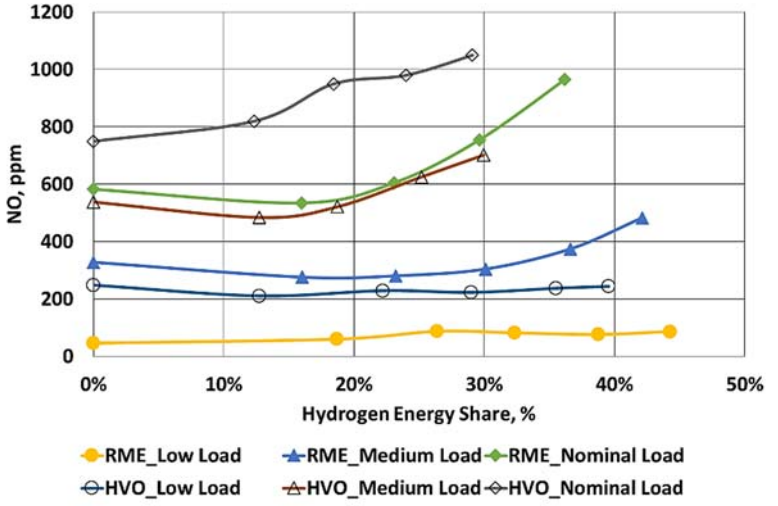

Fig. 3.18. The dependence of NO on fuel used, loads and HES

The HES = 23–26% was found as the optimal percentage with respect to NO emissions when tested with RME. When tested with HVO, the HES = 10–20% was the most suitable range with respect to overall toxic emissions. However, remarkable increase of the *ITE* was noticed when HES exceeds 20% with RME, and 26% with HVO.

Hydrocarbons are formed due to the incomplete combustion of hydrocarbon fuel. The dependance of unburnt hydrocarbon emissions obtained during experiments for various HES and loads with RME and HVO liquid fuels is depicted at the Fig. 3.19. The increase of HC emissions was noticed with lowest HES in compare to pure biodiesel. The combustion with amounts of lower than LFL, at HES = 12–20% was at relatively low temperature and was incompleate. That resulted in higher hydrocarbon emissions. With further increase of HES the HC decreased and with the amouts higher than 30%, it was lower than that with pure biodiesel. The highest decrease of HC was noticed at the nominal load with HVO – 16.7%, while with RME – 12.3% within the same range of HES = 0–35%.

The composition of the fuel influence the composition and magnitude of total hydrocarbons. Fuels containing high amount of aromatics and olefins produce relatively higher concentrations of hydrocarbons. The RME has higher concentration of aromatics therefore produce higher amount of hydrocarbons than that of HVO. The higher value of HC emission for RME compared to HVO could be explained as the poor atomisation and mixing characteristics as a result of high viscosity of the RME.

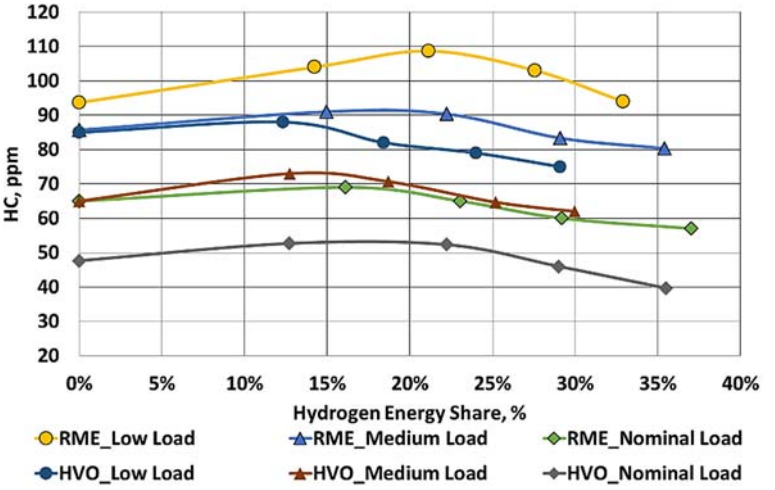

Fig. 3.19. The dependence of unburnt hydrocarbon on fuel used, loads and HES

The emission parameters of hydrogen co-combustion with RME and HVO obtained during experiments can be compared to the results and comments of other authors presented bellow.

Senthil Kumar (2003) and Bika *et al.* (2008) observed NO_x reduction at the low HES of 5%. This NO reduction is due to the slower combustion caused by a shorter auto-ignition dealy that contributes to advanced ignition, which decreases the combustion rate just after start of combustion (Grab-Rogalinski *et al.* 2016). At higher hydrogen rates of the test, NO pollutants increased (Fig. 3.18). The highest increase rate of NO was at the nominal load at the top HES of experiment. However, the increase of HES, led to a reduction of exhaust opacity (Fig. 3.17).

Karim (2007) noticed that with engine operation near stoichiometric mixture the high rate of heat relaese of hydrogen produce high pressures and temperatures, leading to the increased exhaust emissions of NO_x. Higher flame velocity of hydrogen and subsequently more heat release in the premixed combustion phase resulted the higher in-cylinder temperature leading to the increased formation of NO emission (Chelladorai *et al.* 2018, Serin *et al.* 2018).

The reduction in exhaust opacity, HC, CO and CO_2 levels were observed by Chelladorai *et al.* (2018) with hydrogen co-combustion with grapessed oil as the result of improved combustion due to the replacement of a hydrocarbon fuel with a carbonless fuel hydrogen. Serin *et al.* (2018) observed that tea seed oil enriched with 10 l/min of hydrogen also reduced the CO and CO_2 emissions up to 36% and 14%, respectively.

It was observed that during the engine operation with neat *Punica granatum* the NO_x increased with 25% (Tüccar *et al.* 2018). The increase of hydrogen fraction has marginal effect on NO_x emissions. The average of only 1% increase in NO_x emissions has been noticed with hydrogen supply. Increase of diffusion flame temperature was named as the main reason of NO_x increment. While the increased temperature of reaction is highly related to the increment of HES. However engine operation with neat *Punica granatum* revealed the significant decrease of CO emissions, and further decrease was noticed with hydrogen enrichment. The presence of extra hydrogen molecules with abundant amount of oxygen triggers the hydrogen oxygen reaction and formation of OH molecules, leading to the reduction of the CO.

The NO_x emissions was found to be higher of hydrogen co-combustion with neat *Pongamia pinata* to that of biodiesel in all test conditions, due to the increase of exhaust gas temperature up to 652°C (Jagedheesan *et al.* 2017). The formation mechanism of NO_x is directly related to the exhaust gas temperature. The significant reduction in emission of HC, CO, CO_2 is observed with the increase in hydrogen addition.

The summary of the publications of other authors on performance and emissions parameters with various hydrogen fractions referenced to the neat biodiesel is presented at the Annex B.

3.1.6. In-Cylinder Pressure Data Analysis Using AVL BOOST

AVL BOOST software was used to analyse the combustion processes with various HES and biodiesel mixtures of the CI engine. The following data was set into the AVL BURN utility: bore, stroke, compression ratio, clearance volume, length of the connecting road, number of strokes, volumes of intake and exhaust manifolds, engine speed, *BMEP*, SOC, CD, m_v, LHV of fuels. The simulation of the engine operation cycles were performed with created simulation model in AVL BOOST software. The AVL BOOST model depicted at the Fig. 2.9.

The SOC was considered the crank angle at which the curve of the ROHR changes its value from the negative to positive at the zero line cross (Fig. 3.20). The ROHR becomes negative due to the heat transfer to the combustion chamber and and by evaporation of the liquid fuel droplets. The time interval between the start of liquid fuel injection and the start of combustion of the mixture is referred to as auto-ignition delay and is a significant parameter of compression ignition engine.

The analysis of the AVL BOOST results of hydrogen co-combustion with HVO and RME, revealed that the hydrogen fraction affects the combustion intensity of the fuel mixture at the early stage of combustion process, only at ML and NL.

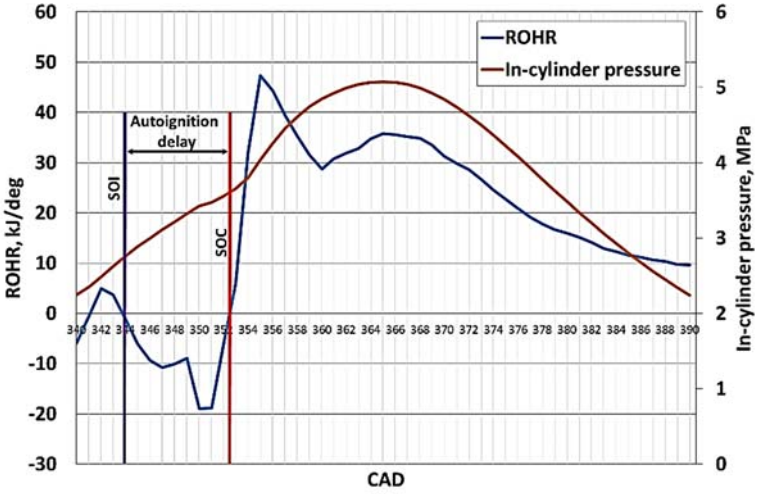

Fig. 3.20. The positions of the SOI and SOC, defined as zero line cross of ROHR

In-cylinder pressure measured during the tests for HVO+$H_2$0%, RME+$H_2$0%, HVO+$H_2$30% and RME+$H_2$30% can verify this phenomenon, presented at the Fig. 3.21 with the position of SOI of corresponding mixtures.

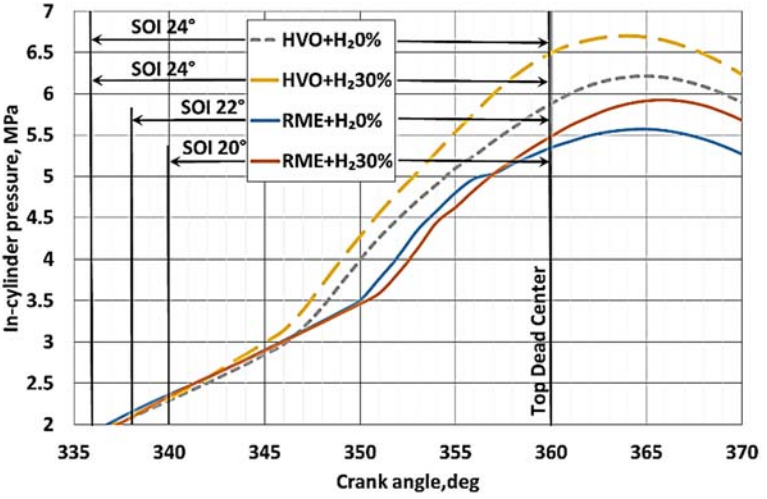

Fig. 3.21. In-cylinder pressure and SOI at the Medium Load

The SOI of 24° was set at the ML of HVO operation: HVO+$H_2$0 % and HVO+$H_2$30% (Table 3.1, test no. 9 and 10), SOI = 22° of RME+$H_2$0% (Table 3.1, no. 3) and SOI = 20° with RME+$H_2$30% (Table 3.1, no. 4).

The position of the SOC determined with SAWIR software was veryfied with AVL BOOST (Fig. 3.22–3.23).

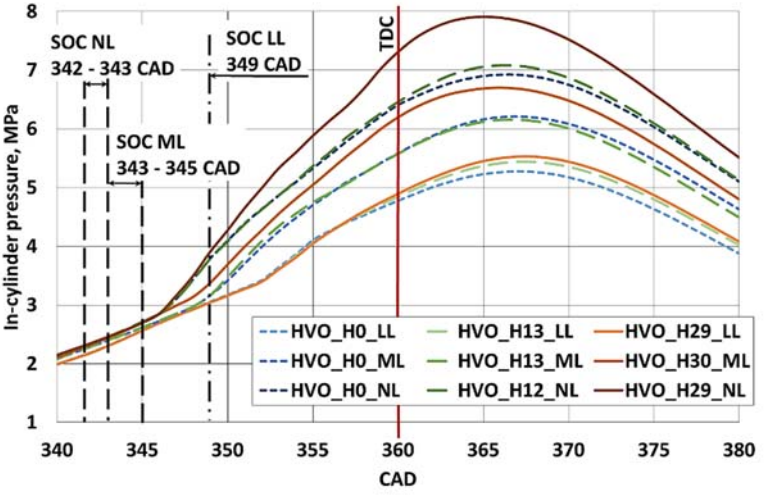

Fig. 3.22. The dependence of in-cylinder pressure of hydrogen co-combustion with HVO vs. CAD at various loads and HES

The SOC of hydrogen and HVO mixture at the LL occurs at the 349 CAD, at the ML and HES 0–25% at 345 CAD, at the ML and HES 30% at 345 CAD, at the NL and HES of 0–24% at 343 CAD, at the NL and HES of 29% at 342 CAD. Very slight influence of HES, was noticed at the LL (HES = 13–29%) and ML (HES = 13%). The more tangible impact of HES was noticed at ML (HES = 30%) and NL (HES = 29%). Due to the very intensive combustion after the SOC, the combustion intensity parameter decreased at ML and NL with increase of HES (Fig. 3.28). The early stage of the combustion of 0–10% MFB has the significant influence on the further combustion process. The combustion at that stage has mainly quasi-laminar character (Heywood 1988; Szwaja 2010) and high laminar flame speed of hydrogen, homogeneity of the mixture can stimulate the combustion process and heat release. However, it depends on the volume fraction of hydrogen and it LFL.

In-cylinder pressure curves for RME+$H_2$0%, RME+$H_2$32% at LL and RME+$H_2$30% at ML – NL are obtained after the AVL BOOST simulation

(Fig. 3.23). Pressure curves provided with the position of SOC of corresponding mixtures.

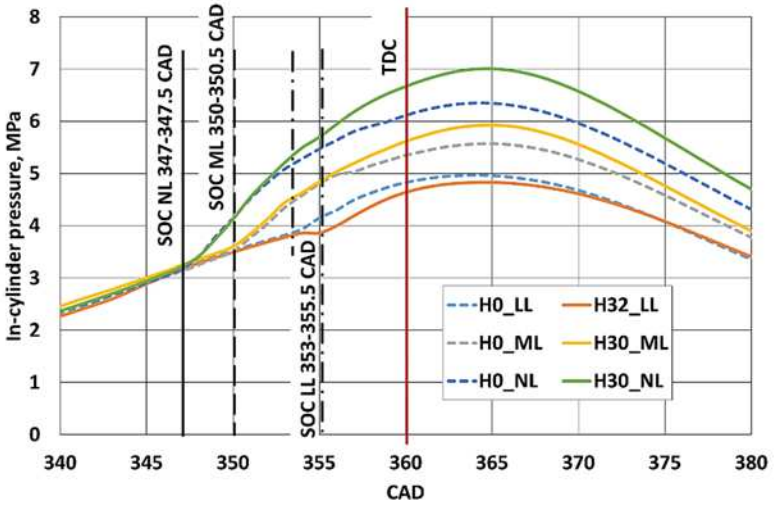

Fig. 3.23. The dependence of in-cylinder pressure of hydrogen co-combustion with RME vs. CAD at various loads and HES

In-cylinder pressure with sole RME at LL was higher than at operation with hydrogen. The hydrogen due to the low volume fraction in the combustion chamber not intensified the combustion. The lean hydrogen – air mixture does not support the flame propagation and results in rather low hydrogen combustion efficiency. After the boundary of hydrogen volume flammability lower limit was exceeded, with HES of 30% at ML and NL, the combustion became more intensive, especially at the premixed phase and in-cylinder pressure as well as p_{max} increased. The engine operation limits was noticed with RME as the abnormal combustion (knocking) appeared when λ reached the rich burn rates of 1.44–1.66 (at the NL) and HES more than 36%, as the injection timing fixed.

3.1.7. Pressure-rise and Heat Relaese Data Analysis Using AVL BOOST

The pressure-rise defined with AVL BOOST revealed that at the LL the hydrogen fraction do not affects significantly the combustion intensity of the fuel mixture. The lean hydrogen – RME mixture does not support the flame propagation and results the slow increase of the pressure-rise, plotted at the Fig. 3.24. The more significant increase of the pressure-rise because of HES noticed at the NL. The

combustion became more intensive at the premixed phase and *dp/dφ* increased from 0.256 MPa/deg to 0.304 MPa/deg. The presence of hydrogen do not influenced the pressure-rise at the LL and lean burn with λ = 3.26–3.92. The marginal increase of *dp/dφ* was only 4.6% with increase of HES from 19% to 32% influenced mainly by the low volumetric hydrogen fraction, which was insufficient to overcome the lower flammability limit of hydrogen.

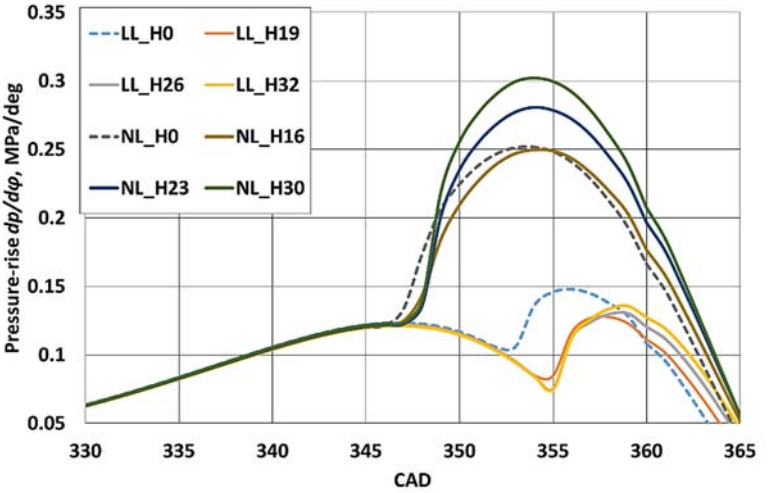

Fig. 3.24. The pressure-rise of hydrogen co-combustion with RME vs. CAD at the LL and NL with various HES

As observed from Fig. 3.25 and 3.26, there is significant difference in SOC with HVO at the various HES and loads investigated. The auto-ignition delay at NL was shorter (and SOC was earlier) by 1.5 CAD at HES = 29% in compare to the HES = 13–22 CAD (Fig. 3.24). The influence of HES at the LL has not been expressed as it was at NL, because the low volume fraction of the hydrogen in the combustion chamber. As mentioned before, the volume fraction of H_2 at LL tests are within the range of 1.38–2.87%, which is below the lower flammability limit of hydrogen – 3.0–3.1% and the combustion has not intensified by presence of the hydrogen.

The peak of ROHR at the NL was 105 J/deg with RME, while 101 J/deg with HVO, nevertheless that *IMEP* of HVO test was higher and mixture was more rich (λ = 1.41–1.54) than that of RME (λ = 1.62–1.98). The RME with high amount of aromatics produce the higher heating value, as it was depicted at the Fig. 3.27, despite that the combustion duration of CA 0–10 was within the same range of 16–22 CAD with both liquid fuels HVO and RME.

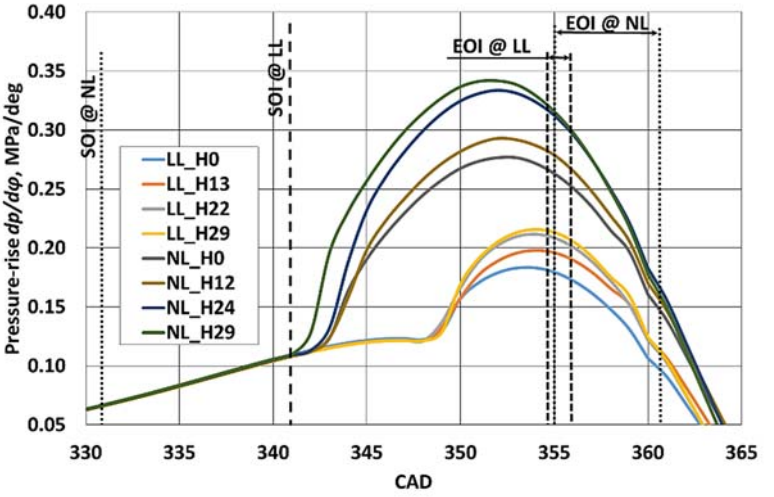

Fig. 3.25. The pressure-rise of hydrogen co-combustion with HVO vs. CAD at the LL and NL with various HES

The evidence of HES influence was the ROHR, which increased by 22% at NL and HES of 24– 29% (Fig. 3.26). The ROHR at LL increased by 21% with HES of 13–29%.

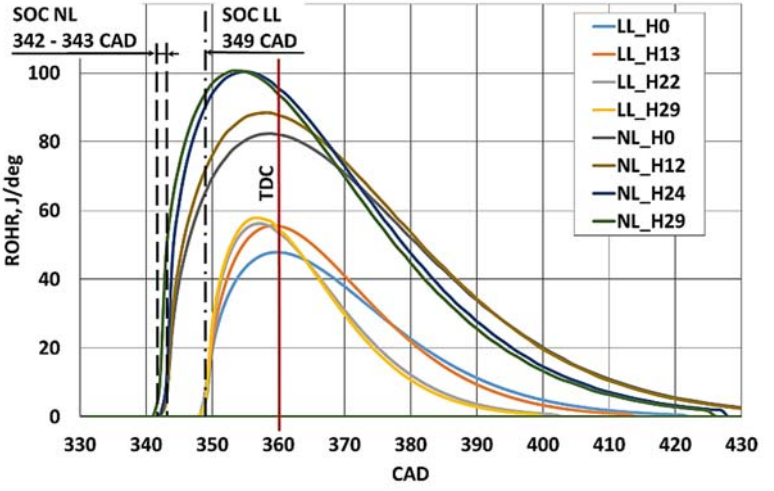

Fig. 3.26. The ROHR of hydrogen co-combustion with HVO vs. CAD at the LL and NL with various HES

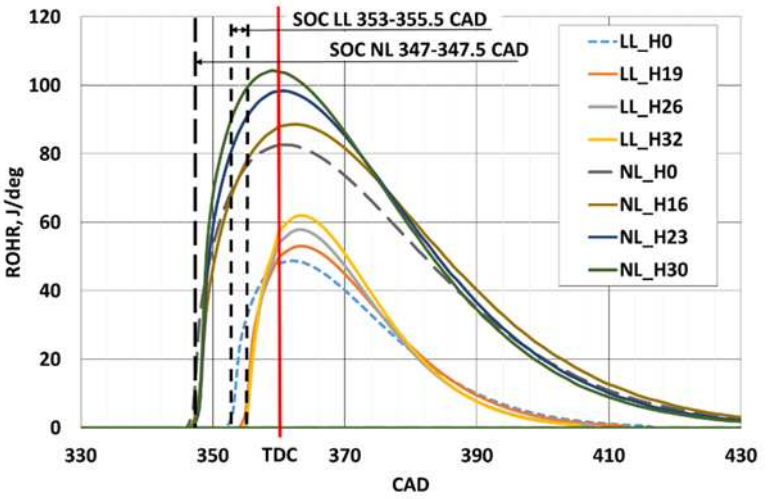

Fig. 3.27. The ROHR of hydrogen co-combustion with RME vs. CAD at the LL and NL with various HES

The increment of HES of the mixture with RME generated the step-by step increase of maximum ROHR by 27.1% from 48.76 J/deg to 61.98 J/deg at the low load (Fig. 3.27). At the nominal load, the ROHR maximum value increased from 82.64 J/deg to 104.35 J/deg. The $ROHR_{max}$ increased by 26.3%, slightly lower than at the low load. This result could lead to the contradiction with conclusion made before, that co-combustion of hydrogen with RME mixture at the LL was sluggish and hydrogen makes positive effect on the engine performance only with the LFL of 3.0–3.1% of hydrogen volume fraction. However, in this case most important factor is the lower heating value of the hydrogen – RME mixture. The lower heating value of the fuel mixture did not changed when λ decreased with increase of engine load at the same HES. Therefore ROHR increased by 26.3–27.1% and λ did not make significant effect. However this gain of ROHR determines the increase of NO with λ = 1.44–1.66, from 535 ppm with HES = 16% to 965 ppm with HES of 32% at the NL and matches well with the test results of other researchers (Barrios *et al*. 2017; Rocha *et al.* 2016).

3.1.8. Combustion Intensity and Duration Data Analysis Using AVL BOOST

During experiments, the engine operation limit was reached and the abnormal combustion (knocking) appeared when λ reached the rates of 1.44 at the NL and

with HES of 36%. The increase of shape parameter m_v was observed at the lean burn LL with HES up to 32% and decrease of shape parameter m_v was observed at the ML – NL with increase of HES to the engine operation limits.The shape parameter of hydrogen – HVO mixture decreased from 0.52 at LL to 0.39 at NL with HES of 29 % (Fig. 3.28). High intensity combustion occurs after the SOC with increase of HES. However, hydrogen fraction affects the combustion intensity of the fuel mixture only at ML and NL. As depicted in Figure 3.29, modeled combustion is getting shorter with higher amounts of hydrogen injected.

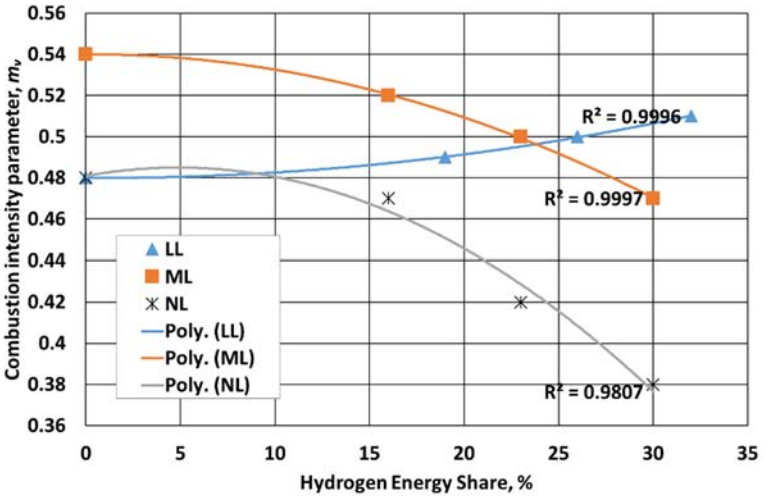

Fig. 3.28. The combustion intensity parameter vs. HES of hydrogen – HVO mixture

The same trend of combustion shape parameter and CD was noticed with RME. The simulation was performed with hydrogen fraction of 49%, 53%, 70%, 80%, i.e. more than during the experiment at LL, with presumption to get the combustion intensity behavior with higher HES. Also the hydrogen – RME mixture mass flow rates determined and input to the AVL BOOST. The numerical simulation was performed at the same engine speed of 960 rpm, and with decreasing λ as the air mass flow rate decreased due to significantly increased hydrogen flow rate. In fact the lower heating value of the fuel mixture reach the value of 73.5–74.2 MJ/kg, twice as the lower heating value of sole RME.

The shape parameter m_v of the Wiebe function increased from 0.48 with sole RME to 0.52 with RME+H_2 32%, due to the low hydrogen combustion efficiency, the intensity moved to the middle of the combustion process when simulated at the LL. Then m_v maintains the decreasing trace to 0.44 with RME+H_2 80%.

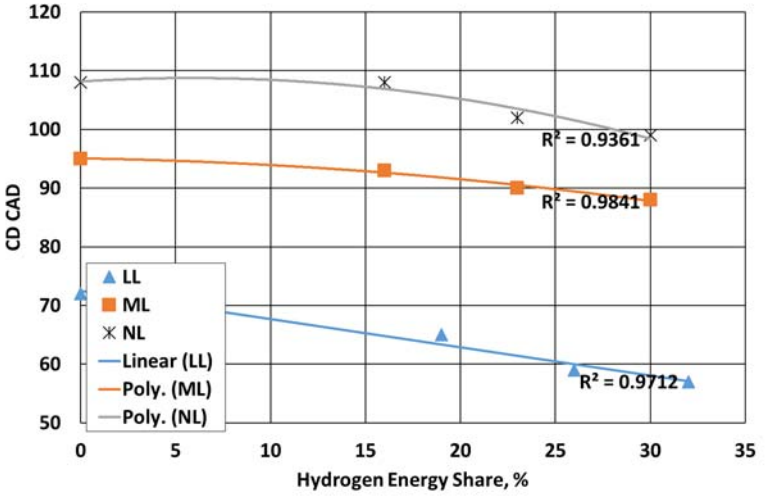

Fig. 3.29. The combustion duration vs. HES of hydrogen – HVO mixture

This simulation case confirms the conclusion that when the LFL was achieved with RME+H_2 32%, the hydrogen co-combustion efficiency with RME increased, with increment of the intensity at the beginning of combustion process, which is confirmed by lower m_v (Fig. 3.30).

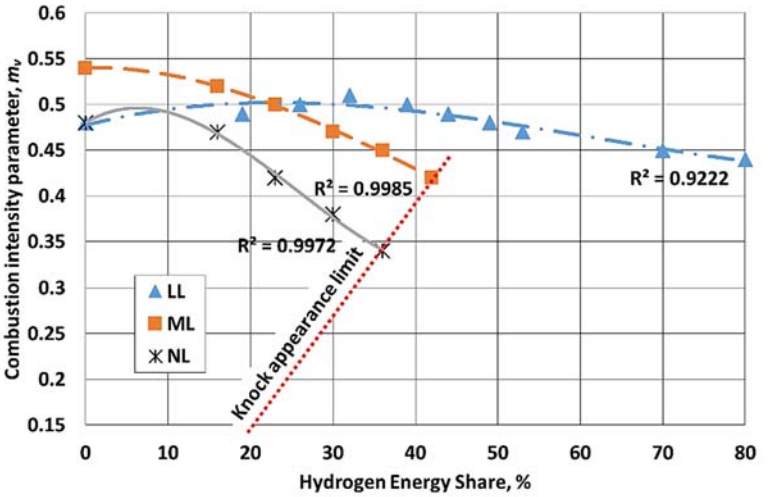

Fig. 3.30. The trend lines of combustion intensity shape parameter m_v vs. HES of hydrogen – RME mixture

The combustion intensity shape parameter m_v decreased with increase of HES at the ML and at the NL. The increasing hydrogen fraction for rich combustible mixtures has inherent ability to accelerate the laminar flame speed and the intensity of combustion at the beginning. Due to the high premixed combustion rate increased the ROHR (Fig. 3.27).

However, with the HES of 42% at the ML and with HES of 36% at the NL abnormal combustion appeared during experiments therefore the AVL BOOST simulation was not performed. Moreover the trend lines of combustion intensity shape parameter m_v, at the HES of knock appearance were sufficient to conclude the decreasing tendency of m_v.

The hydrogen volume fraction was within the range of 6.91–7.83 when knocking started at the ML and NL. The knock appearance limit could dependent on other engine parameters such as SOI, engine speed, compression ratio, hydrogen supply mode.

The combustion intensity was concentrated at the middle of the combustion process until the LFL = 3.0–3.1% of hydrogen was achieved with RME+H32% at the LL. Then concentration of the combustion intensity moved to the beginning of combustion with HES = 39–80%, which was confirmed by lower m_v obtained during the AVL BOOST simulation. The CD shortened with increase of HES without any significant ups and downs when simulated (Fig. 3.31).

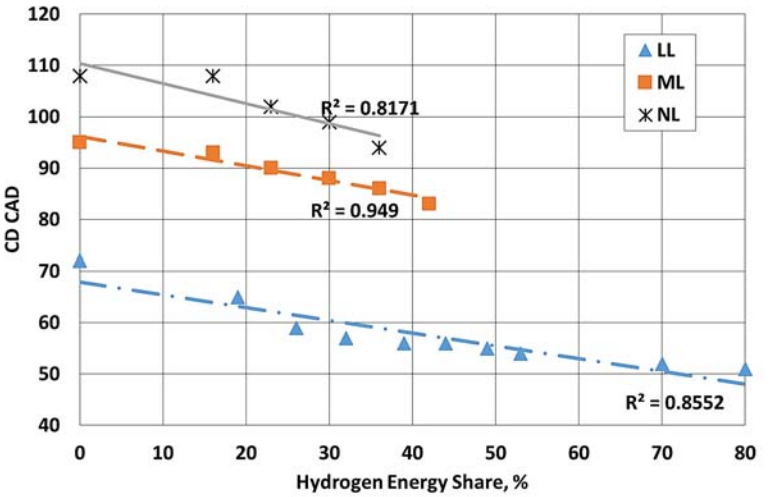

Fig. 3.31. The combustion duration vs. HES of hydrogen – RME mixture

The CD shortened by 29.2% from 72 CAD to 51 CAD at the LL. The presence of hydrogen contributes to decrease the CD due to the high premixed combustion rate and impact of higher laminar speed of hydrogen flame. Increase of hydrogen fraction also reduces the main combustion duration CA 10–90, which was accelerated by the intensified first combustion phase CA 0–10.

3.2. Reaserch of Hydrogen Co-Combustion with Hydrotreated Biodiesel / Petroleum Diesel Mixture and with pure Hydrotreated Biodiesel

3.2.1. Experimental Investigation

Each experiment conducted at the various *IMEP*. The *IMEP* managed by changing the amount of the LRF and HRF supplied to the combustion chamber. The LRF – hydrogen supplied together with air into the intake manifold. In cylinder, homogeneous air – hydrogen mixture under the elevated heat and pressure ignited by injected HRF.

The injection timings φ_{i1} and φ_{i2}, loads corresponding *IMEP* and equivalence ratio (λ) at various composition of combustible mixture presented at the Table 3.2.

Table 3.2. SOI, loads, IMEP and equivalence ratio (λ) at various composition of combustible mixture

Test no.	Composition of combustible mixture	SOI φ_i, bTDC	Loads	*IMEP*, kPa	λ
1	HVO+H_2 0%	φ_{i1} = 18°	LL	344.9	3.78
2	HVO+H_2 (13–35%)	φ_{i2} = 18°	LL	376.0–376.7	3.80–3.31
3	HVO+H_2 0%	24°	ML	519.8	2.22
4	HVO+H_2 (13–30%)	24°	ML	494.8–538.5	2.15–1.93
5	HVO+H_2 0%	28°	NL	651.8	1.55
6	HVO+H_2 (12–24%)	28°	NL	645.8–691.5	1.43–1.42
7	PRO Diesel+H_2 0%	18°	LL	367.6	3.37
8	PRO Diesel+H_2 (17–34%)	18°	LL	406.0–417.7	3.75–3.07
9	PRO Diesel+H_2 0%	26°	ML	533.2	1.99
10	PRO Diesel+H_2 (13–26%)	26°	ML	579.7–620.1	1.91–1.88
11	PRO Diesel+H_2 0%	28°	NL	590.1	1.41
12	PRO Diesel+H_2 (13–24%)	28°	NL	652.9–717.8	1.37–1.28

The analysis of the experiments, presented in thesis, are based on the in-cylinder pressure data acquisition. The term HES could be replaced by premixed energy ratio – PER, which is commonly used in some articles, related to the RCCI startegy. Both HES and PER are defined as the energy ratio of the LRF versus the total delivered energy (Benajes *et al.* 2015). At the each specific HES, the total energy delivered to the cylinder was kept constant during the tests. In order to keep the constant total energy, the mass of LRF and HRF was adjusted as required to compensate the differences in LHV. The impact of HES on combustion properties and combustion duration of the engine operating with the HVO and PRO Diesel at three engine loads studied.

Typically, the reactivity in RCCI combustion mode is characterized by global reactivity and reactivity stratification (Li *et al.* 2014). Most of the subsequent studies are performed using double and triple injection pulses of HRF. Such injection strategy with varied LRF/HRF ratio provides the global and reactivity stratification. However, Li *et al.* (2013) investigated the RCCI startegy with single injection timing φ from 30º to 15º bTDC, while Benajes *et al.* (2014) from 37º to 7º bTDC and Liu *et al.* (2014) from 43º to 35º bTDC. In this article only the global reactivity was studied, which determined by the amount of LRF and HRF and single injection timing φ (from 28º to 18º bTDC) of HRF, which was determined at the position of 50% MFB, corresponding to the peak of indicative pressure in cylinder at the lowest HES at each load (Table 3.2). SOI was fixed with the further HES at the certain load.

3.2.2. Engine Performance

Increase of HES enhances the p_{max} of all tested loads as the result of the considerably higher heating value of hydrogen, higher flame velocity and increasing reaction rates. However, the lean LRF/HRF mixture does not support the flame propagation due to the too low hydrogen volume fraction, which was insufficient to reach the LFL and results the negligible increase of in-cylinder maximum pressure. The efficient hydrogen co-combustion with injected HRF starts with increased HES at ML (HES = 30%) and NL (HES = 29%), corresponding to the LFL = 3.0–3.1% of hydrogen. Fig. 3.32 illustrates the variation of in-cylinder maximum pressure with various HES at LL, ML and NL.

The increasing trend of in-cylinder maximum pressure noticed with increase of HES within all range of loads. The increase of in-cylinder maximum pressure at LL was negligible, it was 7.9% at ML and 14.3% at NL with HVO. The presence of hydrogen increased the maximum pressure at at ML by 14.7% and by 18.2% at NL with PRO Diesel. The negligible influence of hydrogen fraction at the LL and partially at the ML can be explain by the low volume fraction of the

hydrogen in the combustion chamber, which was below of the LFL of hydrogen (Table 1.3).

The flammability limits of the hydrogen-air mixture are changing with increase of temperature and pressure. The temperature was within the range of 404–424 ºC with both fuels during the experiment performed by author. At this temperature, the LFL decreased to 1.5% of hydrogen volume fraction. However with increase of pressure the LFL increased.

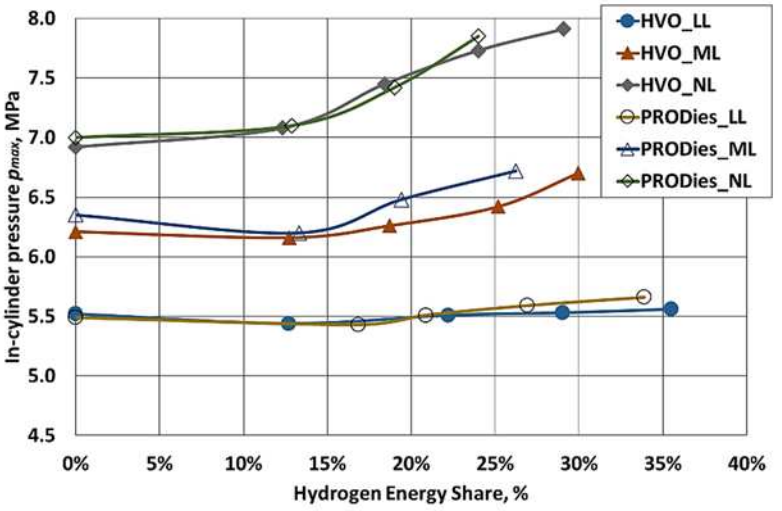

Fig. 3.32. In-cylinder max pressure p_{max} vs. HES at various engine loads

Considering above mentioned, at the moment of the SOC the pressure was 3.52 MPa (35.2 bar) and the LFL was 3.0–3.1% of hydrogen volume fraction. Therefore we can conclude that only when this LFL was achieved, hydrogen effectively co-combusted with injected HRF. Before that, the lean mixture of air – hydrogen with HRF burns incompletely and does not make positive effect on the combustion intensity and engine performance (Verhelst *et al.* 2009). The lean hydrogen – air mixture does not support the flame propagation and results in rather low hydrogen combustion efficiency (Saravanan *et al.* 2007). The same explanation related to the poor performance of p_{max} with low HES and rich fuel mixtures at ML and NL.

The *ITE* increased steadily with increase of the HES with both tested fuels (Fig. 3.33), and that increase was more significant with PRO Diesel noticed. The efficiency of the engine was higher with PRO Diesel, because of the *IMEP* during tests was higher than that of during tests with HVO.

During combustion, the amount of energy released from the combustible mixture is the product of the cyclic mass of the combustible mixture and the calorific value of the mixture or the calorific value. The increase of HES enhanced the fraction of the low-density fuel (hydrogen) of the mixture. Since the cyclic amount of heat during the test of each load was the same, the *ISFC* decreased. With the increase of the hydrogen energy share from 0 to 38%, the *ISFC* decreased and therefore the engine efficiency increased. These changes results the 6% increase of the *ITE* with PRO Diesel at the low load.

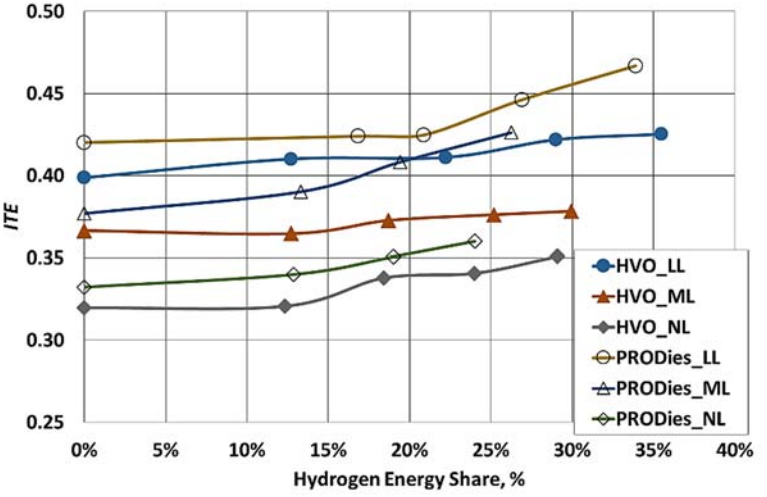

Fig. 3.33. *ITE* vs. HES of HVO and PRO Diesel at various engine loads

The negligible lower auto-ignition temperature of HVO (204 ºC) than PRO Diesel (210 ºC), do not influenced the auto-ignition delay. The biggest influence on the *ITE* was made by increased mass flow rate of the hydrogen as the response to the decreased total fuel mass flow rate. The *ITE* increased by 5.0–6.5% with HVO at whole range of loads, and by 6.5% at the LL and by 13.2–13.9% at the higher loads with PRO Diesel, as the increasing hydrogen fraction affects the combustion intensity more tangible when rich burn with $\lambda = 1.42–1.43$ for HVO and $\lambda = 1.28–1.37$ for PRO Diesel. The *ISFC* decreased steadily with increase of the HES with both tested fuels as presented at the Fig. 3.34.

Due to the increase of LRF – hydrogen, the *ISFC* decreased, because the hourly heat value of the hydrogen directly correlated with HES, while the *ISFC* of HRF decreased with increase of HES. The higher *ISFC* of PRO Diesel at the

NL can be attributed mainly to the higher mass flow rate of liquid fuel – PRO Diesel.

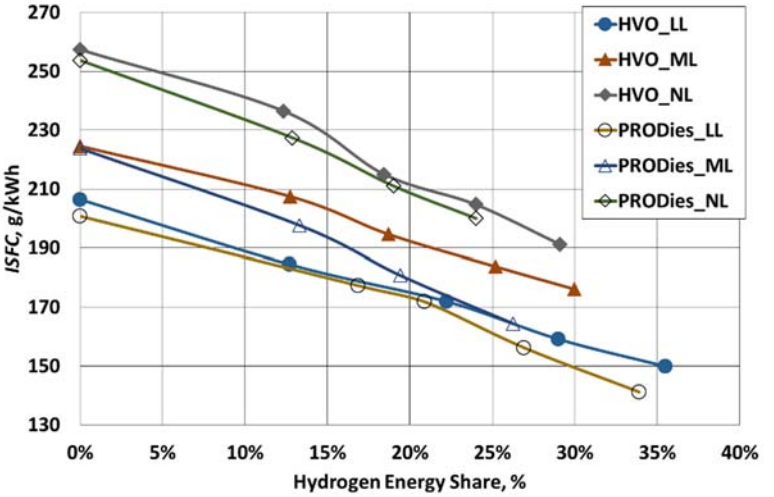

Fig. 3.34. *ISFC* vs. HES of HVO and PRO diesel at various engine loads

The *ISFC* decreased by 18–22% for HVO and by 19–23% for PRO Diesel with increase of the mass flow rate of hydrogen and HES. The substitution of HRF by LRF makes positive affect on the *ISFC*.

3.2.3. Exhaust Emissions

The unburned hydrocarbons are formed when they are prepared insufficiently, i.e. atomized fuel reaches the low temperature regions. The HVO was the fuel with the lowest density of the tested fuels and it has the lowest fraction of aromatics. The evidence of that was lower hydrocarbon emissions in compare to the PRO Diesel (Fig. 3.35), however at the nominal load the difference was marginal, probably due to the inacurate measurements.

With the enhencement of hydrogen energy share, the HC reduction was observed as a result of improved combustion and decrease of carbon to hydrogen ratio at the combustion mixture because of carbonless fuel – hydrogen get in of together with air. Furthermore, the combustion of hydrogen increases the in-cylinder temperature and accelerates the chemical reaction rates exponentially, resulting in increased rate of the oxidation and hydrocarbon emission.

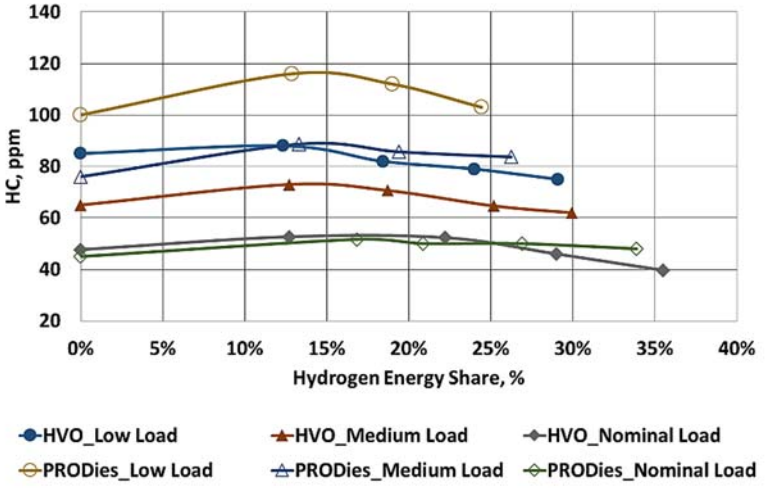

Fig. 3.35. The dependence of HC on fuel used, loads and HES

The CO and CO_2 emission levels (Fig. 3.36, 3.37) were observed with increased hydrogen increment rate, as result of improved combustion and replacement of the certain hydrocarbon fraction.

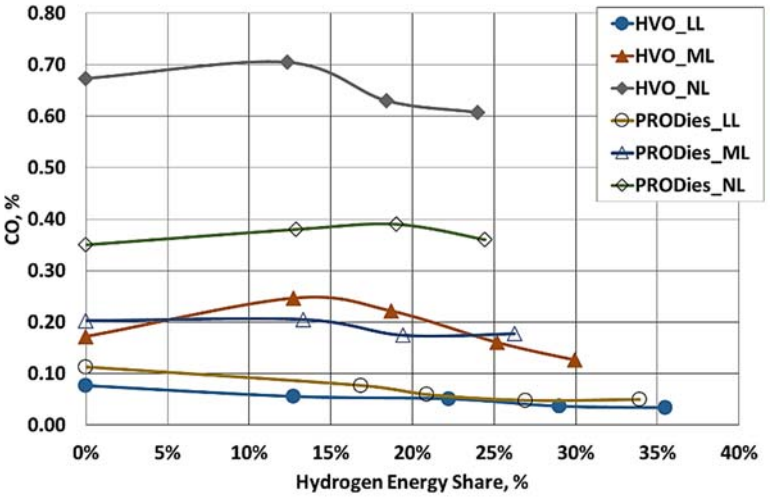

Fig. 3.36. The dependence of CO on fuel used, loads and HES

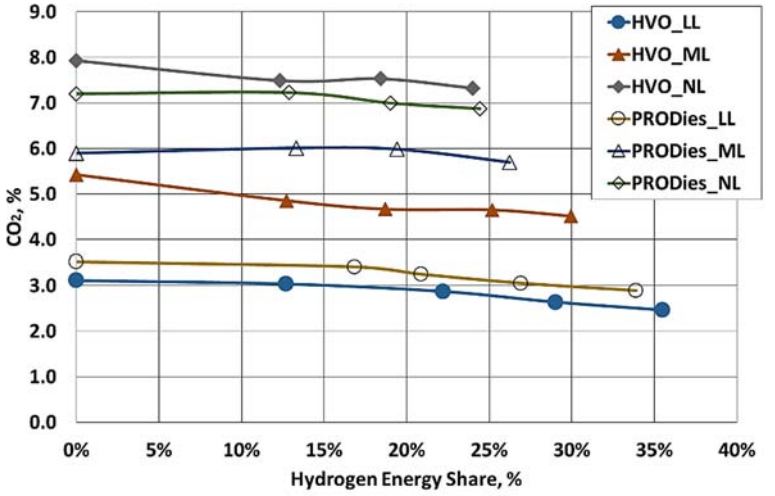

Fig. 3.37. The dependence of CO_2 on fuel used, loads and HES

The HRF used during tests has lower C/H ratio in compare to the petrol DF. On top of that, the increased hydrogen increment rate caused further decrease of C/H ratio and that causes reduction of CO and CO_2 emission in the exhaust gas as well as reduction of its exhaust opacity as shown at the Fig. 3.38.

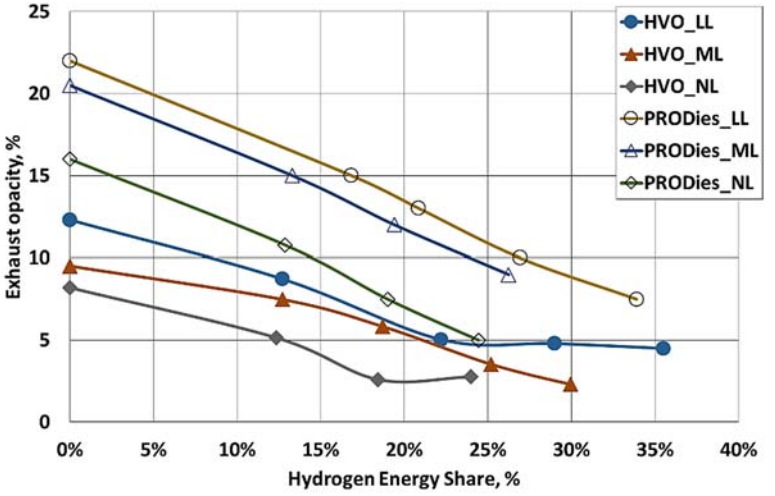

Fig. 3.38. The dependence of exhaust opacity on the load and HES

Other reason is that, increase of HES makes better-homogenized mixture of air and LRF, which leads to the decrease of exhaust opacity.

The addition of hydrogen up to 10–12% HES do not effect NO with both HRF (HVO and PRO Diesel), however with the further HES increase of more than 15% NO increased significantly (Fig. 3.39). At the LL, the increase of NO is negligible at the whole test range of HES because the lean hydrogen – air mixture does not support the flame propagation and results in low combustion temperature.

The increase of HES enhances the temperature, ROHR and contributes the increase of the NO. The HES = 13–17% was found as the optimal percentage with respect to NO emissions.

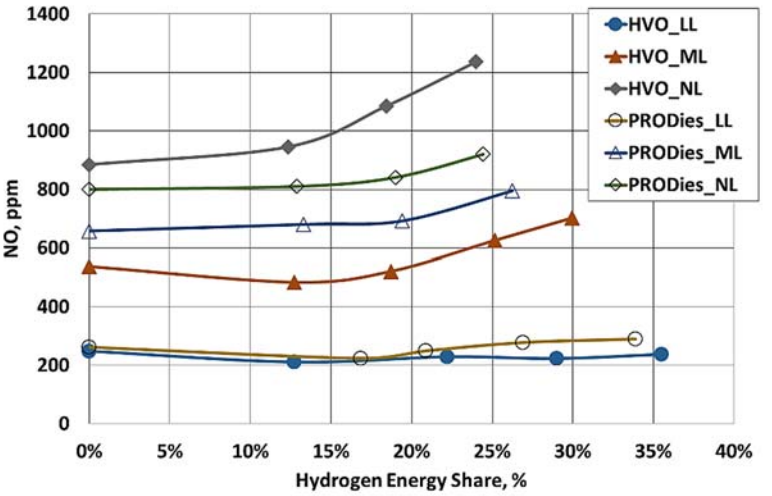

Fig. 3.39. The dependence of NO on the load and HES

The amount of exhaust opacity depends on the CN, soot particles formation and burning rate set up by diffusion phase at the final combustion stages depending on the chemical structure and amount of the fuel injected (Labeckas *et al.* 2014). However, with increase of hydrogen fraction, the combustion became more intensive at the premixed phase, the burning rate at the diffusion phase as well as the CD makes shorter and that can be related to the significant decrease of exhaust opacity with increase of HES (Fig. 3.38). The exhaust opacity measured for the HVO was lower that for PRO Diesel, because of chemical structure and physical properties of the fuel, i.e. lower density and kinematic viscosity than that of PRO Diesel. According to investigations (Chen *et al.* 2013), the HVO presents smaller

SMD than PRO Diesel and better-homogenized mixture guiding to the lower exhaust opacity.

3.2.4. Mass Fraction Burned

The combustion duration of CA 0–10 (Fig. 3.40) and CA 10–90 (Fig. 3.41) calculated at each *IMEP* and with each hydrogen fraction for HVO and PRO Diesel according to the MFB profiles. Additionally, the location of the maximum rate of MFB, the locations of the 50% MFB and the maximum rate of MFB were determined.

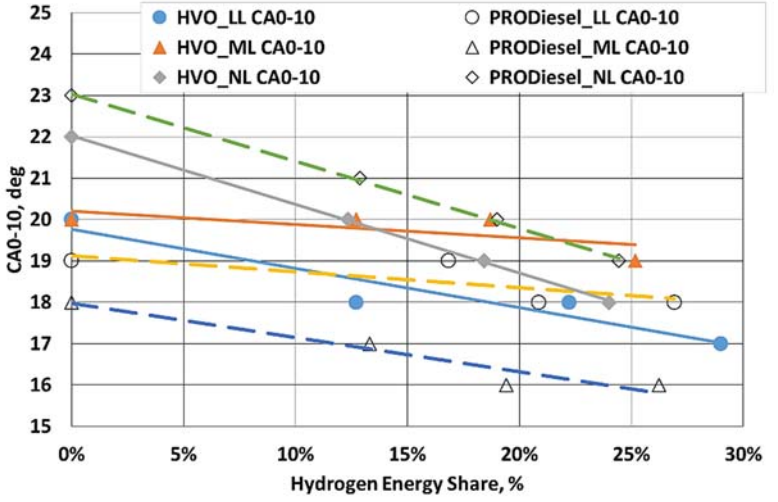

Fig. 3.40. The combustion phase CA 0–10 vs. HES for HVO and PRO Diesel

The test results show that increase of the hydrogen fraction have an impact on the fuel mixture reactivity, which determines the shortened auto-ignition delay (lag). The auto-ignition is the chemical reaction, which releases the energy at the such rate, which is sufficient to sustain combustion without any external energy source. The auto-ignition delay was shortened due to the high premixed combustion rate and development of higher laminar speed of hydrogen flame. In fact, the auto-ignition delay time is defined as the time intervals of chemical and the physical processes of ignition. The physical process includes the heat conduction, diffusion and mixing of reactants and chemical process based on pre-flame reactions, radical concentration governed by chemical kinetics. Thus auto-ignition delay time is important in developing RCCI strategy and it has been frequently used to validate chemical kinetic mechanisms (Tang *et al.* 2014).

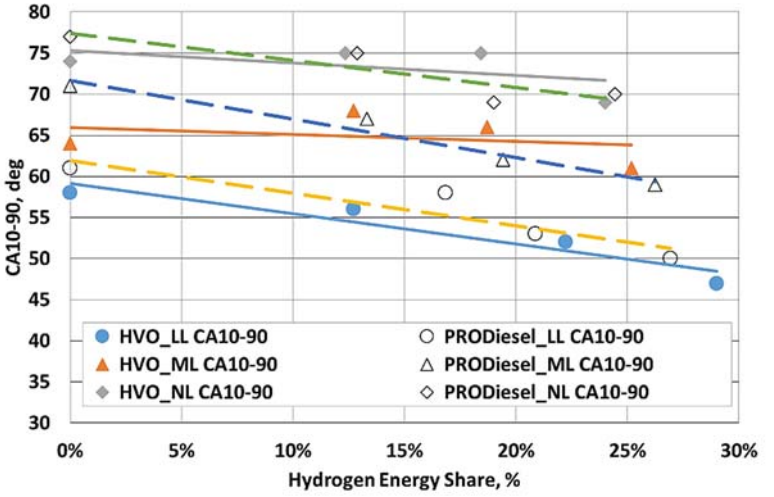

Fig. 3.41. The combustion phase CA 0–90 vs. HES for HVO and PRO Diesel

The combustion starts with the ignition of the injected HRF. Then, the flame propagation across the lean zones of the combustion chamber enhance the temperature and pressure rise. As the LRF/HRF ratio increased, due to the high penetration of hydrogen into the mixture, the mixing time makes shorter and the first combustion stage expressed by CA 0–10 lowered. As the HRF injection timing was fixed at the lowest HES at each load, the further increase of HES shortened auto-ignition delay over combustion process. Increase of hydrogen fraction also reduces the main combustion duration CA 10–90 (Fig. 3.41) which was accelerated by the first combustion phase CA 0–10. The combustion duration of CA0–10 varying with PRO Diesel within the range of 16–23 CAD, while with HVO it was shorter: 17–22 CAD. The CA 10–90 with increase of HES was reduced by 12–16% with both tested fuels.

Different trend of the combustion duration of CA0–10 was noticed at the ML with PRO Diesel in compare to HVO. The CD of PRO Diesel was significantly shorter than that with HVO at ML, while at other two loads (LL and NL) it was vice versa. It occurs due to the different SOI at ML, though at other loads the SOI was the same with both HRF (Table 3.2). The SOI with HVO was 24º bTDC while with PRO Diesel it was more advanced – 26º bTDC. Thus, it additionally confirms that SOI is another tool for adjustment of the performance of RCCI engine tested by several authors (Benajes *et al.* 2015; Li *et al.* 2014; Li *et al.* 2016; Reitz *et al.* 2015).

The maximal rate of MFB was higher with HVO than with PRO Diesel, therefore the CA0–10 was shorter. The CN of HVO is higher and the auto-ignition delay is shorter than PRO Diesel.

The abnormal combustion appeared with the hydrogen volume fraction of 5.0–5.5% at the ML and 6.51–7.15% at the NL, as the SOI of the HRF was fixed. Therefore, the control of the SOI and the amount of HRF is one of challenges for RCCI combustion, especially at rich burn and high loads. With the early injection of 26º bTDC at the ML with PRO Diesel was noticed the shorter combustion duration of CA0–10 in compare to the lean burn of HVO and PRO Diesel.

3.2.5. In-Cylinder Pressure Data Analysis Using AVL BOOST

At the lean mixture (Table 3.2, test no. 1, 2, 7, 8) the combustion of hydrogen with HVO and PRO Diesel is hydrogen assisted and combustion of hydrogen is sluggish, therefore increase of in-cylinder pressure with increase of HES is negligable. The in-cylinder pressure data presented at the Fig. 3.42 and 3.43 with the positions of SOC of corresponding mixtures.

The p_{max} (Fig. 3.32) and in-cylinder pressure for PRO Diesel at the ML was higher than that of HVO at the whole test range of hydrogen fraction starting from 0%, because the SOI (Table 3.2) and SOC with PRO Diesel at ML takes place earlier than with HVO and the pressure-rise in this case faster.

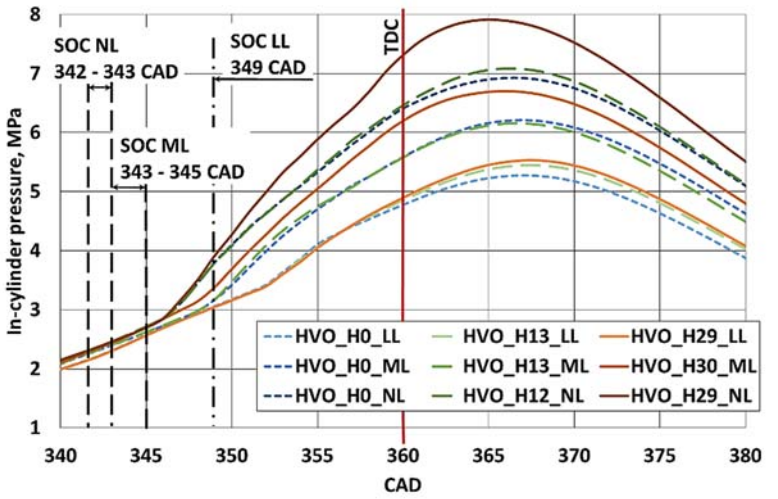

Fig. 3.42. In-cylinder pressure dependence on CAD and position of SOC at various loads and HES with HVO

The heating value of PRO Diesel stoichiometric mixture (on both volume and weight basis) is higher than that of HVO (Table 2.8) and in-cylinder pressure should be higher. However, the CN of HVO has advantage against PRO Diesel, the auto-ignition delay with HVO is shorter and pressure-rise faster. Therefore, at the NL when the SOI was the same at HVO and PRO Diesel, in-cylinder pressure was higher with HVO.

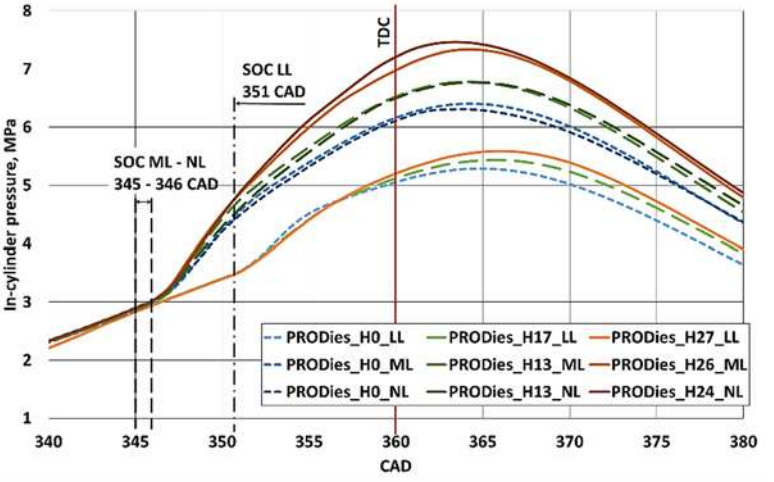

Fig. 3.43. In-cylinder pressure dependence on CAD and position of SOC at various loads and HES with PRO Diesel

The test performed on hydrogen co-combustion with HVO and PRO Diesel revealed the improvement of *ITE*, low CO, CO_2 and exhaust opacity. The addition of hydrogen has a greater effect on the beginning stages of combustion than in later stages of combustion when tests performed with fixed SOI of the HRF. Further optimization of RCCI strategy parameters such as HRF injection strategy modifications are required to realize the potential of dual-fuel operation. Investigation on the abnormal combustion (knocking) of RCCI with development of the model to detect the knock combustion makes it the subject of the research interest (Li *et al.* 2017).

3.2.6. Influence of Injection Timing Adjustment on Performance and Exhaust Emissions Parameters

The further step to perform the RCCI strategy was tests with adjustment of injection timing of HRF: HVO and PRO Diesel at low loads and at nominal loads. The data of obtained during these tests are presented at the Table 3.3. The tests

were performed within the narrow range of HES of 24–29%. In order to determine influence of injection timing on performance and exhaust emission parameters, the test data of the previous test presented at the subchapter 3.2.1, compared to the test data performed with adjusted injection timing (denoted at the Table 3.3 as φ_{i3}). The injection timing φ_{i3} was set at the position of of 50% MFB, which was targeted to be within the range of 8–12 CAD aTDC. Tests performed with adjusted injection timing denoted at the Table 3.3 as 2a, 6a, 7a and 12a, which corresponds to the designation of the tests of Table 3.2. The *IMEP* was set with a small deviation at the same level as before. The *IMEP* was within the range of 370.5–376 kPa at the LL, while 689.6–688 kPa at the NL with HVO and *IMEP* = 416.8–418.8 kPa at the LL, *IMEP* = 675.3–675.7 kPa at the NL with PRO Diesel.

Table 3.3. Dependance of *ITE* and NO emissions on SOI.

Test no.	Composition of combustible mixture	SOI φ_i, bTDC	Loads	*IMEP*, kPa	*ITE*	NO, ppm
2	HVO+H_2 29%	φ_{i2} = 18°	LL	376.0	0.420	223
2a	HVO+H_2 27%	φ_{i3} = 16°	LL	370.5	0.428	178
6	HVO+H_2 24%	φ_{i2} = 28°	NL	689.6	0.341	1236
6a	HVO+H_2 24%	φ_{i3} = 22°	NL	688.0	0.350	734
7	PRO Diesel+H_2 27%	φ_{i2} = 18°	LL	416.8	0.445	278
7a	PRO Diesel+H_2 29%	φ_{i3} = 16°	LL	418.8	0.449	203
12	PRO Diesel+H_2 24%	φ_{i2} = 28°	NL	675.3	0.360	920
12a	PRO Diesel+H_2 24%	φ_{i3} = 20°	NL	675.7	0.363	566

The tests revealed the influence of SOI adjustment with HES, *IMEP* and load were maintained at the same level. The decrease of injection timing with 2 CAD at low load resulted in drop of NO by 20–27% with both tested biofuels. While decrease of SOI with 6 CAD with HVO and 8 CAD with PRO Diesel load resulted in significant decrease of NO by 38–40% at the nominal load. The adjusted SOI of HRF effected the maximum in-cylinder temperature mode. The fast increase of pressure-rise was better controlled with later injection of HRF and lead to the lower in-cylinder temperature. The adjustment of SOI resulted in decrease of T_{max} by 23–24K at the LL, while 60–86K at the NL with both compared fuels. However the exhaust gas temperature gain increase in 9°C at the LL and 26–27°C at the NL. Such the increase could be explained by the later combustion phase in relation to CAD and the shorter time of cool down of the exhaust gases.

The marginal increase of *ITE* was noticed with PRO Diesel at both loads. However, the 1.9–2.6% increase of *ITE* and almost the same decrease of *ISFC* was the result of adjustment of SOI with HVO. The adjustment of SOI makes positive effect on performance parameters due to the initial phase of combustion CA0–10 occurs in the position where piston moves downwards and release the heat more efficiently.

The adjustment of the SOI φ_{i3} makes positive effect on abnormal combustion, which was noticed during tests with SOI timing of φ_{i2}. The increase of HES shortening the auto-ignition delay and sudden increase of pressure-rise and ROHR leads to the abnormal combustion, which reason could be a pin-shape pressure pulse appeared just after the sole hydrogen self-ignition. This self-ignition could be explained as the result of extremely low minimum ignition energy of hydrogen, that provides high probability of coincidental ignitions. However with the adjustment of the SOI φ_{i3} the abnormal combustion was avoided.

The increase of exhaust opacity in 14–18% occured when SOI was adjusted with both fuels at the low load. The HES effected the duration of the initial phase of combustion CA0–10 at the low load not as efficiently as at the nominal load. The low hydrogen volume fraction being below of the LFL of hydrogen not supported the hydrogen oxidation chain of reactions, which are responsible for the auto-ignition delay. The hydrogen volume fraction exceeding LFL at the nominal load and supports the shortening of the auto-ignition dealy. Then combustion of gaseous – liquid fuel mixture makes more efficient resulting in the decrease of exhaust opacity in 8.6–12.8%. The increase-decrease of the exhaust emissions of CO and CO_2 were marginal.

The RCCI combustion avoids the high temperature peaks, and thus improves the emittance of nitrogen oxide. Second, the RCCI combustion improves the control over start of combustion. This improvement allows the combustion timing and duration to be optimized for minimum compression work and maximum expansion work (i.e. maximum *ITE*). The RCCI strategy with adjustment of SOI can be further developed with double- and triple- injection techniques to enhance the performance and efficiency parameters with control of combustion process.

3.3. Reasearch of Hydrogen Co-Combustion with Biodiesel / Petroleum Diesel Mixture and with pure Biodiesel

3.3.1. Experimental Investigation

The tests were conducted with two fuels as follows: RME7 – mixture of ULSD and 7% RME in accordance to the standard EN 590:2013 and pure RME. The

properties of the pure RME along with RME7 and hydrogen are presented at Table 2.8. Tests of the RME7 were performed under the LL, ML and NL corresponding various *IMEP* presented at the Table 3.4. The relative equivalence ratio λ depicted in the Fig. 3.44.

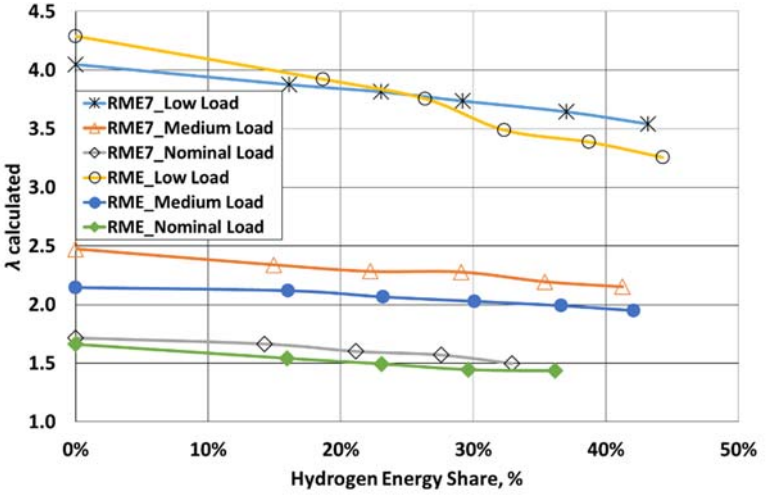

Fig. 3.44. Relative equivalence ratio λ vs. HES at various engine loads

Table 3.4. Injection timings and loads at various composition of combustible mixtures

Test No.	Composition of combustible mixture	SOI φ_i, bTDC	Loads	*IMEP,* kPa
1.	RME7+H_2 0%	φ_{i1} = 18°	LL	259.4
2.	RME7+H_2 (16–43%)	φ_{i2} = 16°	LL	275.9–297.6
3.	RME7+H_2 0%	24°	ML	422.3
4.	RME7+H_2 (15–41%)	20°	ML	458.9–495.2
5.	RME7+H_2 0%	30°	NL	576.4
6.	RME7+H_2 (14–33%)	26°	NL	612.1–661.2
7.	RME+H_2 0%	16°	LL	265.5
8.	RME+H_2 (19–44%)	14°	LL	273.2–295.6
9.	RME+H_2 0%	22°	ML	379.7
10.	RME+H_2 (16–42%)	20°	ML	416.3–508.5
11.	RME+H_2 0%	28°	NL	519.2
12.	RME+H_2 (16–36%)	26°	NL	551.1–625.3

As seen from the test matrix presented at the Table 3.4, the amounts of hydrogen fed to the engine at nominal loads were reduced to 33 and 36% for RME7 and RME respectively, due to the combustion knock occurrence while hydrogen exceeded these limits.

The main objective of the presented research was to examine impact of HES as follows: engine performance including combustion properties and CD, exhaust toxic emissions.

3.3.2. Engine Performance / In-Cylinder Pressure Data Analysis Using AVL BOOST

Hydrogen addition to these fuels increases the LHV of the entire combustible fuel charge trapped in the engine cylinder. Higher fuel‘s LHV usually provides better conditions to obtain higher combustion temperature, hence, it affects other combustion parameters and exhaust emissions.

The positive trends in maximum combustion pressure were observed with increase of HES within all ranges of loads and both tested fuels (Fig. 3.45).

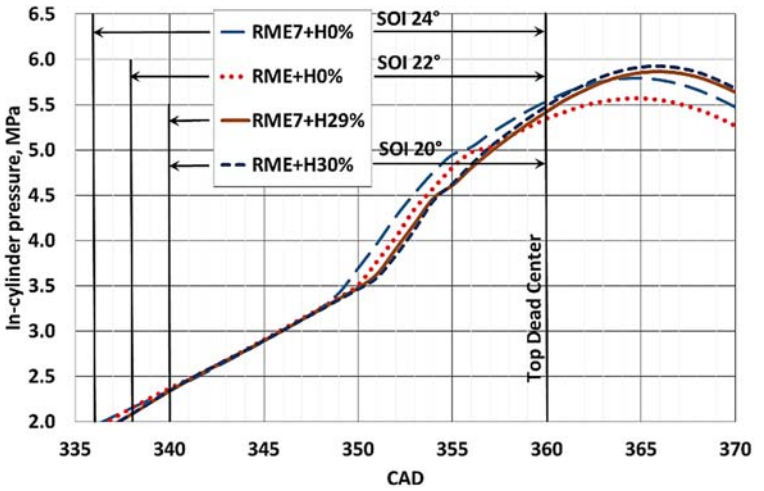

Fig. 3.45. In-cylinder pressure at ML

In fact, at the LL the maximum pressure fluctuates within the ranges of 4.88–5.08 MPa and 4.79–5.04 MPa with RME7 and RME, respectively. The negligible influence of hydrogen fraction at the LL and partially at the MLeNL with low HES was probably caused by low hydrogen fraction in the engine combustion

chamber, which was below LFL for hydrogen (Table 1.3). As hydrogen affects the combustion duration, hence, start of diesel injection timing φ_i was set at fixed position during tests of hydrogenediesel mixture, that makes it possible to compare and analyze combustion phases with various HES. Experiments revealed that the hydrogen–diesel mixture combustion leads to higher in-cylinder peak pressure with HES over 20% as depicted in Fig. 3.46.

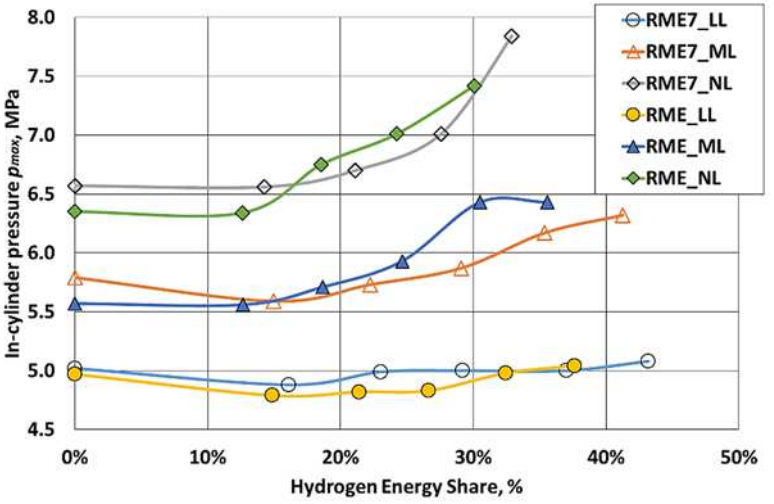

Fig. 3.46. In-cylinder maximum pressure p_{max} vs. HES

ISFC decreases with increase of HES. RME at medium and nominal loads has the highest decrease of *ISFC* by 23.3% in comparison to 19.8% for RME7 (Fig. 3.47). Hydrogen due to high flame speed and short quenching distance extends the flammability limits of RME – hydrogen mixture, provides RME completely combusted especially under higher loads, what leads to reduce *ISFC* as it was stated by Baltacioglu *et al.* (2016). Main reason that *ISFC* is remarkably reduced, comes from relatively high calorific value of hydrogen. Hence, higher hydrogen addition, lower *ISFC*. Additionally, as observed, the engine load is limited by abnormal combustion (knocking), which might appear at nominal loads and HES higher 35%. At those conditions knock can be easily transformed to heavy knock and form extremely high incylinder pressure pulsations over 1 MPa (Szwaja *et al.* 2013) leading to increase heat transfer rate to the piston crown and can quickly damage the piston.

ITE is inversely proportional to *ISFC* taking into account LHV for entire combustible mixture consisted of RME, DF and hydrogen. Although, *ISFC* decreases as presented in Fig. 3.47, but *ITE* is approximately at the same level in between 0.33 and 0.36 except test with RME at low load as shown in Fig. 3.48.

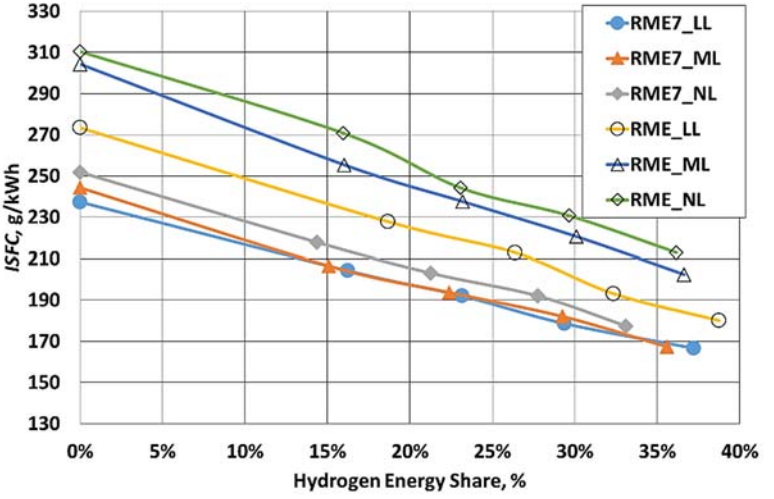

Fig. 3.47. *ISFC* vs. HES of RME and RME7 at various engine loads

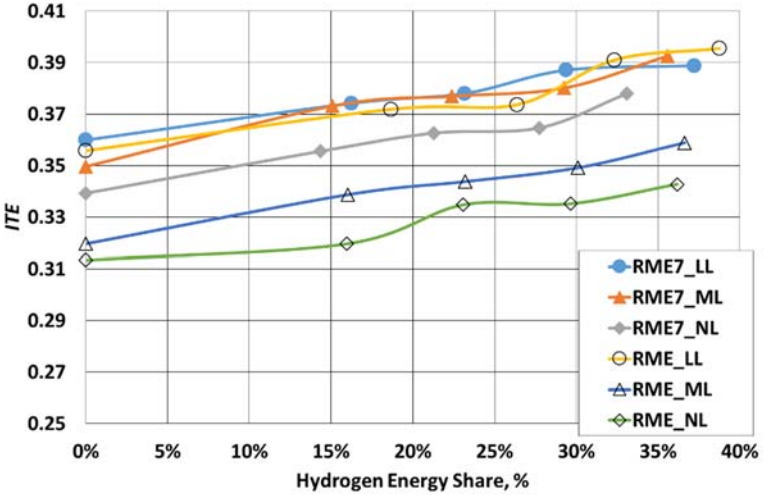

Fig. 3.48. *ITE* vs. HES of RME and RME at various engine loads

The ignition lag can be expressed by the initial combustion phase CA 0–10 starting from the ignition point until 10% fuel burnt. Hence, with increase in HES the ignition delay (lag) gets shorten as depicted in Fig. 3.49 and 3.50. The CA 0– 10 shortens with increase in HES due to high premixed combustion rate and impact of higher laminar speed of hydrogen flame at all engine loads and for both RME and RME7.

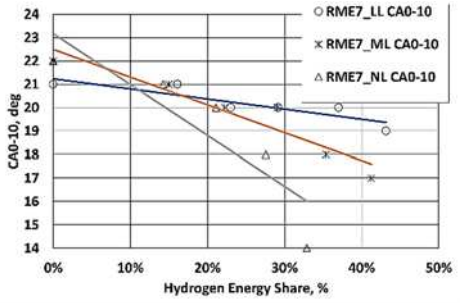

Fig. 3.49. The combustion phase CA 0–10 vs. HES for RME7

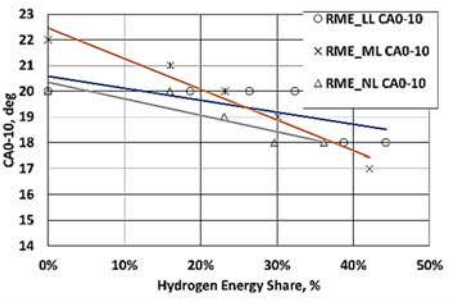

Fig. 3.50. The combustion phase CA 0–10 vs. HES for RME

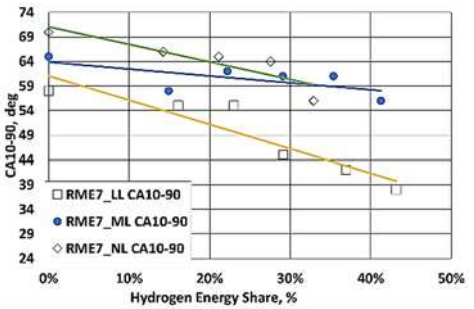

Fig. 3.51. The combustion phase CA 0–90 vs. HES for RME7

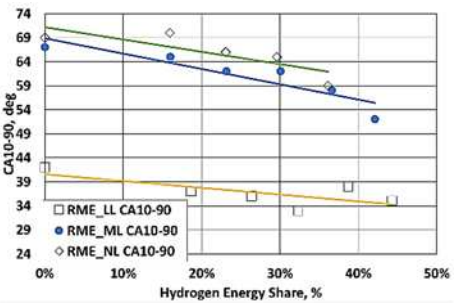

Fig. 3.52. The combustion phase CA 0–90 vs. HES for RME

Increase of hydrogen also reduces the main combustion duration CA 10–90 (Fig. 3.51 and 3.52) which is accelerated by the first combustion phase CA 0–10.

3.3.3. Exhaust Emissions

Investigation on RME and RME7 with hydrogen addition concerns also measurements of exhaust toxic emissions focusing on NO_x, HC and CO. Additionally, CO_2 was also measured with respect to confirm hydrogen impact on CO_2 reduction. As seen in Fig. 3.53, HC emission goes up at the low engine loads, and that was related to the RME and RME7 as well. Hydrogen addition reduces HC emission more significanly at nominal loads.

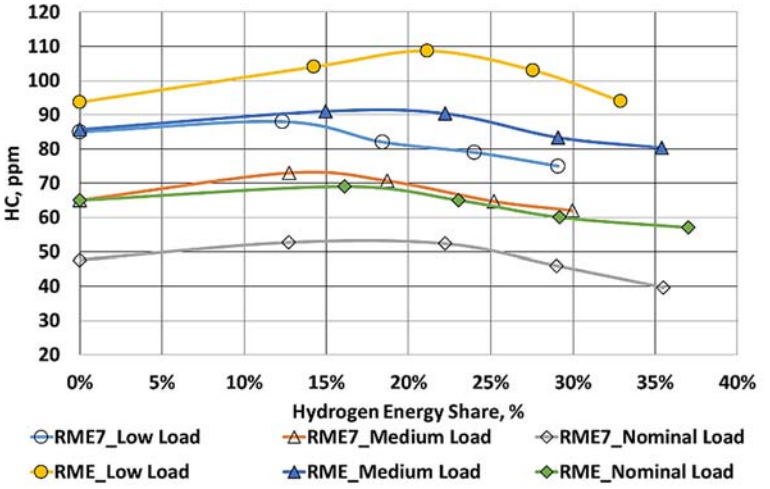

Fig. 3.53. Dependance of HC on HES at various engine loads

The decraese of the unburned HC was observed with higher HES as result of accelerating the combustion process. While at the HES = 12–20% the HC has higher magnitude than the pure biodiesel. Next, the HC drops with further HES increase due to the higher overall combustion temperature and increase of the combustion speed.

The hydrogen induction up to 15% decreases the NO. However, NO increases with HES higher 15% (Fig. 3.54). This trend can be explained with the same phenomenon as it was discussed for HC trend line. Additionally, these trends in both HC and NO are confirmed by well-known NO and HC trade-off, which presents these both emissions inversely proportional to each other. At higher hydrogen rates NO emission increased. The highest increase rate of NO was at the nominal load at max. HES.

Similar trend to HC is observed for CO emission (Fig. 3.55). CO presence in the exhaust gases resulted from incomplete combustion due to both short residence time for fuel molecules in the engine combustion chamber as well as relatively low combustion temperature, which decreases overall combustion reaction rate.

Unlike CO, CO_2 presence in exhaust gases results from complete combustion. Its emission is associated with carbon balance in the combustion reaction, therefore, higher carbon content in fuel implies higher CO_2 emission as far as the CO_2 is the product of complete combustion.

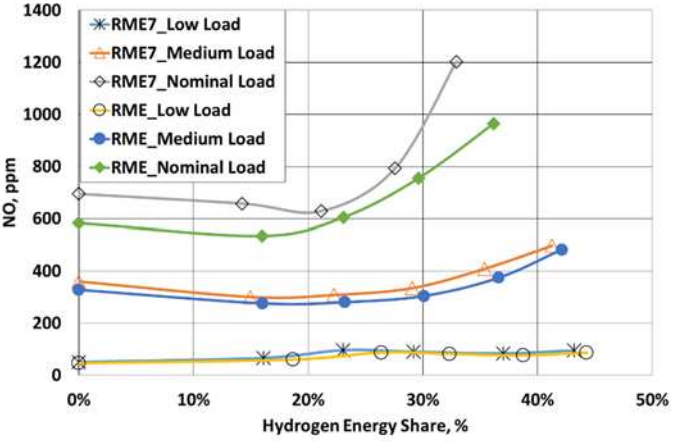

Fig. 3.54. Dependance of NO on HES at various engine loads

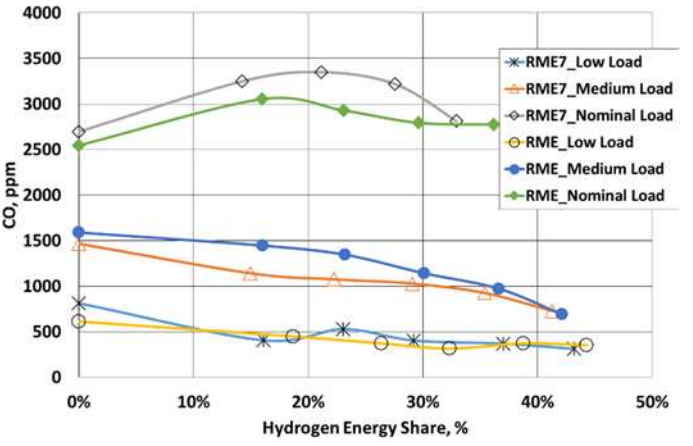

Fig. 3.55. CO vs. HES at various engine loads

The carbon content is usually expressed by the C to H ratio of the specific fuel. Hence, higher hydrogen content in the fuel (denoted with HES) makes the C/H ratio lower, what contributes to lower CO_2 emission as shown in Fig. 3.56.

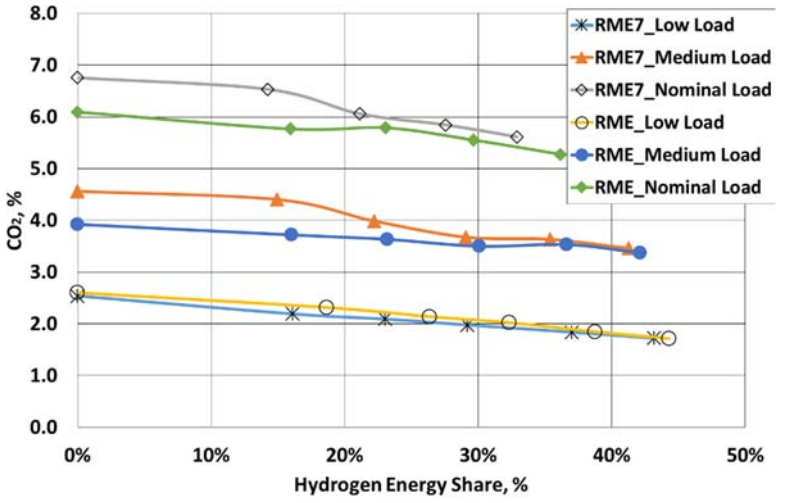

Fig. 3.56. CO_2 vs. HES at various engine loads

Exhaust opacity is a parameter, which characterizes exhaust gases from the CI engine. Exhaust opacity depicts transparency of exhaust gases contaminated with condensed unburnt fuel and soot, which are considered as major substances causing smoke. Unburnt hydrocarbon based molecules and soot are usually inline with each other and they are mostly formed as result of both local oxygen deficiency and short time for complete combustion as it is observed for HC and CO emissions.

As seen in Fig. 3.57, exhaust opacity is in negative trend with HES. It means, that hydrogen assisted diesel fuels provides unfavorable conditions for soot formation. Among all the exhaust emissions tested, exhaust opacity is the parameter which significantly decreases with increase in HES.

The performed test results can be compared to the several publications of the authors. Investigation of Chintala *et al.* (2015) was carried out on the hydrogen based dual-fuel engine with ULSD and B20 (ULSD and 20% biodiesel blend) using low temperature combustion techniques i.e., retarded pilot fuel injection and water injection. With increase of HES nitrogen emission increased while HC, CO and exhaust opacity decreased significantly, however with the low HES, the NO_x emission decreased when the injection timing was retarded and water added.

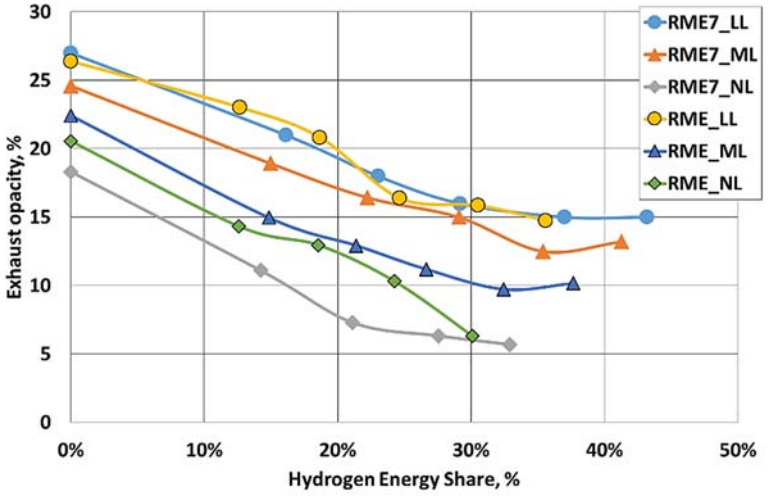

Fig. 3.57. Exhaust opacity vs. HES at various engine loads

The reduction of NO at the low HES was noticed by the author as well as with HES up to 5% was observed decrease of NO and confirmed by Senthil Kumar (2003) and Singh Bika *et al.* (2008). They also explained NO reduction in this HES range as result of slower combustion that forced ignition timing to be more advanced what decreased the combustion rate just after start of combustion (Szwaja *et al.* 2009).

Rocha *et al.* (2017) investigated the co-combustion of the 7% biodiesel-petroleum diesel blend (B7) with hydrogen energy share of 5, 15, 20 and 24% of total fuel energy. With enhance of hydrogen energy share the engine efficiency increased while its *BSFC* and emissions of particulate matter, CO and HC were reduced to the values lower than the reduction of the carbon fraction provided by B7. There was also noticed the decrease of CO_2 emissions, but at lower values than the carbon supplied with the B7 fuel. The increase of hydrogen fraction with higher engine loads increased in-cylinder peak pressure, also raised the in-cylinder temperature, which reflected in the increase of NO_x emissions. All that means that hydrogen promotes faster combustion and higher rates of heat release.

3.4. Conclusions of Chapter 3

1. Co-combustion of the hydrogen and biodiesel with increase of HES enhances the p_{max} of all tested loads as the result of the higher laminar flame

speed of the hydrogen and increased chemical reaction rates. However, lean mixtures does not support the flame propagation due to the too low hydrogen volume fraction, which was insufficient to reach the LFL and results the negligible increase of in-cylinder maximum pressure. The efficient hydrogen co-combustion with biodiesel starts with increased HES, corresponding overstep of the LFL = 3.0–3.1% of hydrogen.

2. Presence of hydrogen contributes to the decrease of the *ISFC* due to decrease of the total fuel mass flow rate. The *ISFC* decreased by 18–22% and 17–28% with HVO and RME respectively, while the decrease with biodiesel blends was as follows: 13–30% with RME7 and 19–23% with PRO Diesel with lower value at LL while higher at NL.
3. The enhancement of *ITE* mainly effected by increased mass flow rate of the hydrogen and it intensive combustions after LFL of hydrogen was oversteped. The *ITE* with increased HES rised remarkably, when hydrogen – biodiesel mixture gets rich burn. The increasing LRF/HRF ratio enhanced the combustion intensity more tangibly at the rich burn with the lowest λ = 1.28–1.37 for PRO Diesel.
4. Even the small HES = 12–13% in co-combustion with biodiesel provides better *ITE* efficiencies than the same engine operated with neat biodiesel. The highest engine efficiency was achieved with the highest HES 30% and with the lean burn mixtures. The favorable outcome of hydrogen fraction defined during tests with respect to performance and emission parameters was HES = 20–23%.
5. HES of less than 15% decreases the NO emissions, but higher hydrogen fraction increases it paticularly at nominal load. NO emission is lower for RME and it blend RME7 in comparison to HVO and it blend PRO Diesel. The HES = 13–17% was found as the optimal percentage at all tested loads with respect to NO emissions. The further increase of HES enhance the NO and at rich burn with λ = 1.28–1.66 the enhancement was 37.5–49.5%.
6. The reduction of exhaust opacity and CO_2 emission levels were observed with increased hydrogen increment rate, as a result of enhanced the temperature, ROHR and and replacement of the certain hydrocarbon fraction. Exhaust opacity decreases due to better premixing, shortening CD and more effective flame proporagion.
7. In general, CO increased with HES of 13–19% at the rich with λ = 1.44–2.15, however further increase of HES resulted decrease to the levels of neat biodiesel CO rate. While at lean burn with λ = 3.26–4.35 presence of hydrogen resulted in decrease of CO by ~ 50% with all tested fuels.
8. The increase of HES influences the combustion phases: the main combustion phase and ignition delay time. As observed, the initial combustion

duration CA 0–10 shortened by 4–6 CAD. It is because hydrogen as very reactive species provides additional combustion precursors, mainly OH group. CA 10–90 also makes shorter by 5–16 CAD with HES increase that makes combustion closer to constant volume conditions, what leads to increase in engine thermal efficiency.

9. The abnormal combustion occures at the rich burn of $\lambda = 1.28–1.50$ with hydrogen volume fraction of 7.83% for RME and 7.51% for it blend RME7. These boundaries for HVO and it blend PRO Diesel was lower: 7.15% and 6.51% respectively. The similar trends were obtained at the leaner burn with $\lambda = 1.89–2.20$.
10. The combustion intensity at the low hydrogen volume fractions of <3% was concentrated at the middle of the combustion process. The increase of HES from 39% to 80% accelerates the intensity of combustion at the beginning of combustion process as it was confirmed by steadlily decreasing combustion shape parameter m_v, obtained in the process of the AVL BOOST simulation.

General Conclusions

The conclusions of each chapter are summarised and presented bellow:

1. The less volume fraction of hydrogen than 3.0–3.1% in the mixture leads to the negligible change of in-cylinder pressure and engine efficiency. The efficient co-combustion of hydrogen with biodiesel starts beyond the LFL with tangible effect on efficiency and emission parameters of the CI engine.
2. The oxidation of hydrogen due to high hydrogen burning rate occurs with lower heat losses to the walls of the combustion chamber. In addition, hydrogen with a low flame quenching distance, spreads the flame closer to the cylinder walls. These factors lead to more efficient combustion of the mixture, higher indicated thermal efficiency and lower fuel consumption.
3. The co-combustion of hydrogen and biodiesel with increase of the HES results in a combustion intensity of the initial (CA0–10) and main (CA10–90) phases of combustion due to the increased laminar flame speed, shortened combustion duration and higher ROHR.
4. The hydrogen fraction increase the combustion intensity and ROHR, which resulted in increase of the NO emission. The HES within the range of 13–17% was determined as the optimum range

for all test loads while NO emissions not exceed the neat biodiesel NO gas emission level.

5. The occurrence of abnormal combustion has limited the increase of the hydrogen fraction in the mixture. The clear boundary of hydrogen fraction has not been defined as the knock appeared within the HES range of 24–36% at ML and 26–42% at NL, while hydrogen volume fraction of 4.97–6.91% at ML and 6.51–7.83% at NL.
6. In order to optimize the performance of the CI engine and reduce the increase in NO emissions, the injection timing was adjusted to φ_3 (because φ_2 was fixed during experiment). Thus abnormal combustion was avoided, the thermal efficiency increased by 1.9–2.6%, and NO emissions decreased by 38–40% at the nominal load.
7. The addition of low reactivity fuel H_2 with increase of HES of the fuel mixture reduce the CN and C/H atom ratio. However, the lowered CN of the mixture due to presence of hydrogen leads to the high ROHR and shortened auto-ignition delay conditioned by the low ignition energy and very fast flame propogation of hydrogen in contrary to the typicaly low CN fuels. The co-combustion of hydrogen is possible with lower CN biofuels.
8. The modeling of AVL BOOST has revealed that at lean mixture and with an increase of hydrogen energy share to the range of 50–80% further intensifies the combustion of the initial combustion phase and shortens the auto-ignition delay period.
9. After the reserach of the hydrogen co-combustion with pure RME and HVO, as well as their blends with petroleum diesel, the knowledge of assessment methods on the RCCI mode engines with use of the alternative fuels has been expanded.

References

Aatola, H.; Larmi, M.; Sarjovaara, T.; Mikkonen, S. 2008. Hydrotreated Vegetable Oil (HVO) as a Renewable Diesel Fuel: Trade-off between NO_x, Particulate Emission, and Fuel Consumption of a Heavy Duty Engine. *SAE Technical Paper* 2008-01-2500.

Aldhaidhawi, M., Chiriac, R., Bădescu, V., Descombes, G., Podevin, P. 2017. Investigation on the mixture formation, combustion characteristics and performance of a Diesel engine fueled with Diesel, Biodiesel B20 and hydrogen addition. *International Journal of Hydrogen Energy* 42, 16793–16807.

Ali, Y.; Hanna, M. A.; Cuppett, S. L. 1995. Fuel properties of tallow and soybean oil esters. *J Am Oil Chemists' Soc* 1995;72:1557–1564.

Alqahtani A.; Shokrollahihassanbarough F.; Wyszynski M. L. 2015. Thermodynamic simulation comparison of AVL BOOST and Ricardo WAVE for HCCI and SI engines optimisation. *Combustion Engines*. 2015; 161(2), 68–72.

Alptekin, E.; Canakci, M. 2009. Characterization of the key fuel properties of methyl ester–diesel fuel blends. *Fuel* 2009;88:75–80.

Antunes, J. M. G.; Mikalsen, R.; Roskilly, A. P. 2009. An experimental study of a direct injection compression ignition hydrogen engine. *International Journal of Hydrogen Energy* 34: 6516–6522. doi:10.1016/j.ijhydene.2009.05.142.

Antunes, J. M. G. 2010. *The Use Of Hydrogen As A Fuel For Compression Ignition Engines*. In Partial Fulfilment of the Requirements for the Degree of Doctor of Philosophy. Newcastle University. 349 p.

Ashraful, A. M.; Masjuki, H.; Kalam, M.; Rizwanul Fattah, I. M.; Imtenan, S.; Shahir, S. A.; Hossain, M. 2014. Production and comparison of fuel properties, engine performance, and emission characteristics of biodiesel from various non-edible vegetable oils: a review. *Energy Convers Manag* 2014;80:202–228.

Atabani, A. E.; Silitonga, A. S.; Badruddin. I. A.; Mahlia, T. M. I.; Masjuki, H. H.; Mekhilef, S. 2012. A comprehensive review on biodiesel as an alternative energy resource and its characteristics. *Renew Sustain Energy Rev* 2012;16:2070–93, https://doi.org/10.1016/j.rser.2012.01.003.

Atabani, A. E.; Mofijur, M.; Masjuki, H. H. *et al.* 2014. Effect of Croton megalocarpus, Calophyllum inophyllum, Moringa oleifera, palm and coconut biodiesel–diesel blending on their physico-chemical properties. *Ind Crops Prod* 2014;60:130–137.

Atadashi, I. M.; Aroua, M. K.; Aziz, A. A. 2010. High quality biodiesel and its diesel engine application: a review. *Renewable Sustainable Energy Review* 2010;14:1999–2008.

Automobile industry pocket guide 2014–2015. 2014. *European Automobile Manufacturers Association – ACEA Communications department*.

Avarzaman, M. B. 2002. *Investigation of Completeness of Combustion in CNG Fueled Spark Ignition Engines.* A Thesis Submitted to the Faculty of Graduate Studies and Research for the Degree of Master of Applied Science at the University of Widsor. Windsor, Ontario, Canada. 20 p. ISBN: 0-494-04961-8.

AVL BOOST v 2011.2. 2011. *AVL BOOST Theory,* Graz, Austria. 113 p.

AVL BOOST v 2011.2. 2011. *AVL BOOST Users Guide*, Graz, Austria. 297 p.

AVL DITEST. 2016. *User Manual AVL DITEST DPM 800*. AVL DiTEST GmbH. 38 p.

Bahadur, N. P.; Boocock, D. G.; Konar, S. K. 1995. Liquid hydrocarbons from catalytic pyrolysis of sewage sludge lipid and canola oil: evaluation of fuel properties. *Energy fuels* 1995;9:248–256.

Baltacioglu, M. K.; Arat, H. T.; Ozcanli, M.; Aydin, K. 2016. Experimental comparison of pure hydrogen and HHO (hydroxy) enriched biodiesel (B10) fuel in a commercial diesel engine. *International Journal of Hydrogen Energy* 41, 8347–8353.

Barrios, C. C.; Domínguez-Sáez, A.; Hormigo, D. 2017. Influence of hydrogen addition on combustion characteristics and particle number and size distribution emissions of a TDI diesel engine. *Fuel* 199 (2017), 162–168.

Benajes, J.; Molina, S.; García, A.; Belarte, E.; Vanvolsem, M. 2014. An investigation on RCCI combustion in a heavy duty diesel engine using in-cylinder blending of diesel and gasoline fuels. *Applied Thermal Engineering* 63:66–76.

Benajes, J.; Molina, S.; García, A.; Monsalve-Serrano, J. 2015. Effects of direct injection timing and blending ratio on RCCI combustion with different low reactivity fuels. *Energy Conversion and Management* 99; 193–209.

Bhardwaj, O. P.; Lüers, B.; Holderbaum, B.; Körfer, T.; Pischinger, S.; Honkannen, M. 2015. Utilization of HVO fuel properties in a high efficiency combustion system *SAE Research Paper* 20154062. *Int J Automot Eng* 2015; 6:75–82.

Bhuiya, M.; Rasul, M.; Khan, M. *et al.* 2016. Prospects of 2nd generation biodiesel as a sustainable fuel–Part 2: properties, performance and emission characteristics. *Renew Sustain Energy Rev* 2016;55:1129–1146.

Canakci, M.; Sanli H. 2008. Biodiesel production from various feedstocks and their effects on the fuel properties. *J Ind Microbiol Biotechnol* 2008;35:431–441.

Cardera, D.; Ryskampa, R.; Bescha, M.; Thiruvengadam, A. 2017. Emissions Control Challenges for Compression Ignition Engines. *4th International Congress of Theoretical and Applied Mechanics.* Procedia IUTAM 20 (2017) 103–111.

Chaichan, M. T. 2018. Performance and emission characteristics of CIE using hydrogen, biodiesel, and massive EGR. *International Journal of Hydrogen Energy* 2018; 43:5415–5435. https://doi.org/10.1016/j.ijhydene.2017.09.072.

Chauhan, B. S.; Kumar, N.; Jun, Y. D.; Lee, K. B. 2010. Performance and emission study of preheated Jatropha oil on medium capacity diesel engine. *Energy* 2010;35:2484–2492.

Chauhan, B. S.; Kumar, N.; Cho, H. M. 2012. A study on the performance and emission of a diesel engine fueled with Jatropha biodiesel oil and its blends. *Energy* 2012;37:616–622.

Chelladorai, P.; Varuvel, E. G.; Martin, L. J.; Bedhannan, N. 2018. Synergistic effect of hydrogen induction with biofuel obtained from winery waste (grapeseed oil) for CI engine application. *International Journal of Hydrogen Energy* 2018; 43:12473-12490. https://doi.org/10.1016/j.ijhydene.2018.04.155.

Chemkin 10112. 2011. *CHEMKIN Tutorials Manual.* Reaction Design; San Diego, 274 p. Retrived from: https://www.ems.psu.edu/~radovic/ChemKin_Tutorial_2-3-7.pdf.

Chen, P. C.; Wang, W. C.; Roberts, W. L.; Fang, T. 2013. Spray and atomization of diesel fuel and its alternatives from a single-hole injector using a common rail fuel injection system. *Fuel.* 103:850–861.

Chintala, V.; Subramanian, K. A. 2015. An effort to enhance hydrogen energy share in a compression ignition engine under dual-fuel mode using low temperature combustion strategies. *Applied Energy* 146 (2015) 174–183.

Choi, C.; Reitz, R. 1999. A numerical analysis of the emissions characteristics of biodiesel blended fuels. *J Eng Gas Turbines Power* 1999;121:31–37.

CO_2 EMISSIONS FROM FUEL COMBUSTION. Overview. *International Energy Agency Highlights.* 2017. [online cit.: 2018-05-07]. Available from: http://www.iea.org/publications/freepublications/publication/CO2EmissionsFrom-FuelCombustion2017Overview.pULSD

Conference of the Parties. 2015. Twenty-first session Paris, 30 November to 11 December 2015. *Framework Convention of the Climate Change*/CP/2015/L.9/Rev.1.

Deb, M.; Sastry, G. R. K.; Bose, P. K.; Banerjee, R. 2015. An experimental study on combustion, performance and emission analysis of a single cylinder, 4-stroke DI-diesel engine using hydrogen in dual fuel mode of operation. *International Journal of Hydrogen Energy* 2015;40:8586–8598.

Demirbas A. 2008. *Biodiesel: a realistic fuel alternative for diesel engines*. London: Springer. 207 p. DOI: 10.1007/978-1-84628-995-8.

Dimitriou, P.; Kumar, M.; Tsujimura, T.; Suzuki, Y. 2018. Combustion and emission characteristics of a hydrogen-diesel dual-fuel engine. *International Journal of Hydrogen Energy* 2018;43:13605–13617.

Dimitriou, P.; Tsujimura, T. 2017. A review of hydrogen as a compression ignition engine fuel. *International Journal of Hydrogen Energy,* 42 (2017):24470–24486. http://dx.doi.org/10.1016/j.ijhydene.2017.07.232.

Directive of the European Parliament and of the Council on the deployment of alternative fuels infrastructure. 2013. COM (2013) 18 final 2013/0012 (COD). Brussels, 24.1.2013.

Dyzelinių variklių valdymo sistemos. 2009. *Robert Bosch GmbH.* Kaunas: Smaltijos leidykla. ISBN 978-9955-707-67-7. 496 p.

Dwivedi, G.; Sharma, M. P. 2014. Prospects of biodiesel from Pongamia in India. *Renewable Sustainable Energy Review* 2014;32:114–122.

Energy Agency of Lithuania. 2012. *Report from the Republic of Lithuania under Article 4(1) of Directive 2003/30/EC of the European Parliament and of the Council on the promotion of the use of biofuels or other renewable fuels for transport*. Retrieved from: http://www.ena.lt .

Engman, A.; Hartikka, T.; Honkanen, M.; Kiiski, U.; Kuronen, Lehto, K. *et al.* 2016. *Neste Renewable Diesel Handbook*. Espoo: Neste Proprietary Publication.

Erkkila, K.; Nylund, N. O.; Hulkkone, T.; Tilli, A.; Mikkonen, S.; Saikkonen, P.; Makinen, R.; Amberia, A. 2011. Emission performance of paraffinic HVO diesel fuel in heavy-duty vehicles. *SAE paper* 2011-01-1966.

Ewphun, P.-P.; Tan Vo, Ch.; Srichai, P.; Charoenphonphanich, Ch.; Sato, S.; Kosaka, H. 2017. Combustion characteristics of hydrotreated vegetable oil – diesel blend under EGR and supercharged conditions. *International Journal of Automotive Technology.* August 2017, Volume 18, Issue 4, p. 643–652.

European Comission Decision C. 2016. 4614. Work Programme 2016 – 2017 "*Smart, green and integrated transport"*. Brussels.

Fayaz, H.; Saidur, R.; Razali, N.; Anuar, F. S.; Saleman, A. R.; Islam, M. R. 2012. An overview of hydrogen as a vehicle fuel. *Renewable and Sustainable Energy Reviews* 16 (2012) 5511–5528.

Flach, B.; Lieberz, S.; Rossetti, A. 2017. EU Biofuels Annual 2017. USDA Foreign Agricultural Service. *Global Agricultural Information Network*. Hague. Report No. NL7015. Retrived from: http://gain.fas.usda.gov/Pages/Default.aspx.

Fukuma, T.; Fujita, T.; Pichainarong, P.; Furuhama, S. 1986. Hydrogen Combustion Study in Direct Injection Hot Surface Ignition Engine. *SAE Paper* 861579.

Gill, S. S.; Tsolakis, A.; Dearn, K. D.; Rodríguez-Fernández, J. 2011. Combustion characteristics and emissions of Fischer-Tropsch diesel fuels in IC engines. *Progress in Energy and Combustion Science* 37 (2011) 503–523.

Ghazali, W. N. M. W.; Mamat, R.; Masjuki, H.; Najafi, G. 2015. Effects of biodiesel from different feedstocks on engine performance and emissions: a review. *Renewable and Sustainable Energy Reviews* 2015;51:585–602.

Ghojel, J.I. 2010. Review of the development and applications of the Wiebe function: a tribute to the contribution of Ivan Wiebe to engine research. *Int. Journal Engines*. Vol. 11. DOI: 10.1243/14680874JER06510.

Glassman I. 1987. *Combustion.* Orlando, FL: Academic Press, Inc. ISBN 0-12-285851-4, 501 p.

Grab-Rogalinski K, Szwaja S. 2017. Combustion Of The Biomethane In An IC Over-Expanded Engine. *Conference Proceedings by IEEE, International Conference on Green Energy and Applications ICGEA 2017*, IEEE Xplore, doi:10.1109/ICGEA.2017.7925473.

Grab-Rogalinski, K.; Szwaja, S. 2016. The combustion properties analysis of various liquid fuels based on crude oil and renewables. *IOP Conference Series: Materials Science and Engineering* 148 (1), 012066 doi:10.1088/1757-899X/148/1/012066.

Hancsok, J.; Krar, M.; Magyar, S.; Boda, L.; Hollo, A.; Kallo, D. 2007. Investigation of the production of high cetane number bio gas oil from pre-hydrogenated vegetable oils over Pt/HZSM-22/Al2O3. *Microporous Mesoporous Mater* 2007;101:148–152.

Heywood, J. B. 1988. *Internal combustion engine fundamentals*. McGraw-Hill Inc. International Editions Automotive Technology Series. ISBN 0-07-100499-8. p. 930.

Hilbers, T. J.; Sprakel, L. M. J.; van den Enk, L. B. J.; Zaalberg, B.; van den Berg, H.; van der Ham, L. G. J. 2015. Green Diesel from Hydrotreated Vegetable Oil Process Design Study. *Chemical Engineering Technology*, ISSN 0930-7516, Vol. 38, No. 4, Pages 651– 657.

Hoekman, S. K.; Broch, A.; Robbins, C.; Ceniceros, E.; Natarajanb, M. 2012. Review of biodiesel composition, properties, and specifications. *Renewable and Sustainable Energy Reviews* 16; 143–169.

Holman, J. P. 2011. Experimental methods for engineers. 8th edition. Published by McGraw-Hill, New York, NY 10020. ISBN 978-0-07-352930-1.

Homan, H. S.; Reynolds, R. K.; De Boer, P. C. T.; McLean, W. J. 1979. Hydrogen-fueled diesel engine without timed ignition. *International Journal of Hydrogen Energy* 1979;4(4):315–325.

Ikegami, M.; Miwa, K.; Shioji, M. 1982. A study of hydrogen fuelled compression ignition engines. *International Journal of Hydrogen Energy* 1982; 7(4):341–353.

Imperato, M.; Tilli, A.; Sarjovaara, T.; Larmi, M. 2011. Large-bore compression-ignition engines: high NOx reduction achieved at low load with hydro-treated vegetable oil. *SAE paper* 2011-01-1956; 2011.

International Energy Agency Highlights. 2017. *CO_2 emissions from fuel combustion. Overview*. Retrieved from http://www.iea.org/publications/freepublications/publication/CO2EmissionsFromFuelCombustion2017Overview.pULSD

Jegadheesan, C.; Somasundaram, P.; Meenakshipriya, B.; Vignesh, U. P. 2017. Investigation effect of hydrogen addition on the performance and exhaust emissions of Pongamia pinnata biodiesel fueled compression ignition engine. *International Journal Of Green Energy*. 2017, Vol. 14, No. 15, 1256–1268. https://doi.org/10.1080/15435075.2017.1399134.

Jain, S.; Sharma, M. P. 2010. Prospects of biodiesel from Jatropha in India: a review. *Renewable Sustainable Energy Review* 2010;14:763–771.

Kalsi, S. S.; Subramanian, K. A. 2017. Experimental investigations of effects of hydrogen blended CNG on performance, combustion and emissions characteristics of a biodiesel fueled reactivity controlled compression ignition engine (RCCI). *International Journal of Hydrogen Energy* 42, 4548–4560.

Karagoz, Y.; Sandalci, T.; Yuksek, L.; Dalkilic, A. S. 2015. Engine performance and emission effects of diesel burns enriched by hydrogen on different engine loads. *International Journal of Hydrogen Energy* 2015;40:6702–6713.

Karim, G. A. 2003. Hydrogen as a spark ignition engine fuel. *International Journal of Hydrogen Energy*, Vol. 28, 569–577.

Karim, G. A. 2007. Hydrogen as an Engine Fuel Some Pros and Cons. *Journal of KONES Powertrain and Transport,* Vol.14, No. 4, 2007.

Karim, G. A. 2015. *Dual-fuel Diesel Engines*. CRC Press. Taylor & Francis Group. ISBN: 978-1-4987-0308-6. 295 p.

Kinast, J. 2003. Production of biodiesels from multiple feedstocks and properties of biodiesels and biodiesel/diesel blends. *NREL Final Report*, SR-510-31460.

Knothe, G.; Matheaus, A. C.; Ryan, T. W. 2003. Cetane numbers of branched and straight-chain fatty esters determined in an ignition quality tester☆. *Fuel* 2003;82:971–975.

Knothe, G.; Razon, L. F. 2017. Biodiesel fuels. *Progress in Energy and Combustion Science* 58 (2017) 36–59.

Knothe, G.; Gerpen, J. V.; Krahl, J. 2005. *The Biodiesel Handbook.* AOCS Press Champaign, Illinois, USA.

Kokjohn, S. L.; Hanson, R. M.; Splitter, D. A.; Reitz, R. D. 2009. Experiments and modeling of dual-fuel HCCI and PCCI combustion using In-Cylinder fuel blending. *SAE paper*; 2009-01-2647.

Koten H. 2018. Hydrogen effects on the diesel engine performance and emissions. *International Journal of Hydrogen Energy* 2018;43:10511–10519.

Kuronen, M.; Mikkonen, S.; Aakko, P.; Murtonen, T. 2007. Hydrotreated vegetable oil as fuel for heavy duty diesel engines. *SAE Technical Paper* 2007-01-4031. DOI: https://doi.org/10.4271/2007-01-4031.

Labeckas, G.; Slavinskas, S. 2005. The effect of diesel fuel blending with rapeseed oil and rme on engine performance and exhaust emissions. *Journal of KONES Internal Combustion Engines*, vol. 12, 1–2.

Labeckas, G.; Slavinskas S. 2015. Combustion phenomenon, performance and emissions of a diesel engine with aviation turbine JP-8 fuel and rapeseed biodiesel blends. *Energy Convers Manag* 2015;105:216–29.

Labeckas, G.; Slavinskas, S.; Mažeika, M. 2014. The effect of ethanol–diesel–biodiesel blends on combustion, performance and emissions of a direct injection diesel engine. *Energy Conversion and Management* 79, 698–720.

Lapuerta, M.; Villajos, M.; Agudelo, J. R.; Boehman, A. L. 2011. Key properties and blending strategies of hydrotreated vegetable oil as biofuel for diesel engines. *Fuel Processing Technology* 92 (12), 2406–2411.

Lata, D.B. 2011. *Investigation of dual fuel diesel engine with hydrogen and LPG fuel.* LAP LAMBERT Academic Publishing GmbH&Co. KG. ISBN: 978-3-659-15025-8. 273 p.

Lebedevas, S.; Makareviciene, V.; Sendzikiene, E.; Žaglinskis, J. 2013. Oxidation stability of biofuel containing Camelina sativa oil methyl esters and its impact on energy and environmental indicators of diesel engine. *Energy Conversion and Management* 65, 33–40.

Lehto, K.; Elonheimo, A.; Hakkinen, K.; Sarjovaara, T.; Larmi, M. 2011. Emission reduction using hydrotreated vegetable oil (HVO) with miller timing and EGR in diesel combustion. *SAE paper* 2011-01-1955; 201.

Lewis, B.; von Elbe, G. 1987. Combustion, Flames and Explosions of Gases. (3rd edition), Academic Press, New York. ISBN-13: 978-0123958884. 764 p.

Li, J.; Yang, W. M.; Goh, T. N.; An, H.; Maghbouli, A. 2014. Study on RCCI (reactivity controlled compression ignition) engine by means of statistical experimental design. *Energy* 78:777–787.

Li, J.; Yang, W.; Zhou, D. 2017. Review on the management of RCCI engines. *Renewable and Sustainable Energy Reviews* 69: 65–79.

Li, Y.; Jia, M.; Chang, Y.; Xie, M.; Reitz, R. D. 2016. Towards a comprehensive understanding of the influence of fuel properties on the combustion characteristics of a RCCI (reactivity controlled compression ignition) engine. *Energy* 99: 69–82.

Liaquat, A. M.; Masjuki, H. H.; Kalam, M. A. *et al.* 2013. Effect of coconut biodiesel blended fuels on engine performance and emission characteristics. *Proc Eng* 2013;56:583–590.

Liaquat, A. M.; Masjuki, H. H.; Kalam, M. A. *et al.* 2012. Application of blend fuels in a diesel engine. *Energy Proc* 2012;14:1124–1133.

Lithuanian Department of Statistics. 2017. *Fuel and Energy final consumption of Transport consumers*. https://osp.stat.gov.lt/statistiniu-rodikliu-analize?theme=all#/.

Liu, H.; Wang, X.; Zheng, Z.; Gu, J.; Wang, H.; Yao, M. 2014. Experimental and simulation investigation of the combustion characteristics and emissions using n-butanol/biodiesel dual-fuel injection on a diesel engine. *Energy*.

McCarthy, P.; Rasul, M. G.; Moazzem, S. 2011. Analysis and comparison of performance and emissions of an internal combustion engine fuelled with petroleum diesel and different bio-diesels. *Fuel* 2011;90:2147–2157.

Melaika, M. 2016. *Research of a combustion process in a spark ignition engine, fuelled with gaseous fuel mixtures*. Dissertation Thesis, Vilnius Gediminas Technical University: 156 p.

Meng, X.; Chen, G.; Wang, Y. 2008. Biodiesel production from waste cooking oil via alkali catalyst and its engine test. *Fuel Process Technol* 2008;89:851–857.

Miyamoto, T.; Hasegawa, H.; Mikami, M.; Kojima, N.; Kabashima, H. 2011. Effect of hydrogen addition to intake gas on combustion and exhaust emission characteristics of a diesel engine. *International Journal of Hydrogen Energy* 36: 13138 – 13149.

Misra, R. D.; Murthy, M. S. 2011. Performance, emission and combustion evaluation of soapnut oil-diesel blends in a compression ignition engine. *Fuel* 2011;90:2514–2518.

Mofijur, M.; Hazrat, M. A.; Rasul, M. G.; Mahmudul, H. M. 2015. Comparative evaluation of edible and non-edible oil methyl ester performance in a vehicular engine. *Energy Proc* 2015;75:37–43.

Mofijur, M.; Masjuki, H. H.; Kalam, M. A. *et al.* 2014. Comparative evaluation of performance and emission characteristics of Moringa oleifera and Palm oil based biodiesel in a diesel engine. *Ind Crops Prod* 2014;53:78–84.

Mofijur, M.; Masjuki, H. H.; Kalam, M. A.; Atabani, A. E. 2013. Evaluation of biodiesel blending, engine performance and emissions characteristics of Jatropha curcas methyl ester: Malaysian perspective. *Energy* 2013;55:879–887.

Mollenhauer, K.; Tschoeke, H. 2010. *Handbook of Diesel Engines*. Springer Heidelberg. Dordrecht, London, New York. DOI 10.1007/978-3-540-89083-6. 636 p.

Molnarne, M.; Schendler, T.; Schroeder, V. 2003. *Explosionsbereiche von Gasgemischen. In: Sicherheitstechnische Kenngroessen, Band 2*. Wirtschaftsverlag NW. Verlag fuer neue Wissenschaft. Bremen, Germany. ISBN-10: 3897017466. 360 p.

Momirlan, M; Veziroglu, T. N. 2005. The properties of hydrogen as fuel tomorrow in sustainable energy system for a cleaner planet. *International Journal of Hydrogen Energy* 2005;30:795–802. https://doi.org/10.1016/j.ijhydene.2004.10.011.

Murray, J.; King, D. 2012. Oil's tipping point has passed. *Nature* 481 (7382), 433–435.

Murtonen, T.; Aakko-Saksa, P.; Kuronen, M.; Mikkonen, S.; Lehtoranta, K. 2009. Emissions with heavy-duty diesel engines and vehicles using FAME, HVO and GTL fuels with and without DOC + POC aftertreatment. *SAE paper* 2009-01-2693; 2009.

Naber, J.; Siebers, D. L. 1998. Hydrogen combustion under diesel engine conditions. *International Journal of Hydrogen Energy,* 1998; 23(5):363–371.

National Academy of Science. 2004. *The Hydrogen Economy: Opportunities, Costs, Barriers, and R&D Needs.* National Academies Press, Washington DC, USA.

Neste Certificate of Analysis. 2017. No. TT-17-001095. Date of issue: 2017.03.31. Neste Corporation, Technology Centre, Engine Laboratory, P.O. Box 310, 06101 Porvoo, Finland.

Neste PRO Diesel Product Data Sheet. 2017. Abbreviation: DIP-12/-22. Date of issue: 2017.01.01. Neste Oyj, Neste Retail POB 95 FIN-00095 Neste Oyj, Finland.

No, S.Y. 2014. Application of hydrotreated vegetable oil from triglyceride based biomass to CI engines – A review. *Fuel* 115; 88–96.

Ono, R.; Nifuku, M.; Fujiwara, S.; Horiguchi, S.; Oda, T. 2007. *Minimum ignition energy of hydrogen–air mixture: effects of humidity and spark duration*. Journal of Electrostatics. 2007;65:87–93. DOI: 10.1016/j.elstat.2006.07.004.

Othman, M. F.; Adama, A.; Najafic, G.; Mamata, R. 2017. Green fuel as alternative fuel for diesel engine: A review. *Renewable and Sustainable Energy Reviews* 80 (2017) 694–709.

Perry, R. H.; Green, D. W. 1997. editors. Perry's chemical engineers' handbook – 7th edition. McGraw-Hill. ISBN 0-07-049841-5.

Pflaum, H.; Hofmann, P.; Geringer, B.; Weissel, W. 2010. Potential of hydrogenated vegetable oil (HVO) in a modern diesel engine. *SAE paper* 2010-32-0081; 2010.

Piaszyk, J. 2012. *Animal fat (tallow) as fuel for stationary internal combustion engines.* A PhD thesis submitted to The University of Birmingham. 167 p.

Pirjola, L.; Rönkkö, T.; Saukko, E.; Parviainen, H.; Malinen, A.; Alanen, J.; Saveljeff, H. 2017. Exhaust emissions of non-road mobile machine: Real-world and laboratory studies with diesel and HVO fuels. *Fuel.* Volume 202, 15 August 2017, Pages 154–164. https://doi.org/10.1016/j.fuel.2017.04.029.

Pischinger, S. 2014. *Alternative vehicle propulsion systems.* Lecture notes. Rheinisch – Westfalische Technische Hochschule Aachen. Institute for Combustion Engines. 286 p.

Rao, P.V. 2011. Experimental investigations on the Influence of properties of Jatropha biodiesel on performance, combustion, and emission characteristics of a DI-CI engine. *World Acad Sci Eng Technol* 2011;75:855–68.

Rahman, M. M.; Rasul, M.; Hassan, N. M. S. 2017. Study on the Tribological Characteristics of Australian Native First Generation and Second Generation Biodiesel Fuel. *Energies* 2017:10–55.

Rapsoila Certificate of Analysis No. 03/17. 2017. LST EN 14214:2014. Date of issue: 2017.03.17. SGS Klaipeda Ltd., UAB „Rapsoila".

Raslavičius, L.; Keršys, A.; Starevičius, M.; Sapragonas, J.; Bazaras, Ž. 2014. Biofuels, sustainability and the transport sector in Lithuania. *Renewable and Sustainable Energy Reviews* 32 (2014) 328–346.

Rassweiler, G. M.; Withrow, L. 1938. *Motion Pictures of Engine Flames Correlated with Pressure Cards*, *SAE Transactions,* Vol. 38, pp. 185–204.

Reitz, R. D.; Duraisamy, G. 2015. Review of high efficiency and clean reactivity controlled compression ignition (RCCI) combustion in internal combustion engines. *Progress in Energy and Combustion Science* 46, 12–71. https://doi.org/10.1016/j.pecs.2014.05.003.

Resitoglu, I. A.; Keskin, A. 2017. Hydrogen applications in selective catalytic reduction of NOx emissions from diesel engines. *International Journal of Hydrogen Energy* 2017;42:23389–23394.

Rheonik. 2005. *RHM 015 – Ultimate Low Flow Coriolis Mass Flowmeter*. M015/18 November 2005 – v5. 7 p.

Rimkus, A.; Matijošius, J.; Bogdevičius, M.; Bereczky, A.; Torok, A. 2018. An investigation of the efficiency of using O_2 and H_2 (hydrooxile gas - HHO) gas additives in a CI engine operating on diesel fuel and biodiesel. *Energy* 152 (2018) 640–651. https://doi.org/10.1016/j.energy.2018.03.087.

Rimkus, A.; Žaglinskis, J.; Rapalis, P.; Skačkauskas, P. 2015. Research on the combustion, energy and emission parameters of diesel fuel and a biomass-to-liquid (BTL) fuel blend in a compression-ignition engine. *Energy Conversion and Management* 106 (2015) 1109–1117. http://dx.doi.org/10.1016/j.enconman.2015.10.047.

Rocha, H. M. Z.; Pereira, R. S.; Nogueira, M. F. N.; Belchior, C. R. P.; Tostes, M. E. L. 2017. Experimental investigation of hydrogen addition in the intake air of compressed ignition engines running on biodiesel blend. *International Journal of Hydrogen Energy* 42(2017):4530–4539. https://doi.org/10.1016/j.ijhydene.2016.11.032.

Sajjad, H.; Masjuki, H. H.; Varman, M.; Kalam, M. A.; Arbab, M. I.; Imtenan, S.; Ashrafur Rahman, S. M. 2014. Engine combustion, performance and emission characteristics of gas to liquid (GTL) fuels and its blends with diesel and bio-diesel. *Renewable and Sustainable Energy Reviews* 30 (2014) 961–986.

Salvi, B. L.; Subramanian, K. A. 2015. Sustainable development of road transportation sector using hydrogen energy system. *Renewable and Sustainable Energy Reviews* 51(2015)1132–1155.

Saravanan, N.; Nagarajan, G.; Sanjay, G.; Dhanasekaran, C.; Kalaiselvan, K. M. 2008. Combustion analysis on a DI diesel engine with hydrogen in dual fuel mode. *Fuel* 87 (2008) 3591–3599.

Saravanan, N.; Nagarajan, G.; Narayanasamy, S. 2007. Experimental investigation on performance and emission characteristics of DI diesel engine with hydrogen fuel. *SAE Technique Paper* 2007-01-17.

Schroeder, V.; Emonts, B.; Janssen, H.; Schulze, H.-P. 2004. Explosion Limits of Hydrogen/Oxygen Mixtures at Initial Pressures up to 200 bar. *Chem. Eng. Technolog.* 27, No. 8, pp. 847–851. https://doi.org/10.1002/ceat200403174

Schroeder, V.; Holtappels, K. 2004. Explosion Characteristics of Hydrogen-Air and Hydrogen-Oxygen Mixtures at Elevated Pressures. *Bundesanstal für Materialforschung und Pruefung (BAM) Research report* – Project SAFEKINEX, contract EVG1-CT-2002-00072.

Senthil Kumar, M. 2003. Use of hydrogen to enhance the performance of a vegetable oil fueled compression ignition engine. *Int J Hydrogen Energy* 28(10):11, 43–54.

Serin, H.; Yıldızhan, Ş. 2018. Hydrogen addition to tea seed oil biodiesel: Performance and emission characteristics. *International Journal of Hydrogen Energy*, 2018; 43:18020 –18027. https://doi.org/10.1016/j.ijhydene.2017.12.085.

Sharma, P.; Dhar, A. 2018. Effect of hydrogen supplementation on engine performance and emissions. *International Journal of Hydrogen Energy*, 2018;43:7570–7580.

Simacek, P.; Kubicka, D.; Sebor, G.; Pospisil, M. 2010. Fuel properties of hydroprocessed rapeseed oil. *Fuel* 2010;89:611–615.

Simacek, P.; Kubicka, D.; Kubickova, I.; Homola, F.; Pospisil, M.; Chudoba, J. 2011. Premium quality renewable diesel fuel by hydroprocessing of sunflower oil. *Fuel* 2011;90:2473–2479.

Singh Bika, A.; Franklin, L. M.; Kittelson, D. B. 2008. Emissions effects of hydrogen as a supplemental fuel with diesel and biodiesel. *SAE Paper* 2008-01-0648.

Singh, D.; Subramanian, K. A.; Singal, S. K. 2015. Emissions and fuel consumption characteristics of a heavy duty diesel engine fueled with Hydro processed Renewable Diesel and Biodiesel. *Applied Energy* 155 (2015) 440–446.

Standard EN 590: 2013. *Automotive fuels - Diesel - Requirements and test methods*.

Standard EN 12916: 2016. *Petroleum products - Determination of aromatic hydrocarbon types in middle distillates - High performance liquid chromatography method with refractive index detection*.

Standard JCGM 100: 2008. *Evaluation of measurement data – Guide to the expression of uncertainty in measurement* 132 p.

Stone, C. R.; Green-Armytage, D. I. 1987. Comparison of methods for the calculation of mass fraction burnt from engine pressure–time diagrams. Proc. *Instn Mech Engrs, Part D: J. Automobile Engineering*, 201(1), 61–67. https://doi.org/10.1243/PIME_PROC_1987_201_158_02.

Sugiyama, K.; Goto, I.; Kitano, K.; Mogi, K. *et al.* 2012. Effects of Hydrotreated Vegetable Oil (HVO) as Renewable Diesel Fuel on Combustion and Exhaust Emissions in Diesel Engine. *SAE Int. J. Fuels Lubr.* 5(1):205-217, 2012, https://doi.org/10.4271/2011-01-1954.

Syu-Ruei, J.; Kang-Shin, C.; Sheng-Lun, L.; Yuan-Chung, L.; Way Lee, C. 2015. Reducing pollutant emissions from a heavy-duty diesel engine by using hydrogen additions. *Fuel* 2015;172:89–95.

Sunde, K.; Brekke, A.; Solberg, B. 2011. Environmental impacts and costs of hydrotreated vegetable oils, transesterified lipids and woody BTL-A review. *Energies*, 4 (6) (2011) 845–877.

Szybist, J. P.; Song, J.; Alam, M.; Boehman, A. L. 2007. Biodiesel combustion, emissions and emission control. *Fuel Process Technol* 2007;88:679–691.

Szwaja, S. 2010. *Studium pulscji ciśnienia spaliania w tłokowym silniku spalinowym zasilanym wodorem.* Wydawnitstwo Politechniki Częstochowskiej. ISBN 978-83-7193-459-9. 229 p.

Szwaja, S. 2011. Knock and combustion rate interaction in a hydrogen fuelled combustion engine. *Journal of KONES Powertrain and Transport,* Vol. 18, No. 3.

Szwaja, S.; Grab-Rogalinski, K. 2009. Hydrogen combustion in a compression ignition diesel engine. *International Journal of Hydrogen Energy* 2009; 34, 4413–4421.

Szwaja, S.; Naber, J. D. 2013. Dual nature of hydrogen combustion knock. *International Journal of Hydrogen Energy* 2013;38:12489–12496.

Talibi, M.; Hellier, P.; Morgan, R.; Lenartowicz, C.; Ladommatos, N. 2018. Hydrogen-diesel fuel co-combustion strategies in light duty and heavy duty CI engines. *International Journal of Hydrogen Energy* 2018;43:9046–9058.

Tamilselvan, P.; Nallusamy, N.; Rajkumar, S. 2017. A comprehensive review on performance, combustion and emission characteristics of biodiesel fuelled diesel engines. *Renewable and Sustainable Energy Reviews* 79 (2017) 1134–1159. http://dx.doi.org/10.1016/j.rser.2017.05.176.

Tang, Ch.; Zhang, Y.; Huang, Z. 2014. Progress in combustion investigations of hydrogen enriched hydrocarbons. *Renewable and Sustainable Energy Reviews* 30: 195–216.

Tsujimura, T.; Suzuki, Y. 2017. The utilization of hydrogen in hydrogen/diesel dual fuel engine. *International Journal of Hydrogen Energy* 2017;42:14019–14029.

Tsujimura, T.; Mikami, S.; Achiha, N.; Takunaga, Y.; Senda, J.; Fujimoto, H. 2003. A study of direct injection diesel engine fueled with hydrogen. *SAE paper* 2003-01-0761.

Tüccar, G..; Uludamar, E. 2018. Emission and engine performance analysis of a diesel engine using hydrogen enriched pomegranate seed oil biodiesel. *International Journal of Hydrogen Energy* 2018;43:18014–18019. https://doi.org/10.1016/j.ijhydene.2017.11.124.

U.S. Department of Energy. 2006. Freedom Car and Vehicle Technologies Multi-Year Program Plan 2006 – 2011. [online cit.: 2018-12-01]. Available from: https://www1.eere.energy.gov/vehiclesanULSDuels/pULSDs/mypp/1_prog_over.pULSD.

U.S. Department of Commerce. 2018. National Oceanic & Atmospheric Administration. *Earth System Research Laboratory.* [online cit.: 2018-05-07]. Available from: www.esrl.noaa.gov/gmd/aggi/aggi.html.

Verhelst, S.; Wallner, T. 2009. Hydrogen-fueled internal combustion engines. Science Direct: *Progress in Energy and Combustion Science* 35, 490 – 527.

Vibe, I.I. 1970. *Brennverlauf und Kreisprozeß von Verbrennungsmotoren*. VEB Verlag Technik. Berlin. 286 p.

Welch, A. B.; Wallace, J. S. 1990. Performance characteristic of a hydrogen-fueled diesel engine with ignition assist. *SAE paper* no. 902070.

White, C. M.; Steeper, R. R.; Lutz, A. E. 2006. The hydrogen-fueled internal combustion engine: a technical review. *International Journal of Hydrogen Energy* 2006;31:1292–1305.

Wiebe, I. I. 1962. Progress in engine cycle analysis: Combustion rate and cycle processes. Moscow; Sverdlovsk: Mashgiz. 271 p. (Вибе, И.И. 1962. Новое о рабочем цикле двигателей. Скорость сгорания и рабочий цикл двигателя. Москва; Свердловск: Машгиз.)

Wierzba, I.; Kilchyk, V. 2001. *Flammability limits of hydrogen–carbon monoxide mixtures at moderately elevated temperatures*. International Journal of Hydrogen Energy 2001;26(6):639–43.

Yang, Z.; Chu, C.; Wang, L.; Huang Y. 2015. Effects of H_2 addition on combustion and exhaust emissions in a diesel engine. *Fuel* 139:190-7. https://doi.org/10.1016/j.fuel.2014.08.057.

Yeliana, Y.; Cooney, C.; Worm, J.; Michalek, D.; Naber, J. 2008. Wiebe function parameter determination for mass fraction burn calculation in an ethanol-gasoline fuelled SI engine. *Journal of KONES Powertrain and Transport*, Vol. 15, No. 3.

Zaccheria, F.; Psaro, R.; Ravasio, N. 2009. Selective hydrogenation of alternative oils: a useful tool for the production of biofuels, *Green Chem*. 11 (2009) 462, http://dx.doi.org/10.1039/b817625f .

Zhou, J. H.; Cheung, C. S.; Zhao, W. Z.; Leung, C. W. 2016. Diesel & hydrogen dual-fuel combustion and its impact on unregulated gaseous emissions and particulate emissions under different engine loads and engine speeds. *Energy* 2016; 94:110–123.

Zhou, J. H.; Cheung, C. S.; Leung, C. W. 2014. Combustion, performance, regulated and unregulated emissions of a diesel engine with hydrogen addition. *Applied Energy* 126 (2014) 1–12.

List of Scientific Publications by the Author on the Topic of the Dissertation

Papers in the Reviewed Scientific Journals

Juknelevičius, R.; Rimkus, A.; Pukalskas, S.; Matijošius, J. 2019. Research of performance and emission indicators of the compression-ignition engine powered by hydrogen – diesel mixtures. *International Journal of Hydrogen Energy*. Vol. 44, Issue 20, Pages 10129–10138. ISSN 0360-3199. https://doi.org/10.1016/j.ijhydene.2018.11.185.

Mehra, R.K.; Duan, H.; Juknelevičius, R.; Ma, F.; Li, J. 2017. Progress in hydrogen enriched compressed natural gas (HCNG) internal combustion engines - A comprehensive review. *Renewable and Sustainable Energy Reviews* 80 (2017) 1458–1498. ISSN 1364-0321. https://doi.org/10.1016/j.rser.2017.05.061.

Juknelevičius, R. 2018. Experimental investigations of hydrogen effects on performance and emissions of renewable diesel fueled RCCI. *Science – future of Lithuania: civil and transport engineering, aviation technologies,* Vol. 10, Article ID: mla.2018.4593, p. 1–10. ISSN 2029-2341. https://doi.org/10.3846/mla.2018.4593.

Rimkus, A.; Juknelevičius, R. 2018a. RME co-combustion with hydrogen in compression ignition engine: performance, efficiency and emissions. *Science – future of Lithuania: civil and transport engineering, aviation technologies,* Vol. 10, Article ID: mla.2018.4093, p. 1–9. ISSN 2029-2341. https://doi.org/10.3846/mla.2018.4093.

Juknelevičius, R.; Szwaja, S.; Pyrc, M.; Gruca, M.; Pukalskas, S. 2018c. Combustion of rme – diesel and NExBTL – diesel blends with hydrogen in the compression ignition engine. *Journal of KONES Powertrain and Transport*, Vol. 25, No. 3, p. 261–274. ISSN 1231-4005. https://doi: 10.5604/01.3001.0012.4341.

Rimkus, A.; Pukalskas, S.; Juknelevičius, R.; Matijošius, J.; Kriaučiūnas, D. 2018b. Evaluating combustion, performance and emission characteristics of CI engine operating on diesel fuel enriched with HHO gas. *Journal of KONES Powertrain and Transport*, Vol. 25, No. 2, p. 303–312. ISSN 1231-4005. https://doi: 10.5604/01.3001.0012.2845.

Juknelevičius, R.; Mehra, R.K.; Ma, F.; Szwaja, S. 2018d. In-cylinder combustion analysis of a SI engine fuelled with hydrogen enriched compressed natural gas (HCNG): engine performance, efficiency and emissions. *Journal of KONES Powertrain and Transport*, Vol. 25, No. 3, 253–260. ISSN 1231-4005. http://doi: 10.5604/01.3001.0012.4340.

Papers in other Reviewed Publications

Juknelevičius, R.; Szwaja, S; Pyrc, M.; Gruca, M. 2018a. Biomass based oil and hydrogen co-combustion in the compression ignition engine. *IOP Conf. Series: Materials Science and Engineering* Vol. 421, art. No. 042032, p. 1–10. ISSN 1757-8981. https://doi:10.1088/1757-899X/421/4/042032.

Juknelevičius, R.; Szwaja, S.; Pukalskas, S. 2018b. Influence of Hydrogen Co-Combustion with HVO on Performance, Emissions and Combustion in the Compression Ignition Engine. *Transport Means 2018: Proceedings of 22nd International Scientific Conference*, p. 395–405. ISSN 2351-7034.

Mehra, R.K.; Ma, F.; Hao, D.; Juknelevičius, R. 2018. Study of Turbulent Entrainment Quasi-Dimensional Combustion Model for HCNG Engines with Variable Ignition Timings. *SAE Technical Paper* 2018-01-1687. ISSN 0148-7191. https://doi:10.4271/2018-01-1687.

Rimkus, A.; Berioza, M.; Melaika, M.; Juknelevičius, R.; Bogdanovičius, Z. 2015. Improvement of the compression-ignition engine indicators using dual fuel (diesel and liquefied petroleum gas). *Procedia Engineering. Transbaltica 2015: Proccedings of the 9th international scientific conference* 134: 30–39. ISSN 1877-7058. https://doi: 10.1016/j.proeng.2016.01.035.

Summary in Lithuanian

Įvadas

Problemos formulavimas

Pasaulio pramonės ir gyvenimo kokybės vystymasis yra neatsiejamas nuo augančio iškastinio kuro vartojimo, sukeliančio vis didėjantį klimato atšilimą, kurio rezultatas yra vis labiau tirpstantys ledynai, išaugęs potvynių ir uraganų intensyvumas.

2015 m. gruodžio mėn. Paryžiaus tarptautinėje klimato kaitos konferencijoje 195 šalys pasirašė visuotinį susitarimą dėl klimato kaitos ir nustatė veiksmų planą, kaip išvengti pavojingų klimato pokyčių. Šalių Vyriausybės susitarė dėl ilgalaikio tikslo – išlaikyti vidutinės temperatūros augimą mažiau nei 2 °C, palyginus su priešindustriniu laikotarpiu, o EK įsipareigojo iki 2050 m. sumažinti išmetamųjų teršalų kiekį 80–95 % palyginus su 1990 m. Tačiau reikia pastebėti, kad šie reglamentavimai daro įtaką naftos gavybai ir energijos žaliavų tiekimui, o tuo pačiu ir pasaulio ekonomikos augimui. Be to energijos žaliavų tiekimo grandines įtakoja neramumai Artimuosiuose Rytuose, Irano branduolinė krizė, Ukrainos ir Rusijos karas, JAV ekonominės sankcijos Rusijai. Rūpestis dėl energijos šaltinių stabilumo privertė pramonę ieškoti tvarių, alternatyvių energijos šaltinių, kuriuos gali tiekti patikimesni tiekėjai, išvengiant brangių transportavimo kaštų.

ES nustatė griežtus išmetamųjų teršalų reglamentus, tačiau Volkswagen dyzelinių variklių skandalas atskleidė, kad su šiuolaikine programine įranga ir interneto prieiga variklio parametrai gali būti lengvai valdomi ir bet kokie tarptautiniai susitarimai neužkerta

kelio nesąžiningiems pažeidimams. Siekiant patenkinti griežtus išmetamųjų teršalų reikalavimus naudojamos brangios išmetamųjų teršalų apdorojimo sistemos, kurios didina degalų sąnaudas. Kadangi šiandien transportas priklauso nuo naftinio dyzelino, techniniai sprendimai šiltnamio efektą sukeliančių dujų kiekiui mažinti bus vis sudėtingesni ir brangesni. Sumažinti išmetamųjų teršalų kiekį pagal ES taisykles ir išlaikyti 26,5 l/100 km dyzelino sąnaudas sunkvežimiuose įmanoma tik su visiškai kompiuterizuota, brangia išmetamųjų teršalų apdorojimo sistema ir gerai subalansuota visos transporto priemonės energijos vartotojų kontrole.

Mažiausiai taršia energija ateityje būtų elektra ir vandenilio kuro elementų technologija, tačiau ribota akumuliatorių talpa yra pagrindinė plėtros kliūtis šiandienos elektrinėms transporto priemonėms, o didelė vandenilio kaina, vandenilio degalinių stoka ir brangios medžiagos riboja vandenilio kuro elementų panaudojimą automobiliuose.

JAV Energetikos departamentas laikosi nuomonės, kad tol, kol vandenilio kuro elementų technologija pasieks didesnį efektyvumą, vandenilio panaudojimas vidaus degimo varikliuose gali pasitarnauti jungtimi ir technologinė platforma, kuri padėtų plėtoti vandenilio infrastruktūrą. Vandenilio panaudojimas dyzeliniame variklyje gali sumažinti išmetamą teršalų kiekį ir klimato atšilimą. Dėl savo savybių vandenilis galėtų tapti patraukliu alternatyviu energijos šaltiniu kelių transportui. Nors gryno vandenilio panaudojimas vidaus degimo varikliams sunkiai įmanomas, jo bendras degimas su biodegalais pagamintais iš tvarių šaltinių, yra naujas ir mažai tyrinėtas būdas / procesas kuris ateityje gali pasitarnauti sprendžiant ekologines problemas.

Darbo aktualumas

2013 m. Europos Parlamento direktyvoje dėl alternatyvių degalų infrastruktūros diegimo buvo paskelbta, kad vandenilis ir biodegalai, gali pakeisti naftinius degalus ir mažinti išmetamųjų teršalų rodiklius. 2016 m. Europos Komisija paskelbė 2016–2017 m. programą „Pažangus, ekologiškas ir integruotas transportas“, kurios tikslas – sukurti mažiau taršią Europos transporto sistemą, tausojančią išteklius, naudojančią alternatyvius išteklius ir kuri būtų naudinga ekonomikai ir visuomenei. Šioje programoje ypatingas dėmesys skiriamas transporto priklausomybei nuo iškastinio kuro mažinimui, alternatyvių degalų įsisavinimui ir klimato kaitos, taršos, bei triukšmo mažinimui.

Šiuolaikiniai dyzeliniai varikliai dirbantys liesu mišiniu, turės būti dar ekologiškesni, tačiau tuo pačiu būti pakankamai efektyvūs. Vienas iš būdų tai pasiekti yra vandenilio ir biodyzelino panaudojimas. Biodyzelinas gali būti tiekiamas ta pačia tiekimo sistema kaip ir naftinis dyzelinas, o vandenilis gali būti tiekiamas tiek į įsiurbimo kolektorių, tiek tiesiogiai į cilindrą.

Bendras vandenilio ir biodyzelino degimas galėtų būti tinkamas sprendimas dyzeliniams varikliams, kad patenkinti jiems keliamus ekologiškumo reikalavimus. Tačiau mažas vandenilio tankis, vandenilio degimo ciklų skirtumai, vandenilio energijos dalies priklausomybė nuo oro pertekliaus koeficiento, apkrovos ir variklio sūkių, sukelia sunkumus panaudojant vandenilį dyzeliniam variklyje.

Atsižvelgiant į skirtingus vandenilio ir biodyzelino cetaninius skaičius, apsprendžiančius jų reaktyvumo savybes, šių dviejų degalų (skystų ir dujinių) panudojimą dyze-

liniame variklyje galima nagrinėti kaip RCCI (angl. *reactivity controled compression ignition*) režimu veikiantį variklį. Įvairaus reaktingumo mišiniai gali būti naudojami esant skirtingoms dyzelinio variklio veikimo sąlygoms: aukšto reaktingumo degalų mišinys esant mažai apkrovai ir mažo reaktingumo mišinys esant nominaliai apkrovai. Todėl RCCI režimas įgalina variklio veikimą su degalų mišiniais, apimančiais platų diapazoną. Keičiant vandenilio energijos dalį galima valdyti variklio veikimą esant įvairiems oro pertekliaus koeficientams ir apkrovoms. Tačiau didelis vandenilio laminarinis liepsnos sklidimo greitis, aukšta savaiminio užsiliepsnojimo temperatūra ir nedidelis vandenilio liepsnos malšinimo atstumas yra savybės įtakojančios vandenilio panaudojimo RCCI režimu veikiančiame variklyje galimybes. Įpurškimo laikas, trukmė ir kelios įpurškimo porcijos yra biodegalų įpurškimo įrankiai, kuriais gali būti valdomas degiojo mišinio reaktingumas ir kuo tolygesnis šilumos išsiskyrimo procesas, užtikrinantis optimalų variklio veikimą ir mažas degalų sanaudas.

Tyrimo objektas

Vandenilio bendrojo degimo su pirmosios ir antrosios kartos biodegalais (bei jų mišiniais su mineraliniu dyzelinu) slėginio uždegimo vidaus degimo variklio proceso parametrai, vandenilį tiekiant į įsiurbimo kolektorių, o biodegalus – tiesiogiai į cilindrą.

Darbo tikslas

Ištyrus vandenilio bendro degimo procesus slėginio uždegimo variklyje su grynu biodyzelinu ir jų mišiniais su mineraliniu dyzelinu, pasiūlyti vandenilio panaudojmo įtakos variklio veikimo parametrams vertinimo metodiką.

Darbo uždaviniai

Siekiant įgyvendinti iškeltą tikslą suformuluoti tokie disertacijos uždaviniai:

1. Išanalizuoti vandenilio ir biodegalų bei jų mišinių su mineraliniu dyzelinu savybes, suplanuoti slėginio uždegimo variklio eksperimentą ir išplėtoti skaitinio tyrimo algoritmą.
2. Ištirti vandenilio energetinės dalies poveikį, variklyje bendrai degant vandeniliui su RME, HVO bei jų mišiniais su mineraliniu dyzelinu: maksimaliam slėgiui cilindre, pirminio (CA 0–10) ir pagrindinio degimo (CA 10–90) trukmėms, degimo gaišties periodui ir šilumos išsiskyrimo pokyčiui.
3. Nustatyti vandenilio energetinės dalies įtaką variklio veikimo ekologiniams rodikliams.
4. Nustatyti ribinę vandenilio energetinę dalį, kuriai esant susidaro neįprasto degimo (slėgio šuolių) atvejai esant skirtingoms variklio apkrovoms.

Tyrimų metodika

Disertacijoje taikomi eksperimentiniai, teoriniai ir skaitmeniniai modeliavimo tyrimo metodai.

Eksperimentai buvo atlikti su vieno cilindro, slėginio uždegimo varikliu be turbokompresoriaus ir EGR. Duomenų rinkimas ir apdorojimas buvo atliktas *SAWIR* programine įranga, sukurta Delphi 6.0 programavimo aplinkoje.

Stendinių bandymų metu buvo naudojami: slėgio cilindre jutiklis *Kistler 6061B*, įsiurbiamo oro ir išmetamųjų dujų temperatūros jutikliai, išmetamųjų dujų analizatorius Bosch BEA 350, dūmų analizatorius *Maha MDO 2 LON*, biodegalų įpurškimo trukmės reguliatorius, biodegalų sąnaudų matuoklis, vandenilio dujų srauto matuoklis *COMMON CGR- 01*.

Eksperimentinio variklio skaitinis modelis buvo sukurtas naudojant *AVL BOOST* programinę įrangą ir pritaikytas degimo proceso duomenims gauti ir variklio degimo procesui imituoti.

Temperatūros pokyčių modeliavimas buvo atliktas pastovaus tūrio degimo kameroje *CHEMKIN* programine įranga.

Mokslinis naujumas

1. Nustatyta vandenilio energinės dalies įtaka vandenilio bendrojo degimo su biodyzelinu ir/ arba jo mišiniais su mineraliniu dyzelinu slėginio uždegimo variklio efektyvumo ir ekologiniams rodikliams.
2. Sukurta nauja degalų energinių verčių santykio skaičiavimo metodika skystųjų degalų įpurškimo trukmei ir vandenilio tūrio srautui apskaičiuoti pagal pasirinktą vandenilio energijos dalį ir vidutinį indikatorinį slėgį, įvertinus indikatorinį naudingumo koeficientą.
3. Vandenilio bendras degimas su biodyzelinu ir/ arba jo mišiniais su mineraliniu dyzelinu realizuotas RCCI (angl. *reactivity controled compression ignition*) režimu veikiančiame variklyje.
4. Išplėtota ir pritaikyta skaitinio modeliavimo metodika variklio parametrų analizei, veikiant liesu mišiniu su vandenilio energijos dalimi (50–80 %) viršijančia eksperimento bandymų ribas.

Darbo rezultatų praktinė reikšmė

1. Automobilių dyzelių lyginamųjų naftinių degalų sąnaudoms ir išmetamųjų dujų toksiškumui sumažinti galima panaudoti vandenilį (20–23 % dalis energijos). Tai ypač aktualu sprendžiant didžiųjų miestų oro taršos problemą. Atitinkamai reguliuojant skystųjų degalų įpurškimo momentą, periodiškumą ir trukmę, gali būti pasiektas dar didesnis dyzelių efektyvumas.
2. Panaudojant lokomotyvų energijos regeneravimo sistemą vandeniliui pagaminti, jis gali būti panaudotas naftinių degalų sąnaudų ir išmetamųjų dujų kenksmingumui mažinti.

3. Remiantis autoriaus gautais tyrimų rezultatais, galima sudaryti rekomendacines metodikas įmonių transporto priemonių parko atnaujinimo strategijoms kurti, dyzeliniams varikliams panaudojant vandenilį.

Ginamieji teiginiai

1. Mažesnė nei 3,0–3,1 % vandenilio tūrio dalis mišinyje yra nepakankama, kad pasiekti žemutinę vandenilio užsiliepsnojimo ribą (LFL), o tai lemia mažą liepsnos sklidimo greitį degimo metu, lėtą šilumos išsiskyrino greitį ir sąlygoja mažesnį p_{max}, lyginant su gryno biodyzelino degimu.
2. Vandenilio bendrojo degimo su RME, HVO bei jų mišiniais su mineraliniu dyzelinu metu vandenilio energijos dalies didinimas esant skirtingoms apkrovoms didina indikatorinį naudingumo koeficientą ir mažina lyginamąsias degalų sąnaudas.
3. Vandenilio bendrojo degimo su RME, HVO bei jų mišiniais su mineraliniu dyzelinu metu vandenilio energijos dalies didinimas trumpina ir pradinės, ir pagrindinės degimo fazių trukmes.
4. NO koncentracija mažėja dėl lėtesnio liepsnos sklidimo esant mažai vandenilio energijos daliai, o toliau didinant vandenilio energijos dalį, NO didėja. CO ir CH atvirkščiai: didėja esant mažai vandenilio energijos daliai, o toliau didinant energijos dalį mažėja.
5. Dūmingumas mažėja didinant vandenilio energijos dalį, bandymus atliekant visoms variklio apkrovoms.

Darbo rezultatų aprobavimas

Disertacijos tema publikuota 11 mokslinių straipsnių: 2 – *Clarivate Analytics Web of Science* duomenų bazės leidiniuose, turinčiuose citavimo rodiklį; 1 – *Clarivate Analytics Web of Science* duomenų bazės *Conference Proceedings* leidiniuose; 5 – kitų tarptautinių duomenų bazių leidiniuose; 3 – kituose recenzuojamuose mokslo leidiniuose.

Tyrimų rezultatai disertacijos tematika buvo paskelbti penkiose mokslinėse konferencijose:

- „44-oji Tarptautinė transmisijos ir transporto priemonių mokslinė konferencija European KONES 2018“. Czestachwa – Wisla, Lenkija.
- „22-oji Tarptautinė mokslinė konferencija Transport means 2018“. Trakai, Lietuva.
- „3-ioji Tarptautinis vandenilio technologijų kongresas (IHTEC-2018)“. Alanya/Antalya, Turkija.
- „9-oji Tarptautinė vandenilio gamybos konferencija (ICH2P/ICRIC-2018)“. Zagrebas, Kroatija.
- „SAE International. Tarptautinė degalų & alyvų, transmisijų konferencija 2018“. Heidelberg, Vokietija.

Disertacijos struktūra

Disertaciją sudaro įvadas, trys skyriai, bendros išvados, literatūros sąrašas, autoriaus publikacijų disertacijos tema sąrašas, santrauka lietuvių kalba ir priedai.

Disertacijos apimtis – 146 puslapiai (išskyrus priedus), 60 numeruotų formulių, 68 iliustracijos ir 15 lentelių. Rengiant disertaciją panaudotos 174 publikacijos ir kiti šaltiniai.

1. Biodyzelino ir vandenilio savybės, aktualumas ir panaudojimas dyzeliniame variklyje

Šiuolaikinių iš biomasės pagamintų biodegalų panaudojimas slėginio uždegimo varikliuose gali sumažinti išmetamų teršalų kiekį, dėl mažesnio biodegalų C / H santykio. Dauguma biodegalų šiandien gaminami iš įprastai prieinamų žaliavų ir klasifikuojami kaip pirmos kartos biodegalai. Biodegalai, pagaminti iš antrosios kartos biomasės, nekonkuruoja su maisto gamyba, tačiau aukšta žaliavų kaina reikalauja sprendimo, kad biodegalai taptų ekonomiškai patrauklūs (Hilbers *et. al.* 2015). Kita problema, susijusi su biodegalų gamyba, yra išgautos energijos kainos santykis su jos gamybos sąnaudomis (Murphy *et. al.* 2010). Šis santykis turėtų būti ne didesnis kaip 3:1, kad energijos kaina padengtų infrastruktūros ir transportavimo kaštus, o dabar šis santykis tėra 1,3:1 (Hilbers *et. al.* 2015).

Pagrindiniai biodegalų šaltiniai yra augaliniai aliejai ir gyvūnų riebalai. Augaliniai aliejai sudaro trigliceridų mišinys. Trigliceridų esterinimo būdu panaudojant katalizatorių (metanolį) išgaunamas riebiųjų rūgščių metilo esterio (FAME) ir glicerolio mišinys. FAME paprastai vadinamas įprastiniu biodyzelinu. Trigliceridų esterinimo alternatyva yra trigliceridų apdorojimas vandeniliu, dar vadinamas hidrolizavimas. Šio proceso metu augalinis aliejus yra termocheminiu būdu apdorojamas vandeniliu ir taip išgauanamas hidrinimu valytas augalinis aliejus (angl. *hydrotreated vegetable oil*, HVO). HVO pagamintas iš tos pačios trigliceridų žaliavos, kuri naudojama FAME arba rapsų metilo esteriui (RME) gaminti. Tačiau FAME ir HVO yra skirtingi produktai, turintys skirtingą cheminę struktūrą ir fizines savybes.

RME gali būti sumaišytas su naftiniu dyzelinu iki 30 % pagal masę, tačiau pagal EN 590 standartą naftinis dyzelinas gali būti skiedžiamas ne didesne kaip 7 % RME masės dalimi. Suomijos mokslininkai kartu su *Neste Oil Corporation* sukūrė hidrinimu valyto augalinio aliejaus technologiją ir ją pavadino NExBTL. Tai yra iš atsinaujinančių žaliavų išgaunamas biodyzelinas, pagamintas iš antrosios kartos biomasės: palmių, sojos pupelių, rapsų aliejaus, o taip pat iš maisto parmonės (Engman *et. al.* 2016).

FAME sudėtyje yra didesnis deguonies kiekis (10–11 %), todėl žemutinė šiluminė vertė (LHV) pagal masę yra mažesnė nei mineralinio dyzelino. Tačiau dėl 6 % didesnio tankio ir mažesnio stechiometrinio oro-degalų masės santykio jo stichiometrinio mišinio energijos kiekis yra maždaug 1,8 % didesnis nei mineralinio dyzelino. Žemutinė FAME šiluminė vertė priklauso nuo žaliavos ir skiriasi: palmių biodyzelino šiluminė vertė yra 36,5–36,9 MJ/kg, o iš *Pongamija* aliejaus išgauto biodyzelino – 43,4 MJ/kg.

Didelė FAME kinematinė klampa yra pagrindinė priežastis, kodėl grynas biodyzelinas negali būti naudojams kaip automobiliniai degalai. Riebiųjų rūgščių metilo esterių ki-

nematinę klampą įtakoja anglies atomų grandinės ilgis ir dvigubų ryšių skaičius. Kuo ilgesnė atomų grandinė ir didesnis prisotinimo laipsnis tuo didesnis biodyzelino klampumas (Knothe *et. al.* 2016). HVO pasižymi mažesniu tankiu nei naftinis dyzelinas ir biodyzelinas (FAME). HVO yra lengvos frakcijos angliavandenilis, kuriame yra mažai aromatinių frakcijų bei nėra deguonies. HVO savybės yra panašios į tas kuriomis pasižymi dyzelinas, gaminamas Fischer-Tropsch sintezės būdu (Aatola *et. al.* 2008).

Dėl mažo HVO tankio – 779,7 kg/m^3 jis neatitinka EN 590:2013 nustatyto reikalavimo – 820 kg/m^3. Dėl šios priežasties tik iki 30 % masės HVO gali būti maišomas su mineraliniu dyzelinu, kad atitiktų EN 590 specifikaciją. Mažas tankis lemia 6% mažesnę šiluminę vertę pagal tūrį lyginant su mineraliniu dyzelinu, todėl norint pasiekti tą patį vidutinį efektyvų slėgį reikia sunaudoti didesnį tūrį HVO degalų.

HVO pasižymi aukštu cetaniniu skaičiumi – daugiau nei 75, nes jis yra *n*-parafinų (alkanų) ir *i*-parafinų mišinys (Engman *et al.* 2016). Dauguma *n*-parafinų turi 70–90 % *n*-heptadekano ir *n*-oktadekano, o tai padeda pasiekti aukštą CN. Tačiau šie parafinai įtakoja prastas savybes žemoje temperatūroje ir tokiu būdu riboja HVO panaudojimą jį maišant su mineraliniu dyzelinu. Aukštasis HVO cetaninis skaičius ir mažas C/H santykis (5,60) nulemia trumpesnį gaišties periodą, todėl degimo metu susidaro mažiau suodžių.

Aukštas HVO cetaninis skaičius ir maža aromatinių frakcijų dalis esanti HVO (Sugiyama *et al.* 2012) sumažina HC ir kietųjų dalelių emisijas ir sumažina specifines degalų sąnaudas. Dyzelinio variklio veikiančio degalais, kurių sudėtyje yra 30 % tūrio *Camelina sativa* biodyzelino (Lebedevas *et al.* 2013), efektyvumo ir ekologiškumo rodikliai pakito nedaug lyginant su naftiniu dyzelinu, tačiau saugojimo metu savybės pablogėjo lyginant su naftiniu dyzelinu, todėl biodyzelino saugojimas turi būti kiek tai įmanoma trumpesnis.

Atliekant eksperimentinį tyrimą su dyzeliniu varikliu (Labeckas *et al.* 2014), veikiančiu 5–15% pagal tūrį etanolio ir dyzelino mišiniu, ir etanolio (15 % tūrio), dyzelino (80 % tūrio), RME (5 % tūrio) mišiniu (E15B). Buvo nustatyta, kad E15B mišinyje esantis deguonies masės kiekis labiau atspindi savaiminio užsidegimo gaišties trukmę nei cetaninis skaičius. Maža NO_x, CO, HC emisija ir teigiami dūmingumo pokyčiai parodė degaluose esančios deguonies jungties svarbą.

Atliekant bandymus su dyzeliniu varikliu esant vidutiniam sukimosi greičiui ir skirtingiems apkrovos momentams, tiekiant į variklį dyzelino ir *BTL* (15 %) mišinį (Rimkus *et al.* 2015) buvo pastebėta, kad *BSFC* sumažėjo 2,6 %, o efektyvumas padidėjo 2,0 %. CO_2 emisijos sumažėjo 1,1 %, o CH sumažėjo 3–7 %. Šiuos pokyčius sąlygojo *BTL* molekulių jungtys ir mažesnis C/H santykis. Dėl mažos aromatinių angliavandenilių dalies bei intensyvaus degimo difuzinėje fazėje buvo pasiektas 16–18 % dūmingumo sumažėjimas. Be to, dėl didesnio *BTL* cetaninio skaičiaus ir mažesnio deguonies kiekio sutrumpėjusi savaiminio užsidegimo gaišties trukmė sukėlė 12–20 % šilumos išsiskyrimo sumažėjimą ir mažesnę degimo temperatūrą. Dėl to 9–12 % sumažėjo NO_x.

Pirjolos *et al.* (2017) atliktų bandymų metu, dyzelinius degalus pakeitus HVO, NO_x emisijos sumažėjo 20 %, o kietųjų dalelių emisija – 44 %. Bhardwaj *et al.* (2015) pastebėjo, kad HVO degalų panaudojimas sumažino dūmingumą apie 50 %, o kietųjų dalelių emisija 43 %. Šie ir kiti tyrimai (Aatola *et al.* 2008; Murtonen *et al.* 2009; Lehto *et al.* 2011; Imperato *et al.* 2011; Pflaum *et al.* 2010; Erkkila *et al.* 2011) atlikti su HVO parodė, kad HVO sumažina NO_x, suodžių emisiją ir nuosėdų susidarymą cilindre, todėl HVO turi teigiamą įtaką slėginio uždegimo varikliui.

Vandenilis pasižymi aukšta žemutine šilumos verte (120 MJ/kg), plačiu užsiliepsnojimo diapazonu pagal tūrį (4–75 %), mažą minimalią užsidegimo energija (0.02 mJ), mažą liepsnos malšinimo malšinimo atstumą, labai greitą liepsnos sklidimo greitį (2.65–3,25 m/s) ir didelį mažų molekulių skvarbumą. Vieno vandenilio užsidegimas įmanomas pasiekus aukštą temperatūrą (585 ºC), tačiau pats degimo procesas yra netolygus, todėl vidaus degimo varikliuose vandenilis naudojamas bendrai jam degant su kitais angliavandeniliais. Bendras vandenilio degimas su dyzelinu ir/ arba biodyzelinu sutrumpina užsidegimo gaišties trukmę, paspartina šilumos išsiskyrimo greitį ir padidina variklio efektyvumą.

Antunes *et al.* (2009) išbandęs vandenilį dyzeliniam variklyje išgavo didesnę specifinę galią lyginant su įprastu dyzelinu veikusiu varikliu. Tačiau tam, kad vandenilis degtų slėginio uždegimo variklyje reikėjo panaudoti įsiurbiamo oro šildymą, kad būtų užtikrintas pakankamas degimas. Bandymuose su vandeniliu buvo pasiektas 42,8 % šiluminis efektyvumas, palyginus su 27,9 % efektyvumu pasiektu su dyzelinu.

Gryno vandenilio panaudojimą HCCI režimu veikiančiame variklyje tyrę Szwaja *et al.* (2009) pastebėjo degimo nestabilumą dėl nevaldomos degimo pradžios ir padarė prielaidą, kad vandenilis tikriausiai užsidega nuo karštų degimo kameros vietų ir stūmoklio paviršiaus. Be to, užsidegimas įvykdavo per anksti, ir neišvystydavo tokio sukimo momento, kurį pasiekdavo dyzelinu veikiantis variklis. Norint pagerinti variklio veikimą, reiktų panaudoti EGR ir (arba) oro ir vandenilio mišinio šildymą.

Tolesni slėginio uždegimo variklių tyrimai juose bendrai degant vandenilio ir biodyzelino mišiniams (Serin *et al.* 2018; Chaichan *et al.* 2018; Chelladorai *et al.* 2018; Tüccar *et al.* 2018; Jegadheesan *et al.* 2017; Rocha *et al.* 2017; Aldhaidhawi *et al.* 2017; Baltacioglu *et al.* 2016; Zhou *et al.* 2014) parodė, kad emisijų sumažėjimui ir variklio efektyvumui įtakos turi skystų degalų įpurškimo momentas, trukmė, variklio sūkiai ir vidutinis efektyvusis slėgis. Vandenilis bendrai degdamas su biodyzelinu gali sumažinti CO ir kietųjų dalelių išmetimą ir užtikrinti aukštesnį šiluminį efektyvumą.

Verhelst *et al.* (2009) atliko ilgalaikį vandenilio panaudojimo kaip energijos šaltinio tyrimą, siekdamas įvertinti perėjimą prie švarios ir tvarios energijos panaudojant vandenilį. Efektyviausias būdas naudoti vandenilį yra kuro elementų technologija, kuri yra dvigubai efektyvesnė už vidaus degimo variklį. Vandenilis galėtų būti švaraus kuro energijos nešėju, kad pakeisti dyzelinius variklius traukiniuose, laivuose, tačiau pagrindinė problema yra brangi technologija, didelės vandenilio sąnaudos ir nepakankamas vandenilio užpildymo tinklas (Europos Komisija 2015). Todėl vandenilio panaudojimas vidaus degimo varikliuose galėtų pasitarnauti vandenilio infrastruktūros plėtrai ir vėlesniam perėjimui prie kuro elementų technologijos.

Bendras vandenilio ir biodyzelino degdamas slėginio uždegimo varikliuose užtikrina didesnį šiluminį efektyvumą ir mažina kenksmingų teršalų išmetimą palyginus su dyzelinu veikiančiu varikliu. Vandenilio ir biodyzelino bendro degimo panaudojimas turi galimybę padėti vandeniliui įsiskverbti į pramonę. Didelio darbinio tūrio lokomotyvų varikliai veikdami energijos regeneravimo režimu gali gaminti vandenilį, kuris vėliau gali būti panaudojamas varikliui ir mažinti aplinkos taršą.

2. Vandenilio bendro degimo su biodyzelinu tyrimo metodologija

Tyrimo darbo tikslui pasiekti ir numatytiems uždaviniams įgyvendinti buvo atlikti vandenilio bendro degimo su biodyzelinu eksperimentai slėginio uždegimo variklyje. Tokiame variklyje degalų tiekimo sistema turi užtikrinti dujinių degalų – vandenilio ir skystų degalų – biodyzelino tiekimą. Tokia sistema yra sudėtingesnė nei vieno būvio degalų tiekimo sistema. Ji tampa dar sudėtingesnė jeigu tyrimui naudoti keturių cilindrų variklį, nes reikia keturių purškstukų, keturių jutiklių, t.y. daugiau įrangos, bei su tuo susijusių pakeitimų. Todėl buvo pasirinktas vieno cilindro variklis, kad būtų pigiau ir paparasčiau atlikti būtinus pakeitimus.

Skystų degalų tiekimo sistema buvo pasirinkta tokia, kad būtų galima nustatyti įpurškiamų skystų degalų kiekį, o vandenilio energijos dalis buvo nustatoma pagal tūrio srautą. Įpurškiamų degalų kiekis buvo nustatomas elektroniniu būdu valdomu įrenginiu, kuriuo buvo reguliuojama įpurškimo trukmę μs, kad gauti reikiamą įpurškiamų degalų kiekį. Į esamą slėginio uždegimo variklio įsiurbimo kolektorių buvo įmontuotas vožtuvas, sujungtas su vandenilio tiekimo vazdžiu.

Bandymai buvo atlikti vieno cilindro stacionariuoju slėginio uždegimo varikliu Andoria S320. Skystų degalų tiekimui užtikrinti buvo sumontuotas radialinis aukšto slėgio slėgio siurblys Bosch CR/CP1S3, varomas 2,2 kW elektros varikliu GL-90L2-4. Sinchroninis elektros variklis CELMA Type 2Sf200 L6/4A panaudotas kaip slėginio uždegimo variklio starteris-generatorius. Šiuo elektros varikliu užvedamas dyzelinis variklis, o jam pradėjus veikti sukimo momentas dviem diržais perduodamas elektros varikliui, kuris generuoja elektros energiją. Taip palaikomas pastovus slėginio uždegimo variklio greitis – 965 min^{-1}. Sugeneruota elektros energija tiekiama į elektros tinklą. S.2.1 lentelėje pateikti slėginio uždegimo variklio Andoria S320 pagrindiniai techniniai rodikliai.

S.2.1 lentelė. Variklio Andoria S320 techniniai rodikliai

Rodikliai	Reikšmė
Cilindrų skaičius	1
Cilindro skersmuo, mm	120
Stūmoklio eiga, mm	160
Darbinis tūris, cm^3	1810
Suslėgimo laipsnis	17
Maksimali galia, kW/AG	13,2/18
Maksimalūs sūkiai, min^{-1}	1500
Maksimalus sukimo momentas, Nm (min^{-1})	84,4 (1200)
Švaistiklio ilgis, mm	275
Įsiurbimo vožtuvo atsidaro	23° prieš viršutinį galinį tašką
Įsiurbimo vožtuvo užsidaro	40° po apatinio galinio taško
Išmetimo vožtuvo atsidaro	46° prieš apatinį galinį tašką
Išmetimo vožtuvo užsidaro	17° po viršutinio galinio taško

Slėgio cilindre *p* duomenų surinkimo ir kaupimo sistemą sudaro:

1. Pjezo jutiklis – Kistler 6061B.
2. Slėgio duomenų signalų stiprintuvas – Kistler 5011.
3. Alkūninio veleno kampo padėties matuoklis – Kistler 2612C.
4. Duomenų surinkimo keitiklis – Measurement Computing Corporation PCI-DAS 6036.
5. Programinė įranga SAWIR (lenkų k. System Analizy Wykresu Indykatorowego w Rzeczywistym czasie) – indikatorinių rodiklių analizės sistema realiuoju laiku.

Kiekvieno bandymo metu programa SAWIR surenka duomenis ir įrašo txt formatu, kurį vėliau galima transformuoti į kitas patogias duomenų apdorojimui ir analizei rinkmenas. Bandymų metu yra kaupiami šie duomenys apie kiekvieno ciklo (iš 200 ciklų) parametrus: variklio sūkių skaičius; degimo metu išsiskyręs indikatorinis specifinis šilumos kiekis; indikatorinė galia; maksimalus slėgis cilindre; didžiausias slėgio prieaugis; šilumos išsiskyrimo greitis; didžiausia temperatūra; 50 % sudegusio mišinio padėtis alkūninio veleno posūkio kampo atžvilgiu; oro (ir vandenilio dujų) temperatūra įsiurbimo kolektoriuje; išmetamųjų dujų maksimali temperatūra; skystų degalų (dyzelino arba biodyzelino) temperatūra.

Taip pat apskaičiuojami šie vidutiniai rodikliai (200 ciklų) alkūninio veleno posūkio kampo atžvilgiu (t.y. nuo 0º iki 720º): slėgis cilindre; degimo kameros tūris; slėgio pokytis; šilumos išsiskyrimo greitis; temperatūra cilindre.

Slėginio uždegimo variklio skaitinis modelis, sudarytas AVL BOOST programa. Variklio skaitinio modelio grafinis vaizdas pateiktas S.2.1 paveiksle.

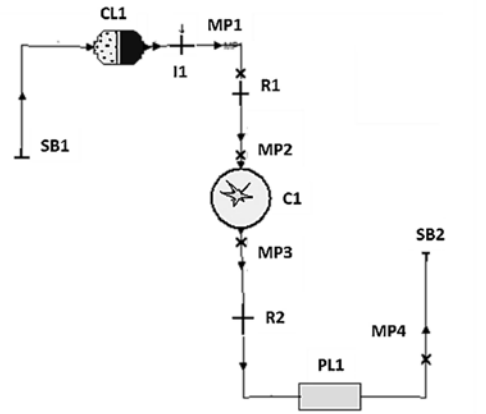

S.2.1 pav. Variklio Andoria S320 AVL BOOST skaitinis modelis:
I1 – H_2 purkštukas; PL1 – išmetimo kolektorius; CL1 – oro filtras; MP1-4 – matavimo taškai; SB1-2 – modelio ribos; C1 – variklio cilindras

Sudarant AVL BOOST modelį į programą įvedami variklio parametrai: cilindro skersmuo, stūmoklio eiga, suslėgimo laipsnis, švaistiklio ilgis, variklio sūkiai, cilindrų

darbo tvarka, vožtuvų fazės ir atidarymo eiga, likusių deginių kiekis cilindre. Nustatomi įsiurbimo bei išmetimo sistemos vamzdžių ilgiai bei skersmenys ir kiti parametrai.

Atliekant degimo proceso sintezę pasirinktas Vibe dvieju zonu šilumos išsiskyrimo modelis. Į programą įvedamas skystų degalų ir vandenilio ciklinis kiekis, jų žemutinė šiluminė vertė; oro pertekliaus koeficientas, degimo pradžia (SOI), degimo trukmė (CD) ir degimo intensyvumo formos parametra m_v. Šie parametrai nustatomi atliekant šilumos išsiskyrimo skaičiavimus – degimo proceso analize. Tai atliekama naudojant AVL BOOST paprogramę BURN. Joje panaudojami eksperimento metu išmatuoti parametrai: slėgis cilindre p, ciklinis skystų degalų ir vandenilio kiekis, ciklinis oro kiekis.

3. Eksperimentinis ir skaitinis vandenilio bendro degimo su biodyzelinu slėginio uždegimo variklyje tyrimas

Bandymai buvo atlikti vieno cilindro slėginio uždegimo varikliu su kombinuotu degiojo mišinio paruošimu. formavimu. Išorinis mišinio paruošimas buvo panaudotas homogeniniam oro ir vandenilio mišinio tiekimui į degimo kamerą. Vidiniu mišinio ruošimo būdu, biodegalai buvo tiesiogiai įpurškiami į degimo kamerą, kuri jau buvo pripildyta oro ir vandenilio mišinio.

Vandenilis dėl savo difuzinių savybių per gan trumpą laiko tarpą, kolektoriuje sudaro homogeninį degujį mišinį su oru ir patenka į degimo kamerą, kurioje į homogeninį oro-vandenilio mišinį įpurškiami skysti degalai. Dėl aukšto slėgio (3,98 MPa) ir padidėjusios temperatūros (415–435 ºC) suslėgimo pabaigoje, įpurkšti skysti degalai savaime užsiliepsnoja, o dėl šį užsiliepsnojimą lydinčios išaugusios temperatūros užsiliepsnoja ir degusis oro ir vandenilio mišinys. Užsiliepsnojimo pradžios momentas yra pereinamasis procesas, susijęs oksidacijos reakcijų vyksmu, kuris prasiseda nuo inertiškų angliavandenilių ir vandenilio radikalų susidarymo prie aktyvių hidroksido radikalų susidarymo bei degimo procesui virstant oksidacijos reakcijų grandine.

Slėgiui cilindre pastebimai daro įtaką vandenilio tūrio dalies didėjimas (S.3.1 pav.).

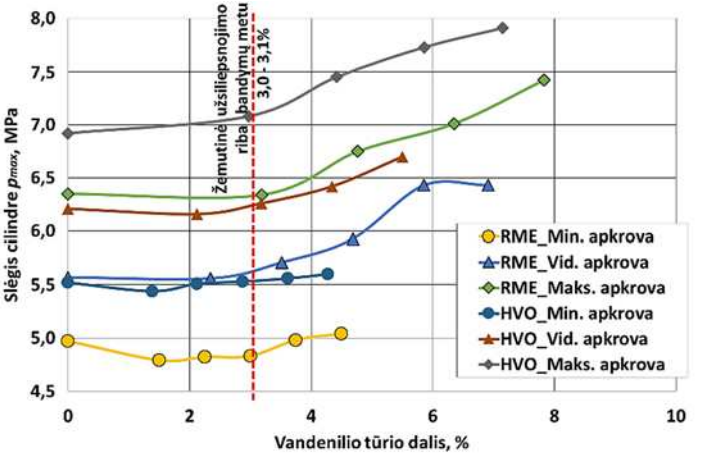

S.3.1 pav. Slėgio cilindre priklausomybė nuo vandenilio tūrio dalies

Tačiau šis slėgio padidėjimas buvo pastebėtas padidinus vandenilio tūrio dalį daugiau kaip 3,0–3,1 %. Slėgio padidėjimas esant minimaliai apkrovai buvo nedidelis (1 %), tačiau vidutinei apkrovai – 9 %, o maksimaliai apkrovai – 14 %.

Esant mažai vandenilio koncentracijai, kol nepasiekta 4 % vandenilio tūrio dalis ore – žemutinė užsiliepsnojimo riba, degimas vyksta gan lėtai. Kai ši riba yra viršyjama, degimas vyksta žymiai sparčiau, kadangi padidėjus vandenilio koncentracijai sudaromos palankesnės sąlygos susidaryti ypač aktyviam hidroksido radikalui, kuris žymiai paspartina vandenilio ir angliavandenilių oksidacijos reakcijų grandinių susidarymą. Kai vandenilio energijos dalis buvo 19 % vandenilio tūrio dalis tesudarė 1,5 %, esant 26 % vandenilio energinei koncentracijai, tūrio dalis sudarė 2,25 %, o esant 32 % vandenilio energinei koncentracijai, tūrio dalis sudarė 3 % ir visos šios vertės buvo mažesnės nei 4 % žemutinė vandenilio užsiliepsnojimo riba.

Reikia pastebėti, kad didėjant temperatūrai ir slėgiui keičiasi vandenilio ir oro mišinio degumo ribos. Autoriaus atliktų eksperimentų metu, užsiliepsnojimo pradžia vyko 415–435 °C temperatūros intervale. Žemutinė užsiliepsnojimo riba 415–435 °C temperatūroje sumažėjo iki 1,5 % vandenilio tūrio dalies (Schroeder *et al.* 2004). Šis žemutinės ribos sumažėjimas iki 1,5 % nesukelia savaiminio vandenilio užsiliepsnojimo, nes temperatūra vis dar yra per maža (415–435 °C) ir nepakankama vandenilio uždegimui ir degimo intensyvumui skatinti.

Tačiau slėgiui padidėjus iki 5 MPa, žemutinė užsiliepsnojimo riba padidėja nuo 4 % iki 5,6 %. Eksperimentų metu užsiliepsnojimo pradžioje slėgis buvo 3.98 MPa, todėl žemutinė užsiliepsnojimo riba yra 3,0–3,1 % vandenilio tūrio dalies. Galima daryti išvadą, kad tik pasiekus vandenilio energijos dalį – 32 %, buvo pasiekta žemutinė užsiliepsnojimo riba ir tada vandenilis efektyviai dega su įpurškiamu RME arba HVO. Iki šios ribos liesas oro ir vandenilio mišinys su RME arba HVO nedaro apčiuopiamo poveikio degimo intensyvumui.

Indikatorinis naudingumo koeficientas (S.3.2 pav.) didėjo bandymus atliekant su RME ir didnant vandenilio energijos dalį. Variklio efektyvumas bandymuose su HVO buvo didesnis, nes bandymų metu vidutinis indikatorinis slėgis (*IMEP*) buvo didesnis nei bandymų su RME metu. Atsižvelgiant į tai, kad RME stechiometrinio mišinio šiluminė vertė yra didesnė (2,79 MJ/kg) nei HVO (2,75 MJ/kg), galima teigti, kad RME šiluminis efektyvumas turėtų būti didesnis nei HVO esant tam pačiam *IMEP*.

Degiojo mišinio šiluminė vertė esant vienodai apkrovai nesikeisdavo, todėl keičiant vandenilio ir skystų degalų šiluminių verčių santykį, tai neturėjo įtakos indikatoriniam naudingumo koeficientui. Didžiausią įtaką šiluminiam naudingumo koeficientui turėjo padidėjęs vandenilio masės srautas, kurio šilumingumas didesnis nei biodyzelino. Dėl mažo vandenilio tankio sumažėjo bendras dujinio ir skystų degalų masės srautas, ir tuo pačiu indikatorinės degalų sąnaudos.

Dėl greito vandenilio degimo greičio vandenilio oksidacija vyksta su mažesniais šilumos nuostoliais į degimo kameros sienas, todėl pagerėja šiluminis efektyvumas. Taigi didinant vandenilio energinę koncentraciją turėtų padidėti ir šiluminis efektyvumas esant riebiam degalų mišiniui su maksimalia apkrova. Tačiau reikia pažymėti, kad vandenilis turi labai mažą liepsnos malšinimo atstumą, mažesnį negu biodyzelino. Todėl vandenilio liepsna gali išplisti arčiau cilindrų sienelių, o tai lemia beveik visišką mišinio sudegimą.

Didinant vandenilio energinę kocentraciją, liepsnos malšinimas vyksta vyskta arčiau cilindro sienelių, o tai padidina šilumos perdavimą per degimo kameros sieneles ir todėl pablogėja šiluminis efektyvumas.

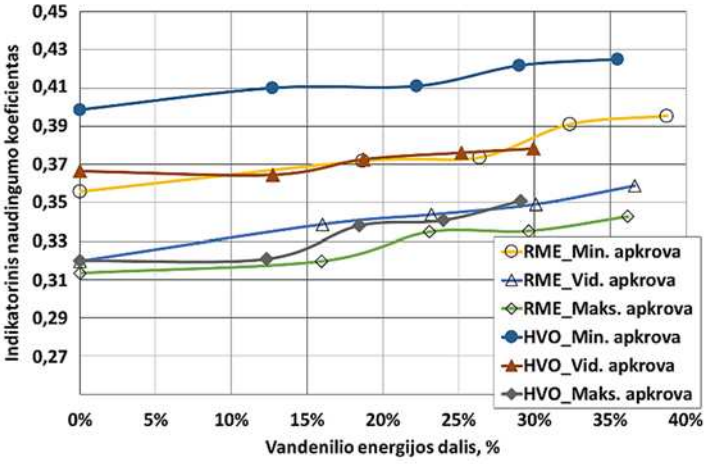

S.3.2 pav. Indikatorinio naudingumo koeficiento priklausomybė nuo H_2 energijos dalies

Sudegusi mišinio dalis (SMD, anglų k. – MFB) buvo apskaičiuota įvertinant šilumos išsiskyrimą kiekviename degimo proceso taške, kurį atitinka alkūninio veleno posūkio kampas. Pradinė degimo fazė (CA 0–10) yra išreikšta alkūninio veleno posūkio kampu, per kurį nuo mišinio užsiliepsnojimo pradžios sudega iki 10% mišinio. Pagrindinė degimo fazė (CA 10–90) yra išreikšta alkūninio veleno posūkio kampu, per kurį sudega nuo 10 % iki 90 % mišinio. CA 0–10 ir CA 10–90 degimo trukmės buvo įvertintos laispniais esant įvairioms indikatorinio vidutinio slėgio reikšmėms, vertinant bendrą vandenilio degimą su biodegalais (RME ir HVO). Didinant vandenilio energijos dalį pradinė CA 0–10 degimo trukmė sutrumpėjo dėl padidėjusio liepsnos sklidimo greičio (S.3.3 pav.). Vandenilio energinės koncentracijos padidėjimas taip pat sutrumpina pagrindinę degimo trukmę CA 10–90, kurią pagreitina pradinė degimo fazė CA 0–10 (S.3.4 pav.).

Analizuojant vandenilio bendro degimo su HVO ir RME rezultatus, nustatyta, kad vandenilio energinė koncentracija turi įtakos degiojo mišinio degimo intensyvumui ankstyvojoje degimo fazėje, varikliui veikiant tik vidutinei ir maksimaliai aprovai. Slėgis cilindre (S.3.5 pav.), išmatuotas bandymus atliekant su HVO + H_20 %, RME + H_20 %, HVO + H_230 % ir RME + H_230 % skystų degalų ir vandenilio mišiniais, patvirtina šį teiginį. Pateiktame paveiksle slėgio cilindre kreivės pavaizduotos kartu su skystų degalų įpurškimo pradžios padėtimi.

Bandymų metu išmatuotos slėgio cilindre reikšmės koreliuoja su tomis, kurios buvo nustatytos modeliuojant su AVL BOOST. Remiantis šilumos išsiskyrimo pokyčio kreivėmis buvo nustatyta užsiliepsnojimo pradžia.

Degiojo mišinio (be vandenilio) užsiliepsnojimo pradžia buvo toje padėtyje kai alkūninio veleno posūkio kampas buvo 349º esant mažai apkrovai (S.3.6 pav.). Alkūninio veleno posūkio kampas buvo 345º padėtyje esant vidutinei apkrovai ir degimui naudojant HVO, o vandenilio energinę dalį keičiant 0–30 %.

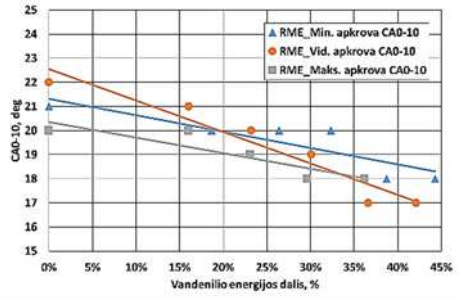

S.3.3 pav. Pradinė degimo fazės trukmė CA 0–10 esant įvairioms vandenilio energijos dalims, bandymuose su RME

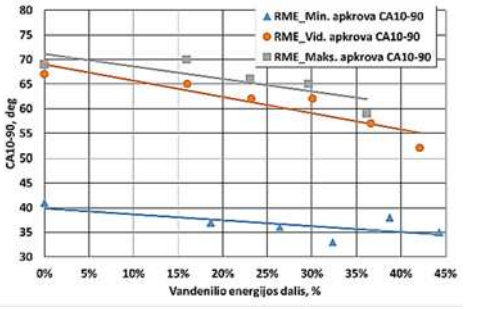

S.3.4 pav. Pagrindinė degimo fazės trukmė CA 0–10 esant įvairioms vandenilio energijos dalims, bandymuose su RME

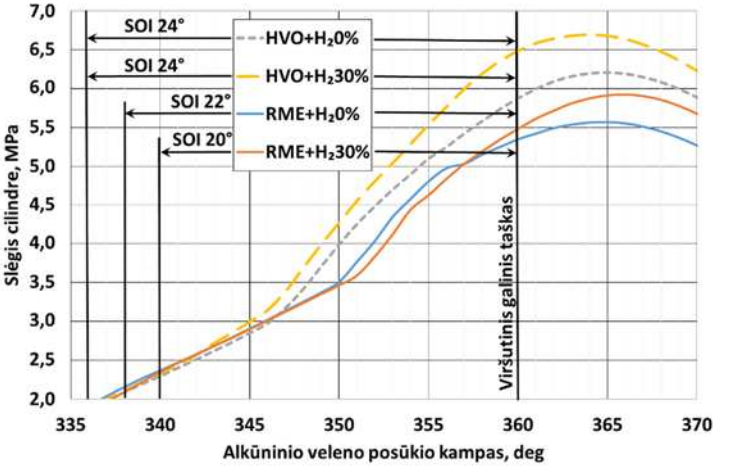

S.3.5 pav. Slėgio cilindre pokyčio kreivės

Užsiliepsnojimo pradžios kampas buvo 343º padėtyje esant maksimaliai apkrovai ir degimui naudojant HVO, o vandenilio energinę dalį keičiant 0–24 %. Kai vandenilio energijos dalis buvo 30%, užsiliepsnojimo kampas buvo 342º padėtyje. Mažas vandenilio kiekis nedaro ženklios įtakos slėgiui cilindre esant mažai apkrovai ir keičiant vandenilio

energijos dalį 13–29 % diapazone. Labiau apčiuopiamas poveikis buvo pastebėtas esant vidutinei apkrovai (30 %) ir esant maksimaliai apkrovai (29 %). Taip vyksta dėl labai intensyvaus degimo po mišinio užsiliepsnojimo pradžios. Tai parodo degimo intensyvumo parametro sumažėjimas esant vidutinei ir maksimaliai apkrovai ir didinant vandenilio energijos dalį.

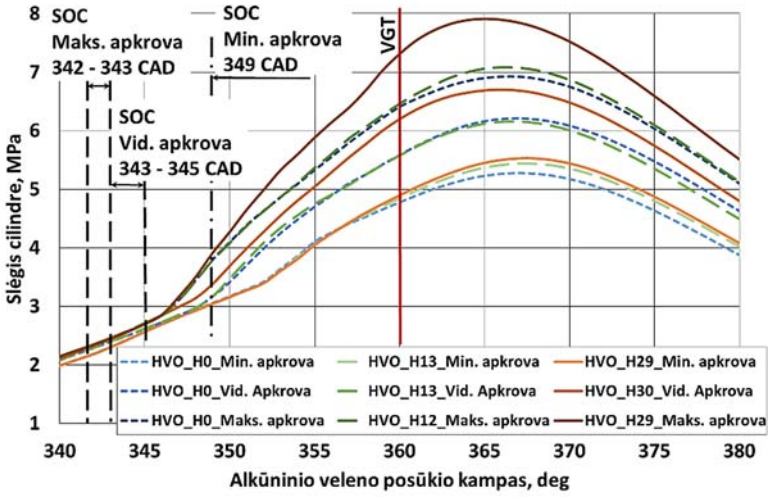

S.3.6 pav. Slėgio cilindre pokyčio kreivės nustatytos AVL BOOST programa

Ankstyvoji degimo fazė CA 0–10, kurios metu sudega iki 10 % degiojo mišinio didelę įtaką tolesniam degimo procesui. Ypatingai tai pasireiškia degimo procese, kai yra naudojami degalų mišiniai, iš kurių vienas yra aukšto reaktingumo (šiuo atveju HVO), o kitas yra žemo reaktingumo (vandenilis) degalai. Šiuo režimu veikiantis variklis vadinamas reaktingumo valdymo režimu veikiantis slėginio uždegimo variklis (anglų k. RCCI – raectivity controlled compression ignition engine). Degimas ankstyvojoje degimo fazėje vyskta liepsnai sklindant kvazilaminariškai, o mišinio vientisumas lemia intensyvų degimo proceso vyksmą ir spartų šilumos išsiskyrimą. Tačiau labai greitai toks degimo proceses pavirsta į turbolentinį kuris vyksta likusioje pagrindinėje degimo fazėje.

Bendrosios išvados

1. Mažesnė nei 3,0–3,1 % vandenilio tūrio koncentracija mišinyje lemia nereikšmingą variklio efektyvumo ir slėgio cilindre pokytį. Efektyvus vandenilio ir biodyzelino bendras degimas prasideda tik viršijus žemutinę vandenilio užsiliepsnojimo ribą, ir pastebimai įtakoja slėginio uždegimo variklio efektyvumo ir emisijos parametrus.

2. Vandenilio oksidacija dėl didelio vandenilio degimo greičio vyksta su mažesniais šilumos nuostoliais į degimo kameros sieneles. Be to vandenilis pasižymi mažu liepsnos malšinimo atstumu, todėl vandenilio liepsna išplinta arčiau cilindro sienelių. Šie veiksniai lemia efektyvesnį mišinio sudegimą, aukštesnį variklio indikatorinį naudingumo koeficientą ir mažesnes lyginamąsias degalų sąnaudas.
3. Bendras vandenilio ir biodyzelino degimas didinant vandenilio energijos dalį, sąlygoja degimo intensyvumą pradinėje (CA 0–10) ir pagrindinėje (CA 10–90) degimo fazėse, kuris vyksta dėl išaugusio laminarinio liepsnos sklidimo greičio, sutrumpėjusios degimo trukmės ir padidėjusio šilumos išsiskyrimo pokyčio.
4. Vandenilio koncentracija padidina degimo intensyvumą ir šilumos išsiskyrimo pokytį, dėl to padidėja NO koncentracija. Vandenilio energijos dalies interavalas tarp 13–17 % buvo nustatytas kaip optimalus intervalas visoms bandymų apkrovoms, o NO koncentracija net neviršija tos NO koncetracijos, kuri gauta bandant su grynu biodyzelinu.
5. Neįprasto degimo atsiradimas apribojo vandenilio energijos dalies didinimą mišinyje. Aiški vandenilio energijos dalies riba nenustatyta, tačiau neįprastas degimas pasireiškė esant vidutinei apkrovai, kai vandenilio energijos dalis 24–36 %, ir esant nominaliai apkrovai kai vandenilio energijos dalis 26–42 %, o vandenilio tūrio dalis ore buvo atitinkamai – 4,97–6,91 %, esant vidutinei apkrovai ir 6,51–7,83 % esant nominaliai apkrovai.
6. Siekiant optimizuoti slėginio uždegimo variklio veikimo efektyvumą ir sumažinti išaugusią NO emisiją, buvo nustatytas kitas (φ_{i3}) įpurškimo kampas (kadangi φ_{i2} buvo fiksuotas eksperimento metu). Taip išvengiama neįprasto degimo reiškinio, efektyvumas padidėjo 1,9–2,6 %, o NO emisija sumažėjo 38–40 % esant nominaliai apkrovai.
7. Dėl mažo reaktingumo degalo (H_2) tiekimo sumažėja mišinio CN ir C/H masės santykis. Tačiau sumažėjęs mišinio CN, sąlygoja didelį šilumos išsiskyrimo pokytį ir sutrumpėjusią užsidegimo gaišties trukmę dėl mažos vandenilio užsidegimo energijos ir labai intensyvaus liepsnos srauto sklidimo greičio, t. y. priešingai nei kitų žemo CN degalų. Bedras vandenilio degimas įmanomas ir su žemo CN biodegalais.
8. Modeliavimas AVL BOOST‘u atskleidė, kad esant liesam mišiniui ir didinant vandenilio energijos dalį 50–80 % dar labiau suintensyvėja degimas ankstyvoje degimo fazėje ir sutrumpėja užsidegimo gaišties periodas.
9. Ištyrus vandenilio bendro degimo procesą su grynais RME ir HVO, o taip pat jų mišiniais su mineraliniu dyzelinu, išplėstos žinios apie vidaus degimo variklių, naudojančių alternatyviuosius degalus ir veikiančių RCCI režimu, vertinimo metodus.

Annexes[1]

Annex A. Methodology of Research on Hydrogen Co-combustion with Biodiesel
Annex B. Summary of Publications of other Authors
Annex C. Declaration of the Authorship
Annex D. Agreements of Co-authors to Provide Publications in the Dissertation
Annex E. Copies of Scientific Publications by the Autor on the Topic of the Dissertation

[1]The annexes are supplied in the enclosed compact disc.

Romualdas JUKNELEVIČIUS

RESEARCH ON BIODIESEL AND HYDROGEN
CO-COMBUSTION PROCESS
IN COMPRESSION IGNITION ENGINE

Doctoral Dissertation

Technological Sciences,
Transport Engineering (T 003)

BIODYZELINO IR VANDENILIO BENDRO
DEGIMO PROCESO SLĖGINIO UŽDEGIMO
VARIKLYJE TYRIMAS

Daktaro disertacija

Technologijos mokslai,
Transporto inžinerija (T 003)

2019 06 06. 14,0 sp. l. Tiražas 20 egz.
Vilniaus Gedimino technikos universiteto
leidykla „Technika“,
Saulėtekio al. 11, 10223 Vilnius,
http://leidykla.vgtu.lt
Spausdino BĮ UAB „Baltijos kopija“,
Kareivių g. 13B, 09109 Vilnius